5-2008

Ductile-Regime Machining of Glass Using the Micromilling Process

Kevin Foy
Clemson University, kfoy@clemson.edu

DUCTILE-REGIME MACHINING OF GLASS USING THE MICROMILLING PROCESS

A Thesis
Presented to
the Graduate School of
Clemson University

In Partial Fulfillment
of the Requirements for the Degree
Master of Science
Mechanical Engineering

---

by
Kevin Austin Foy
May 2008

Accepted by:
Dr. Yong Huang, Committee Chair
Dr. David Angstadt
Dr. John Ziegert

ABSTRACT

Glass is a homogeneous material with amorphous crystal structure that is produced through the rapid cooling of its molten state below the glass transition temperature. Glass exhibits many excellent mechanical and physical properties, and it is widely used in automotive, communications, optics, electronics, architectural, and biomedical industries. For certain applications such as DNA microarrays, glass components with microfeatures are typically produced using a combination of photolithography and etching processes, which is generally time consuming and can involve hazardous chemicals. It would be ideal to fabricate some glass devices through mechanical micromachining for some rapid prototyping applications of glass-based devices, but the brittle nature of glass makes machining difficult. The machined surface is usually fractured and requires additional finishing processes that are costly and time consuming. Fortunately, it is found that the glass can be machined in a ductile regime under certain controlled cutting conditions. Machining in the ductile regime can produce continuous cutting chips.

For micromilling to be used in the manufacturing of glass-based devices, further machining research is required to find optimum cutting configurations to produce high quality micro-scale features. It is known that the cutting regime transition from brittle to ductile cutting regimes is attributed to the effect of pressure and temperature in the cutting zone. The transition has also been correlated to the undeformed chip thickness. However, the mechanism behind ductile regime machining still cannot be fully explained. In this study, the effect of tilt angle on cutting regime transition has been

studied in micromilling crown glass with a micro-ball end mill. Straight glass grooves were machined in a water bath by varying the tool tilt angle and feed rate, and the resulting surface was characterized using a scanning electron microscope and a profilometer to investigate the cutting regime transition. In characterizing the cutting regimes in glass micromilling, rubbing, ductile machining, and brittle machining regimes are hypothesized according to the undeformed chip thickness. In addition, mechanistic stress and temperature models are used in conjunction with experimental data to predict the stress and temperature information in glass micromilling in order to provide insight into why ductile machining happens.

For the conditions investigated in this study, a 45° tool tilt angle was found to produce the highest ductile machining-related feed rate, 0.32 mm/min, and the best surface finish (less than 60 nm R_a) for feed rates less than 0.32 mm/min. The specific cutting energy relationship is determined based on the experimental force data and the effective undeformed chip thickness, which is derived based on the surface roughness measurements. The predicted stresses indicate that the 45° tilt angle easily leads to ductile cutting by increasing the glass fracture toughness while comparing with the performance under the other tilt angles (0°, 15°, 30°, 60°). The temperature rise is estimated negligible under the investigated micromilling conditions. This study offers a better understanding in optimizing the glass micromilling process, and it is expected that the occurrence of the glass ductile-brittle cutting regime transition will be elucidated based on the advances in glass material properties understanding and milling process modeling.

DEDICATION

To my family for their unlimited support

To my friend Harry Cantey (1983-2005)

ACKNOWLEDGMENTS

I would like to thank Dr. Yong Huang, Dr. David Angstadt, and Dr. John Ziegert for serving on my committee and for their assistance with my research. I also greatly appreciate the assistance and contributions from Dr. Zhi Wei in performing this research. I would like to thank the students at Clemson Advanced Manufacturing and Systems Integration Laboratory (CAMSIL) for the good times and their contributions to my work. I certainly appreciate and acknowledge the efforts and contributions of Dr. Yong Huang, Mr. Michael Justice, Mr. Jamie Cole, Mr. David Moline, and Dr. John Ziegert to the development and setup of the equipment needed for this research. Lastly, many thanks to the Department of Bioengineering for profilometer usage and the Clemson Electron Microscope Lab for electron microscope usage.

TABLE OF CONTENTS

Page

Table of Contents (Continued)

Page

LIST OF TABLES

LIST OF FIGURES

List of Figures (Continued)

Figure Page

List of Figures (Continued)

Figure Page

List of Figures (Continued)

Figure Page

List of Figures (Continued)

Figure Page

CHAPTER I

INTRODUCTION

Motivation

Glass is a homogeneous material with amorphous crystal structure that exhibits many excellent mechanical and physical properties, and it is widely used in automotive, communications, optics, electronics, architectural, and biomedical industries. For certain applications such as DNA microarrays glass components with microfeatures are typically produced using a combination of photolithography and etching processes, which is generally time consuming and can involve hazardous chemicals. It would be ideal to fabricate some glass devices through mechanical micromachining for some rapid prototyping applications of glass-based devices, but the brittle nature of glass makes machining difficult. The machined surface is usually fractured and requires additional finishing processes that are costly and time consuming. Fortunately, it is found that the glass can be machined in a ductile regime under certain controlled cutting conditions.

Machining in the ductile regime can occur during the mechanical micromachining of brittle materials under a carefully selected cutting configuration. Machining in the ductile regime can produce continuous cutting chips and a smooth surface that contains few, if any, minute cracks/fracture. In comparison, a surface in brittle cutting consists of many cracks, and discontinuous cutting chips usually appear in a crushed form. Between the brittle and ductile cutting regimes exists a cutting regime transition where cutting and the produced surface exhibit traits of both regimes. This transition is mainly attributed to the effect of pressure and temperature conditions along the cutting shear zone, and it is

usually correlated with the fracture toughness (K_{IC}) of glass (Le Bourhis et al., 2003). The undeformed chip thickness greatly affects the cutting regime transition. If the chip thickness is below a critical value machining is ductile, and this critical value for glass machining was found to be around one micrometer for some applications (Moriwaki et al., 1992; Nakatsuji et al., 1990). While there has been much research interest, it is still not clear as to why ductile machining happens. Further machining and material research must be conducted in order to study the response of brittle materials under the high pressure and/or temperatures typically seen in micromachining.

Recent developments in micro/meso machine tool technology have made the possibility of using traditional mechanical cutting processes, such as micromilling, more realizable. Among the different mechanical micromachining processes, the micromilling process brings new flexibility in machining of a wide array of engineering materials and has the ability to create three-dimensional small-scale features. This new generation of machine tools, in comparison to their conventional-sized counterparts, is more efficient in terms of floor space utilization, energy consumption, and cost in micro/meso-scale manufacturing. To further improve the possibility of implementing micro/meso-scale machine tools, scientific advances must involve a better understanding in the process mechanics at the micro/meso-scale including the scaling effect, effects of the workpiece microstructure on the process, and surface chemistry effects (Williams et al., 2005). The scaling effect presents fundamental differences in various phenomena that more frequently occur in microscale machining than in macroscale machining. These differences can influence changes in the chip-formation process, cutting forces, vibrations

and process stability, and in the generation and subsequent character of the resulting machinined surface (Liu et al., 2004c).

The goals of this thesis are to investigate the cutting configuration required for ductile regime machining in micromilling and to provide insight into the underlying mechanism for cutting regime transition. While there are numerous investigations into the ductile regime machining of various ceramics using turning and grinding, few concern the micromilling of optical glass; and, consequently, there is still a lack of fundamental understanding into why ductile regime machining occurs. In order to study the effect of cutting configuration in micromilling on the cutting regimes, the tilt angle and feed rate were varied in the machining of straight glass grooves with a constant depth. The resulting machined surface was analyzed using a scanning electron microscope (SEM) and a noncontact profilometer. Traditional mechanical/thermal modeling of the ball milling process has been reviewed and used to predict the stress and temperature in the cutting zone. These predictions were used to offer insight into why the cutting regime transition happens. The results of this work may also apply to other silica-based amorphous materials.

Organization

Chapter I gives the motivation and brief background for this experimental work. The overall design of the conducted experiments and stress/temperature predictions are discussed. An outline for this thesis is also offered.

Chapter II gives a brief background into the concepts behind the research conducted for this thesis. In this section, the basic structure and characterization of glass are defined. Methods used to study the high pressure and/or temperature response of the glass microstructure are then examined. A brief overview of the concepts covering the different cutting regimes and machining-related scaling phenomena in glass micromachining is presented.

Chapter III discusses the experimental work behind the study of the effect of tool tilt angle on the cutting regime transition in glass micromilling. The experimental setup and design are introduced with explanations on tool selection, workpiece setup, and chosen cutting conditions. Next, the results of the effect of the controlled machining parameters on the cutting regime transition are examined using scanning electron microscopy and a noncontact surface profilometer. Conclusions from the study are then discussed.

Chapter IV presents the methods and analysis used in predicting the stress and temperature in the cutting zone shear plane. Mechanistic stress and thermal models for ball end milling are introduced based on a review of literature. The experimental methodology and design required to formulate a specific cutting energy curve are presented along with the subsequent prediction of the stresses in the cutting zone shear plane, and the experimental results and predictions are discussed. The findings in estimating the temperature in the cutting zone are presented and examined. Lastly, conclusions are offered.

As an ending to this thesis, Chapter V gives overall conclusions on the conducted experiments and predictions in Chapters III and IV. Recommendations for further research are then proposed.

CHAPTER II

BACKGROUND

Basic Structure and Characterization of Glass

Silicon is one of the most common elements of the Earth's crust and is usually alloyed with other elements to form various materials including metallic alloys, polymers, and hard ceramics. Silicon is rarely found in nature alone and most commonly found in sand where it occurs as silicon dioxide (SiO_2). Silicon dioxide, frequently referred to as silica, is the primary constituent of glass. The structure of silica-based glasses is based on a network of an irregular arrangement of Si-O tetrahedra (Figure 2.1). Each tetrahedron that forms the network consists of one silicon atom in the center and one oxygen atom located at each of the four vertices. The Si-O bonds are covalent in nature and each O-Si-O bond angle varies little from 109.5°. Tetrahedra are connected to each other via sharing of the oxygen atoms at the corner vertices where each corner belongs to exactly two tetrahedra. While the Si-O-Si bond angles hardly vary, the bond angles between tetrahedra (O-Si-O) and the orientation of each tetrahedron (shown as Δ and δ in Figure 2.1) vary significantly which gives glass its amorphous structure (Marians et al., 1987).

This amorphous arrangement of silica tetrahedra is formed during material processing when the silica melt is rapidly quenched below the glass transition temperature. The rapid cooling does not allow enough time for formation of a regular arrangement of silica tetrahedra. During the glass formation process, additional chemical elements or compounds (such as soda, lime, boron, iron, etc.) may be added to the silica

melt. The addition of these chemical elements or compounds may lower the melting point and/or affect the resulting physical and mechanical properties of the processed glass. The integration of the added constituents into the silica network affects the bonding characteristics within the atomic structure of the glass melt (Marians et al., 1987).

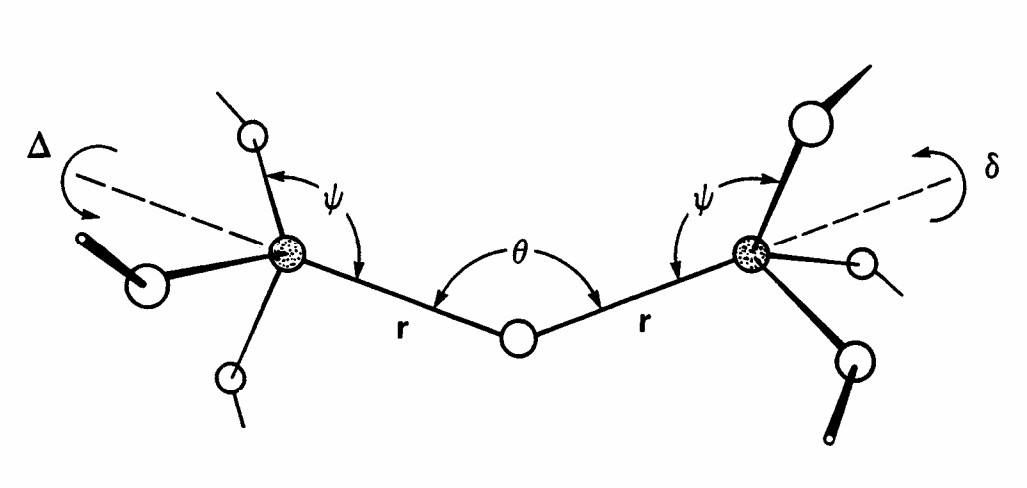

Figure 2.1 - Atomic structure of two connected silica tetrahedra, white atoms – oxygen, dark atoms – silicon – O-Si-O angle (ψ), Si-O-Si (θ), orientation angle of left tetrahedron (Δ), orientation angle of right tetrahedron (δ), distance between Si and O atoms (r) (Galeener, 1987)

The structure of glasses is generally characterized on three main scales: short range order, intermediate range order, and long range order. Short range order involves the bonding environment of each atomic species and may include bond types, distances, and angles. The size of the short range order is approximately on the 0.3-0.5 nm range. The intermediate range order entails the specification of relative atomic positions over a scale in the 0.5-1 nm range. This may take the form of the angles between tetrahedra (Si-O-Si angles) and other network connectivity characteristics. The long range order

considers a much larger range than the short and intermediate range and may include overall bulk properties or characterization of crystalline and non-crystalline structures, such as structure defects. Sometimes the long range order is further classified as crystalline long range order, morphological long range order, or global range order (Galeener, 1987).

Glass Microstructure under High Pressure and Temperature

The microstructure of silica glass under high pressure and/or temperature has been well studied experimentally using high pressure cells, indentation, and molecular simulations. Experiments involving high pressure cells involve exerting high hydrostatic pressure, on order of 1 GPa, at a variety of temperatures up to around the glass transition temperature on specimens in bulk or powder form. Recently, more advanced setups even incorporate an x-ray detector for *in situ* XRD implementation (Inamura et al., 2004). Indentation experiments are useful as a simple analog to basic mechanical machining processes. A rigid, hard indenter with known simple geometry is brought into contact with the specimen using a closely monitored applied force and displacement. The resulting data can then used to predict the surrounding stress field and mechanical properties of the specimen, including hardness. Surface imaging and mapping tools, such as SEM and AFM, provide insight into the modes of deformation of the material near the indenter-workpiece interface, and microstructure analysis using XRD and Raman spectroscopy provide information on structural changes within the intermediate range order. Molecular simulations have been used to verify experimental results as well as

provide possible insight into the mechanisms behind the structural changes on the short and intermediate range orders.

High Pressure Cell and Molecular Simulation Studies

Approaches using high pressure cells produced much of the early works regarding the response of silica-based glasses under high pressure and temperature. Densification in the microstructure was observed above a threshold pressure in the 1-10 GPa range (Bridgman et al., 1953; Cohen et al., 1961; Mackenzie, 1963). Densification was observed to be approximately 6-7 % above this threshold pressure at room temperature (Bridgman et al., 1953; Cohen et al., 1961) and up to 20 % above the threshold pressure at high temperatures (~500 °C) close to the softening temperature (Mackenzie, 1963). The variations in observed threshold pressures were viewed to be due to differences in the degree of applied shear inherent to the experimental setups and techniques. The presence of the shear stresses was found to increase densification and reduce the threshold pressure for densification (Mackenzie, 1963). Densification has been observed to be as high as 20% (Mackenzie, 1963; Susman et al., 1991), and is specifically due to the applied compressive stress in the 8-25 GPa range (Grimsditch, 1984; Polian et al., 1990). Molecular simulations verify a gradual change in the microstructure over a range of temperature and pressure (Huang et al., 2004), characterized by a gradual reversible increase in the oxygen coordination number from 4 to 6 (Lacks, 1998; Huang et al., 2004). The transition has been reasoned to be caused by the occurrence of mechanical instabilities in the structure that lead to a disappearance of the local energy minimum,

leaving the system in a mechanically unstable state which then consequently relaxes into an new state with an unrelated potential energy minimum (Lacks, 1998).

Glass Indentation Studies

Indentation experiments also involve a large applied hydrostatic compressive pressure; but, unlike in high pressure cell experiments, they include a significant degree of shear stress. Consequently, an additional mode of deformation has been observed. In addition to the densification caused by the large pressures exerted by the indenter and observed in high pressure cell experiments, the increase in shear stresses induces volume-conservative plastic flow. The volume under applied shear stress can be displaced through the breaking and joining of bonds and can be observed as pile-up along the outer edges of the indent, as shown in Figure 2.2 (Kese et al., 2005). Microindentation tests have shown evidence of pile-up in silica glass at room temperature (Peter, 1970; Kurkjian et al., 1995).

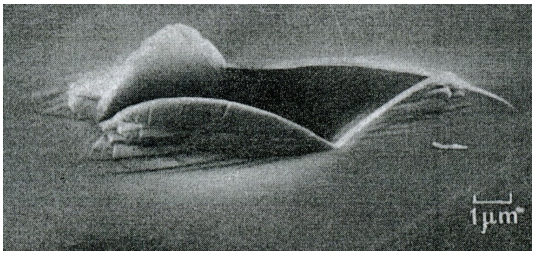

Figure 2.2 - SEM image of indentation imprint on plate glass with a 70° pyramid indenter. Indentation-induced pile-up can be seen on the outer edges of the imprint (Peter, 1970)

The occurrence of volume-conservative plastic flow is due to the change in material behavior under the loading from elastic to viscoelastic. The viscoelastic behavior was observed in microindentation of float glass at temperatures above 300 °C,

which was much lower than the glass transition temperature T_g determined by dilatometry (550 °C) (Le Bourhis et al., 2000). As temperatures approached T_g, the viscous deformation became increasingly dependent on strain rate and was observed to become more and more predominant over the densification (Le Bourhis et al., 2003). Densification volumes were observed to reach 8 and 2.7 times the shear-flow volumes at 373 and 773 K, respectively (Shang et al., 2006). Complete stress relaxation of the workpiece can be achieved if the glass is heated on order of hours at or very close to the glass transition temperature, as shown in Figure 2.3 (Kese et al., 2006).

Both densification and viscous yielding is observed under a typical indentation. The extent of how much of the deformed volume is compacted (densification) and how much is displaced (viscous yielding) is highly dependent on the loading conditions (Le Bourhis et al., 2003), and material composition (Yoshida et al., 2005; Ji et al., 2006). The densified volume of a Vickers indent was found to represent as much as 68% in window glass and 92% in a-SiO_2 (Ji et al., 2006). The higher the composition of SiO_2 in glass the more covalently bonded the network structure and thus the stronger the bonding. Inclusion of network modifiers creates more ionic bonds that are weaker in comparison to the covalent bonds and results in more likelihood of shear-induced yielding (Bridgman et al., 1953).

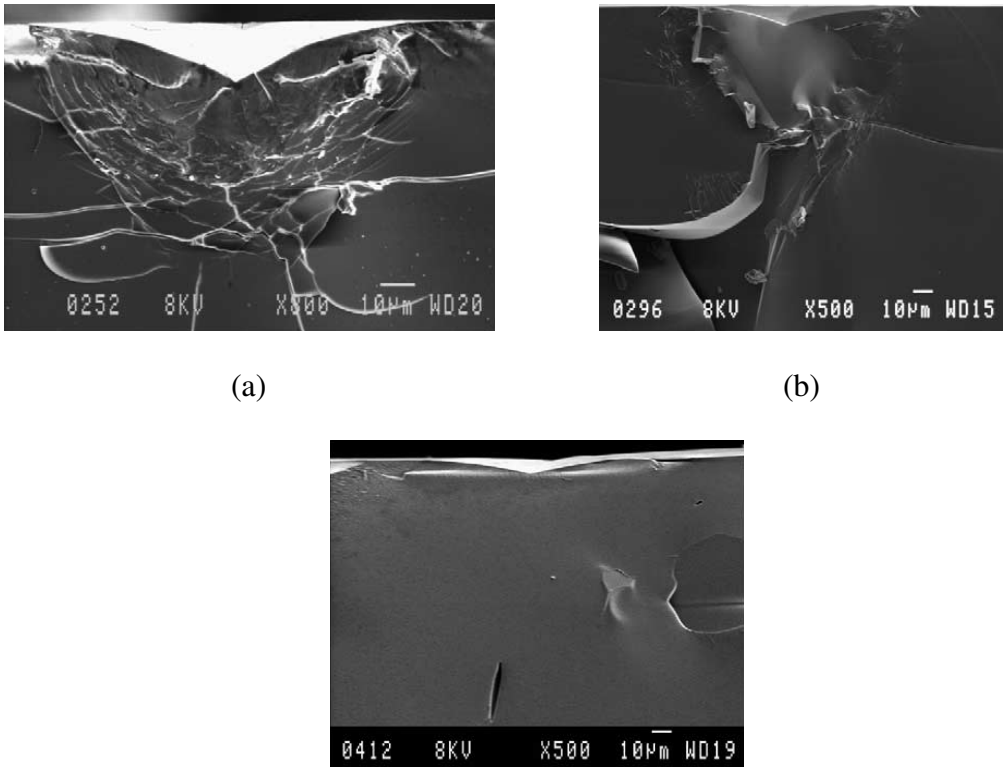

(a) (b)

(c)

Figure 2.3 - SEM pictures of the plastic zone transformation process for selected temperatures and times (a) as-indented, no annealing, (b) annealed 24 h at 550 °C, and (c) annealed 24 h at 600 °C. (Kese et al., 2006)

Temperature Dependence of Glass Mechanical Properties

Microindentation tests have shown that glass can experience material softening under loading at elevated temperatures. As a result, this material softening has an effect on the mechanical properties, such as fracture toughness, hardness, and elastic modulus. Le Bourhis et al. found that the fracture toughness of soda lime glass dramatically increased starting at a temperature around a half of the glass softening temperature (Figure 2.4) (Le Bourhis et al., 2000). As shown in Figure 2.5, when temperature rises from 100 °C through 500 °C, the Vickers hardness decreases from approximately 6 GPa

to 3 GPa [(Le Bourhis et al., 2000; Michel et al., 2004). In addition, as illustrated in Figure 2.6, Rouxel et al. found that the elastic modulus of soda lime glass decreases with increase in temperature and decreases even more rapidly at higher temperatures (Rouxel et al., 2000). Accordingly, the change in mechanical properties leads to a more ductile-viscoelastic response and can be seen through increased pile-up around the edges of indentation.

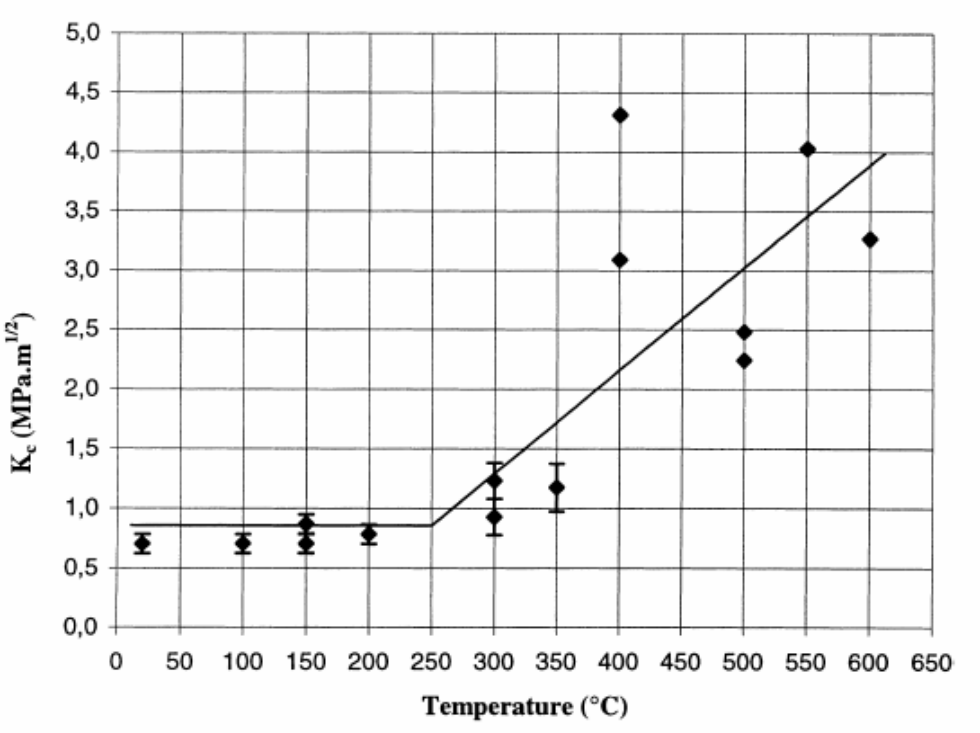

Figure 2.4 - Mean fracture toughness as a function of temperature during microindentation of float glass (~72 wt. % SiO_2) (Le Bourhis et al., 2000)

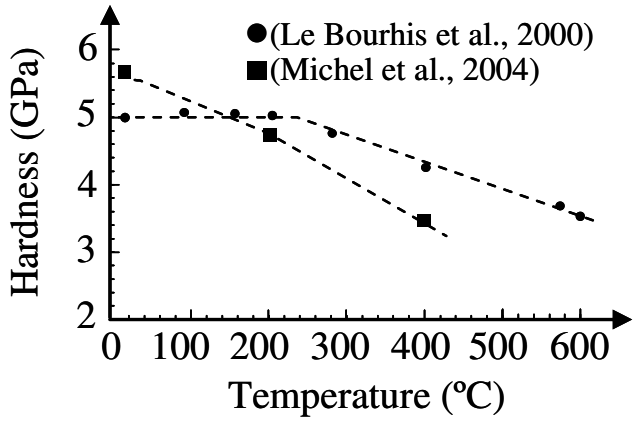

Figure 2.5 - Temperature-dependent Vickers hardness of soda lime glass (Le Bourhis et al., 2000; Michel et al., 2004)

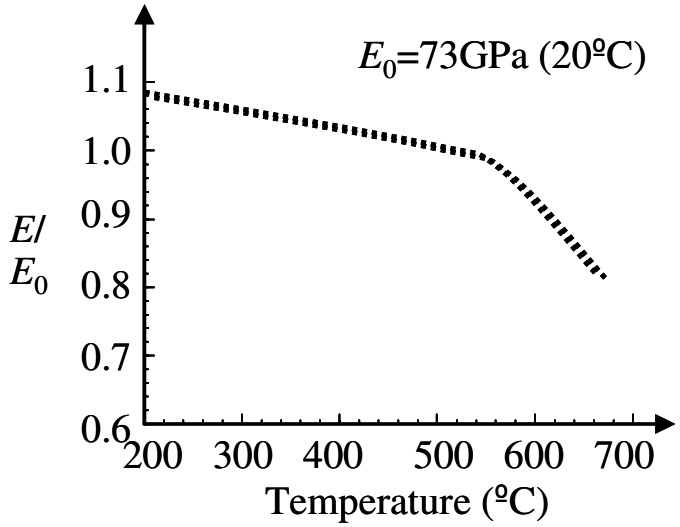

Figure 2.6 - Temperature dependence of Young's modulus of soda lime glass (Rouxel et al., 2000)

Glass Micromachining

As brittle materials including different types of glasses have been studied intensively over the years, it has been found that they can be machined as ductile materials under certain cutting configurations. Advances in grinding technologies led to the first reproducible evidence of glass ductility in machining (Huerta et al., 1976a; Huerta et al., 1976b), and since then research on the cutting regime/mode in grinding of various brittle materials such as ceramics, glasses, and semiconductor has been well documented (Komanduri, 1996; Sreejith et al., 2001). A hypothesis on the ductile regime in grinding was proposed and it was predicted that if the size scale of the removed material is made small enough then any material, regardless of its brittleness, could be machined through plastic shear instead of fracture (Bifano et al., 1991). This size effect has also been illustrated in both molecular dynamics simulations and microindentation (Shimada et al., 1995) and experimental observations in nanoindentation (Fang et al., 2004). For example, when the scale of the load and depth of indentation are reduced to the order of 0.1 N and 1 μm, respectively, plastic yielding-induced pile-ups have been observed along the indentation outer edges (Fang et al., 2004).

The occurrence of the aforementioned cutting regime transition has been associated with a critical undeformed chip thickness (Nakatsuji et al., 1990; Moriwaki et al., 1992). Figure 2.7 shows a schematic illustration of the ductile-brittle transition with respect to the undeformed chip thickness. When the undeformed chip thickness reaches a critical value brittle fracture begins to occur on the machined surface and becomes more dominant as the chip load is further increased. However, when the undeformed chip

thickness is below the critical value the machined surface will turn to be ductile. Research has shown that the change in the failure mechanism from brittle fracture to ductile shear can also occur with a sufficient hydrostatic stress and/or temperature in the deformation zone (Komanduri, 1996) and then the critical undeformed chip thickness can be increased accordingly. An increase in the hydrostatic stress in the cutting zone has been achieved using tools with a negative effective rake angle (Nakatsuji et al., 1990; Chiu et al., 2000; Fang et al., 2004; Patten et al., 2005) or by applying an external hydrostatic pressure (Yoshino et al., 2005). Thermal softening of the brittle workpiece has also been demonstrated using a heat source (Brehm et al., 1979) and lasers (Hwang et al., 2004) to facilitate ductile machining. In addition to the effect of hydrostatic pressure and temperature on the cutting regime transition, the application of ultrasonic vibration in the cutting direction also helps improve ductile machining of brittle materials (Moriwaki et al., 1992; Gan et al., 2003; Zhou et al., 2006).

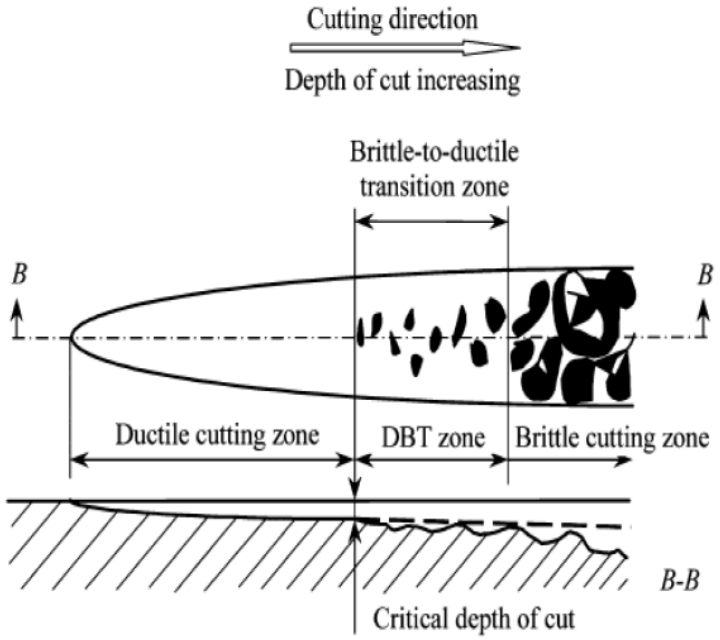

Figure 2.7 - Schematic illustration of ductile-brittle transition in grooving (Liu et al., 2004b)

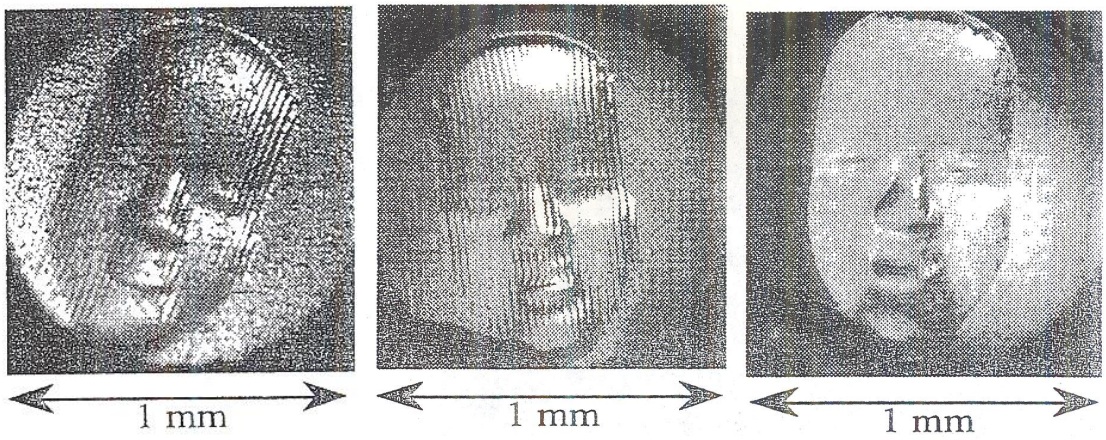

(a) (b) (c)

Figure 2.8 - Contours of a human face machined on a glass mask 1 mm in diameter and 30 μm in height under (a) rough cutting (brittle regime) and (b), (c) subsequent finishing passes under ductile regime (Takeuchi et al., 1996)

Among the different mechanical micromachining processes, the micromilling process brings new flexibility in machining of brittle materials, including glass, due to its ability of creating three-dimensional small-scale features. Takeuchi et al. (Takeuchi et al., 1996) demonstrated this micromilling advantage in ductile regime machining using a pseudo ball end mill to produce a glass-based human face mask shown in Figure 2.8, and the mask was measured to be 1 mm in diameter and 30 μm in height, having a maximum surface roughness of 50 nm (Takeuchi et al., 1996). The practical application of the micromilling process was also demonstrated in ductile regime machining of straight glass grooves for DNA microarray applications (Matsumura et al., 2005; Yoshino et al., 2006). Micromilling is also of interest due to its flexibility and effectiveness for some three-dimensional microfabrication applications. The control of tool tilt angle in ball end milling has been shown to be effective in improving the workpiece surface quality for macro-scale (Ko et al., 2001; Antoniadis et al., 2003) and micro-scale (Matsumura et al., 2005) applications. However, the effect of tilt angle on the cutting regime transition in ductile machining is still not clearly understood.

Evidence of the cutting regime transition has been shown through surface analysis, cutting force data, and cutting chip characterization. Machining in the ductile regime has resulted in a smoother surface, as seen in Figure 2.9 (Liu et al., 2004a; Zhou et al., 2006); and the transition from the ductile to brittle regime can also be indicated by the ratio of cutting force to thrust force (Chiu et al., 2000; Chiu et al., 2001; Sreejith et al., 2005) and appearance of periodic fluctuations in the cutting force signal due to brittle fracture repetition (Figure 2.10) (Matsumura et al., 2004).

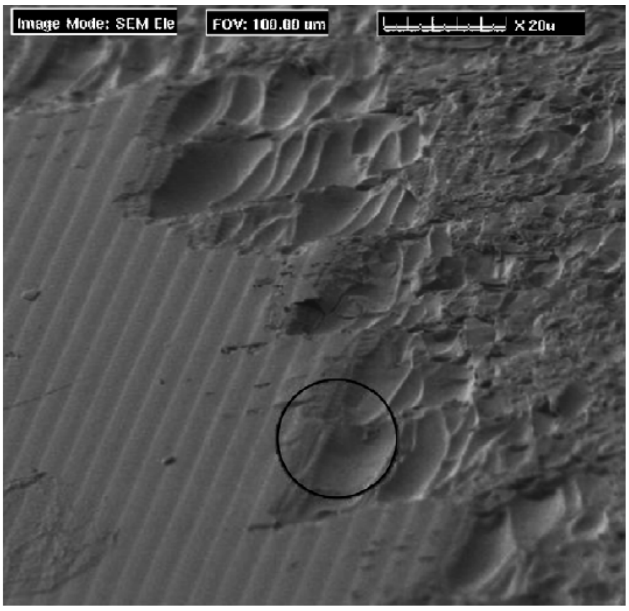

Figure 2.9 - Cutting regime transition shown in diamond cutting of optical glass (Zhou et al., 2006)

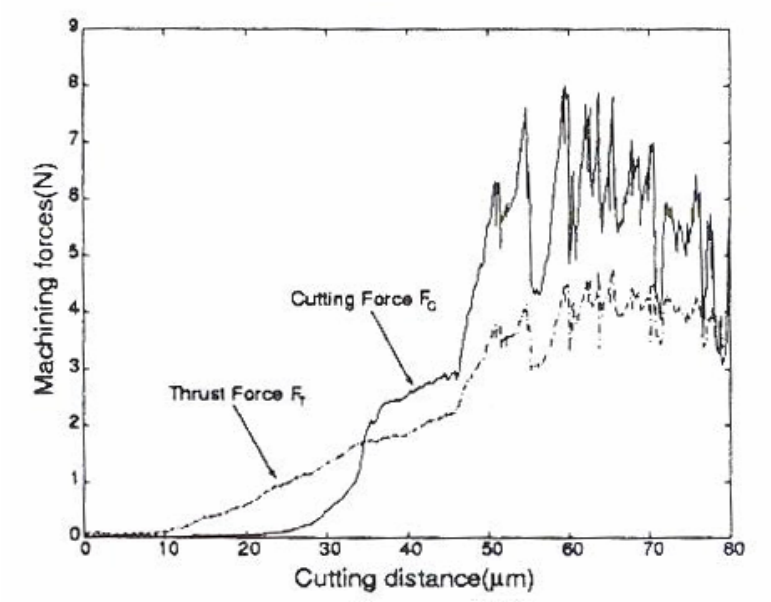

Figure 2.10 - Measured force components during cutting of glass microscope slide - uncut chip thickness increased (left to right) from 0 μm to 0.6 μm (Chiu et al., 2000)

Brittle Fracture in Mechanical Micromachining

A ductile-to-brittle transition has been found to occur in mechanical micromachining of nominally brittle materials, and the occurrence of this transition is believed to exist due to the competition at the micron to sub-micron scale between the minimum energy needed for yielding-induced plastic deformation (volume effects) and the minimum energy needed for brittle fracture (surface effects). Identifying the origins of the brittle crack initiation and subsequent propagation give insight into where focus needs to be applied into suppressing crack formation. Three zones have been identified in cutting experiments as possible areas for brittle fracture (Patten et al., 2004):

1. During chip formation (Figure 2.11(a)),
2. In the trailing tensile stress field (Figure 2.11(b)), and
3. Lateral crack formation after tool pass (Figure 2.11(c)).

Crack formation in brittle machining most commonly occurs in the region of the high pressure zone in front of the tool tip (Figure 2.11(a)) responsible for chip formation. Cracks that form in this region of chip formation may or may not propagate to the finished surface depending on the extent and orientation of the crack initiation. Brittle fracture that occurs due to extension of cracks into the finished surface reveal themselves as small pits on the machined surface with size approximate to the grain size in polycrystalline material. This fracture can be minimized by controlling the size, state, and magnitude of the stress field in front of the tool through control of process parameters (e.g. reducing depth of cut) and tool geometry (e.g. more negative rake angle) (Patten et al., 2004).

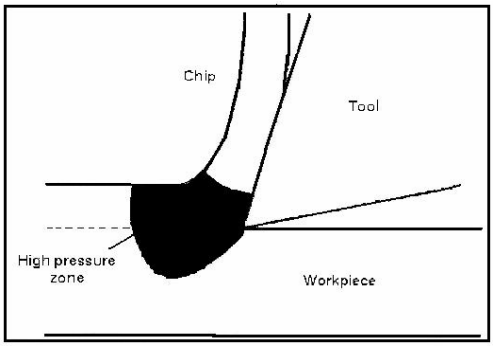

(a)

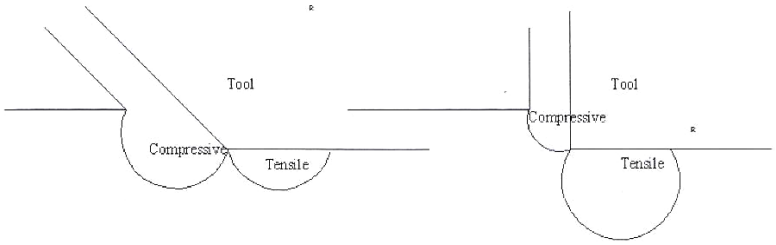

(b)

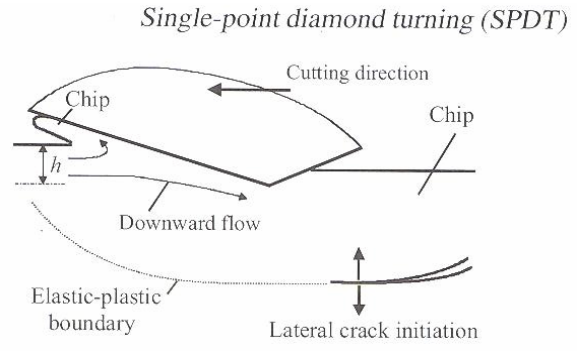

(c)

Figure 2.11 - Candidate regions for occurrence of brittle fracture during mechanical micromachining consist of: (a) the high pressure zone at the tool tip, (b) the trailing stress field, and (c) lateral crack formation at the elastic-plastic boundary (Patten et al., 2004)

Behind the tool edge a trailing tensile stress field exists, as illustrated in Figure 2.11(b), and beyond a critical depth of cut fracture can occur at the finish surface. The difference between this fracture and the fracture that occurs during chip formation is that cracks initiate at the surface and result in the material being ejected from the finished surface – as opposed to the cracks that form during chip formation in front of the tool and propagate towards the finished surface. The occurrence of this fracture in the trailing tensile stress field is more directly correlated to the depth of cut and secondarily to rake angle, and has been found to significantly affect the resultant fracture toughness and surface roughness of the material. Increased rubbing due to tool wear increases the shear stress beneath the tool and the trailing stress field, and thus increases the possibility of brittle fracture (Patten et al., 2004).

The third possible region for crack formation occurs after each pass of the cutting tool edge. The stress exerted on the workpiece by the cutting tool edge results in a surrounding elastic-plastic boundary, as shown in Figure 2.11(c). Once the tool passes the loading on the workpiece is released, and the residual stress at this boundary can initiate lateral cracks. These lateral cracks may or may not propagate to the surface and occur when excessively large thrust loads are directed towards the workpiece, e.g. extreme negative rake angle. Fracture due to lateral crack formation/propagation to the surface and fracture due to the cracks originating in the trailing tensile stress field are found to be more catastrophic in nature in comparison to cracks formed in front of the tool and more adversely affect the material properties of the finished surface and the fracture toughness (Patten et al., 2004).

Cutting Chip Formation in Micro-Cutting

While the occurrence of ductile regime machining of brittle materials has been associated with a critical undeformed chip thickness, more insights are required into the mechanics of material removal in order to develop a better understanding into why ductile machining occurs. Conventional machining models for milling typically assume that a chip is formed during each pass of the cutting edge. However, in micromachining there are scaling-related phenomena that can cause fundamental differences into how material is or is not removed during each cutter pass.

Minimum Chip Thickness in Micro-Cutting

In conventional machining the cutting edge is assumed sharp as the cutting edge radius is much less than the size of the formed chip. However, in micromilling the cutting edge radius (~ 1 micron) is comparable with the size of the chip (1 nm – 1 μm) and impacts how the workpiece material can be deformed. It has been found that a chip may not be formed until a certain critical undeformed chip thickness is reached, and this critical value has been termed the minimum chip thickness. The ratio of minimum chip thickness to cutting edge radius has been found to be approximately 0.2-0.4 in the cutting of aluminum and steels (Weule et al., 2001; Vogler et al., 2004; Liu et al., 2006). When, the undeformed chip thickness is below the minimum chip thickness, the workpiece material will deform either through elastic or mixed plastic-elastic deformation. When the material is deformed elastically it is expected to return to its original position after the cutting edge passes without being removed. Increasing the uncut chip thickness while without reaching the minimum chip thickness results in the mixed plastic-elastic mode

where a certain percentage of the material is elastically deformed and the rest is removed through ploughing or edge rubbing. Ploughing/edge rubbing can adversely affect the machined surface/cutting process through increased surface roughness and cutting forces. Further increasing the uncut chip thickness to the minimum chip thickness results in the deformed material being removed as a chip. Thus, in micromilling where the chip thickness changes as the cutter rotates all three cutting modes can occur during one pass of the cutting edge (Liu, 2004c).

Effect of Microtool Fabrication on Chip Formation

In the modeling of conventional machining processes the cutting edge is considered sharp and well-defined along its length. However, as previously discussed, the edge radius effect in micromilling has a profound impact on how the material is deformed. The cutting edge geometry may not be consistent along the length of the cutting edge due to limitations in microtool fabrication methods. For most widely used WC microendmills, the geometry of the cutting flute edge is primarily restricted by the grain size of the tungsten carbide powder and the grit size of the grinding wheel, which are both in the range of submicron to a few microns. As a result, a serration is produced along the cutting edge with amplitude and wavelength in the same micron range as shown in Figure 2.12. The edge serration produces a variation in the cutting edge radius which can significantly impact the chip formation and resulting cutting forces and surface finish (Liu et al., 2007a; Liu et al., 2007b). The effect of edge serration has also been illustrated in the micro-cutting of soda lime glass using a polycrystalline diamond (PCD) tool with a conical-shaped tip that had been produced through micro electro discharge machining

(μEDM) (Morgan et al., 2004). The grains of the PCD tool were found to leave feed marks on the machined surface corresponding to the rotation of the tool. Since the sub-micron to micron size of both the grains composing the tool and the amplitude/wavelength of the serrated cutting edge are on the same order as the feed rate used in micromilling, the effect of edge serration can be profound.

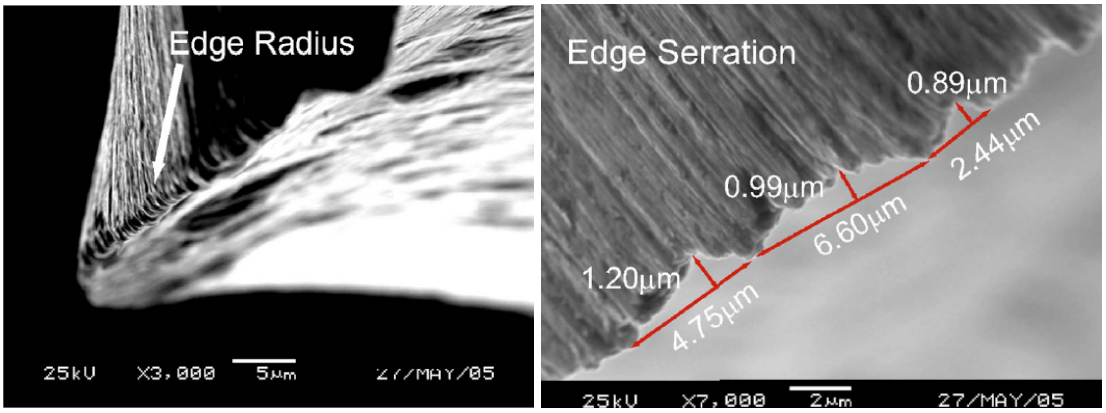

(a) (b)

Figure 2.12 – (a) Edge radius and (b) edge serration of a cutting flute of a microendmill (Liu et al., 2007a)

Summary

An extensive literature review has been conducted and presented in this chapter. First, the basic structure and characterization of glass was presented. Then the results from various studies on the response of glass microstructure to high stress/temperature through high pressure cell and indentation experiments and molecular simulations were discussed. For instance, microindentation tests have shown glass ductility through the evidence of pile-up along the outer edges of indentation under small indentation loads (~ 1 N) and penetration depths (~ 1 μm). Furthermore, various studies have revealed that

certain mechanical properties (fracture toughness, elastic modulus, and hardness) of glass have been found to exhibit increased ductility as the temperature in the deformation zone is increased towards the glass softening temperature. A review of glass mechanical micromachining studies has revealed that glass can be machined in a ductile regime under certain controlled cutting conditions (Nakatsuji et al., 1990; Moriwaki et al., 1992). Machining in the ductile regime can produce continuous cutting chips and a smooth surface that contains few, if any, minute cracks/fracture. In comparison, a surface in brittle cutting consists of many cracks, and discontinuous cutting chips usually appear in a crushed form. Between the brittle and ductile cutting regimes exists a cutting regime transition where cutting and its resulting surface exhibit traits of the both regimes. This transition is mainly attributed to the effect of pressure and temperature conditions along the cutting shear zone, and it is usually correlated with the fracture toughness (K_{IC}) of glass (Le Bourhis et al., 2003). The undeformed chip thickness greatly affects the cutting regime transition. If the chip thickness is below a critical value, machining is ductile, and this critical value for glass machining was found to be around one micrometer for some applications (Nakatsuji et al., 1990; Moriwaki et al., 1992). Lastly, other micro-scale machining phenomena, such as minimum chip thickness and edge serration effect, and their possible effect on the machining process have been presented and discussed.

However, favorable ductile regime machining instead of brittle regime machining in micromilling is still not fully understood as a function of cutting conditions, glass properties, and tool geometry and properties. In order for ductile regime machining of glass to be viable for practical applications, further machining research must be

performed to better understand how and why ductile machining happens. The following two chapters implement the important aforementioned principles in studying the ductile-brittle cutting regime transition in glass machining using the micromilling process. First, Chapter III presents an investigation into the effect of tilt angle on the cutting regime transition in micromilling of crown glass. Straight grooves with a constant depth were cut under different levels of tilt angle and feed rate. Machined surfaces are characterized to observe the cutting regime transition using a scanning electron microscope (SEM) as well as a profilometer. Conclusions are offered based mainly on surface finish in order to appreciate the effect of tilt angle on the cutting regime transition. Through investigating the cutting regime transition, Chapter IV presents a study of the fracture strength of glass as a function of the tilt angle and feed rate in the micromilling process. The mechanistic model implemented in the study for the prediction of the stress state in the cutting zone is first presented. The experimental design and methodology for predicting the stress state and temperature in the cutting zone are then offered. The predicted stresses are discussed and compared with previous experimental observations from Chapter III to draw conclusions regarding the effect of compressive stress on glass ductility. The findings from estimating the temperature in the cutting zone are offered and discussed. Conclusions are made to help provide a better understanding of the stress and temperature dependence of the glass fracture toughness, during machining as well as insight into why ductile machining happens.

CHAPTER III

EFFECT OF TILT ANGLE ON CUTTING REGIME TRANSITION IN GLASS

Introduction

Glass is a homogeneous material with amorphous crystal structure that is produced through the rapid cooling of its molten state below the glass transition temperature. Glass exhibits many excellent mechanical and physical properties such as high hardness, transparency, good corrosion and chemical resistance, and high electrical resistivity. It is widely used in automotive, communications, optics, electronics, architectural, and biomedical industries. For certain applications, such as DNA microarrays used in DNA analysis, glass components with microfeatures are typically produced using a combination of photolithography and etching processes (Voldman et al., 1999), which is generally time consuming and can involve hazardous chemicals. It would be ideal to fabricate them through mechanical micromachining for some rapid prototyping applications of glass-based devices, but the brittle nature of glass makes machining difficult. The machined surface is usually fractured and requires additional finishing processes that are costly and time consuming. Fortunately, it has been found that glass can be machined in a ductile regime under certain controlled cutting conditions (Nakatsuji et al., 1990; Moriwaki et al., 1992).

Machining in the ductile regime can produce continuous cutting chips and a smooth surface that contains few, if any, minute cracks/fracture. In comparison, a surface in brittle cutting consists of many cracks, and discontinuous cutting chips usually appear in a crushed form. Between the brittle and ductile cutting regimes exists a cutting

regime transition where cutting and its resulting surface exhibit traits of the both regimes. This transition is mainly attributed to the effect of pressure and temperature conditions along the cutting shear zone, and it is usually correlated with the fracture toughness (K_{IC}) of glass (Le Bourhis et al., 2003). The undeformed chip thickness greatly affects the cutting regime transition. If the chip thickness is below a critical value, machining is ductile, and this critical value for glass machining was found to be around one micrometer for some applications (Nakatsuji et al., 1990; Moriwaki et al., 1992).

In order for ductile regime machining of glass to be viable for practical applications, further machining research must be performed to better understand how and why ductile machining happens. In this experiment, the effect of tilt angle on the cutting regime transition was investigated in micromilling of crown glass (72% SiO_2, 18% K_2CO_2, 10% $CaCO_2$), which was also used in the works by Matsumura et al. and Yoshino et al. (Matsumura et al., 2005; Yoshino et al., 2006). Straight grooves with a constant depth were cut under different levels of tilt angle and feed rate. Machined surfaces were characterized to observe the cutting regime transition using a scanning electron microscope (SEM) as well as a profilometer. This chapter first examines the experimental setup and design, and then it is followed by experimental observations and discussion in order to appreciate the effect of tilt angle on the cutting regime transition, mainly in terms of the machined workpiece surface finish.

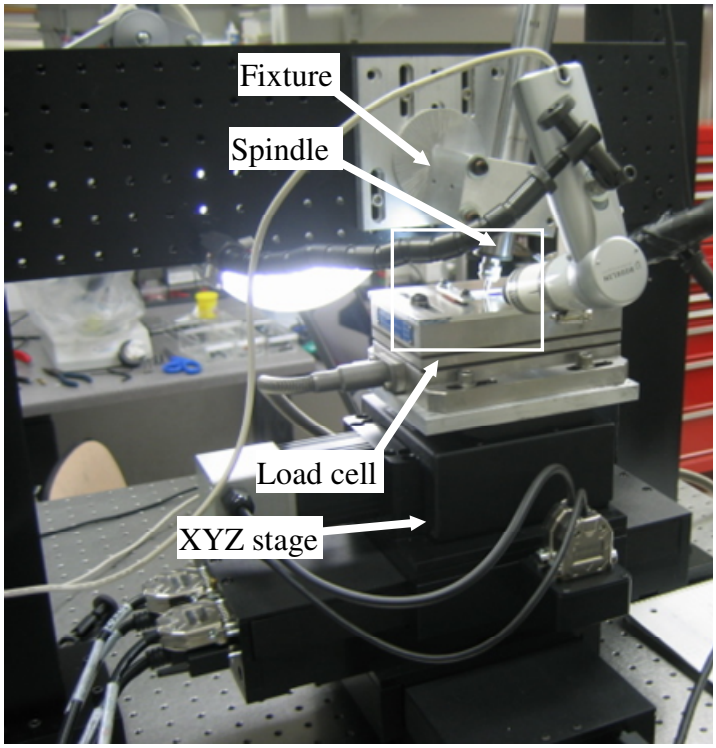

(a)

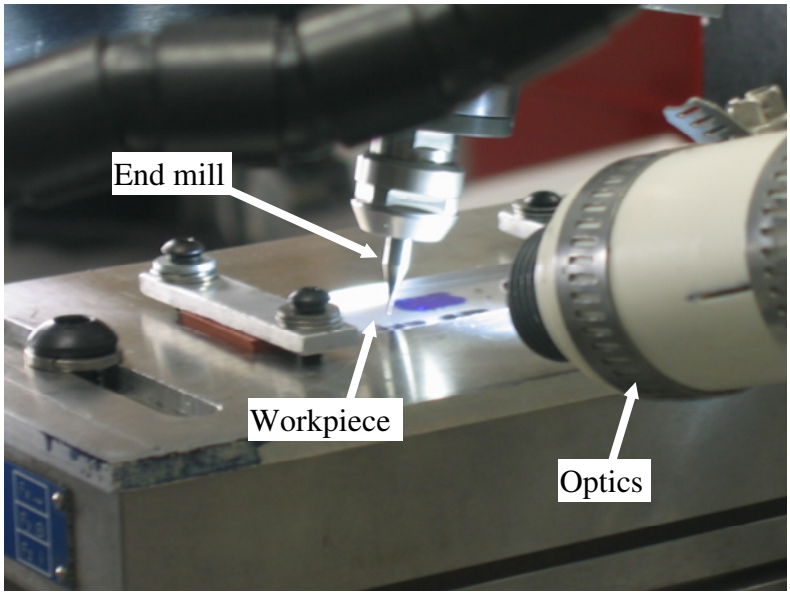

(b)

Figure 3.1 - (a) Micromilling setup and (b) closer view of the machining process

Experimental Setup and Design

Machining experiments were carried out on a vertical micromilling center as shown in Figure 3.1. The spindle/motor set used in the experiments was the NSK Astro-E 500Z with a highest spindle rotational speed of 50 kRPM and a less than 1 μm runout. The tool used was a cemented carbide ball end mill with 2 flutes and a 0.2 mm nose radius. Scanning force ion microscopy images of the rake face and edge roundness of the cutting edge are shown in Figure 3.2. More detailed information can be found in Appendix B. Such a ball end mill was expected to exert a large hydrostatic stress for suppressing crack propagation in micromilling (Matsumura et al., 2005). The spindle was attached to a rigid support structure that allowed the tool to be tilted with respect to the vertical axis in a -70° to 70° range.

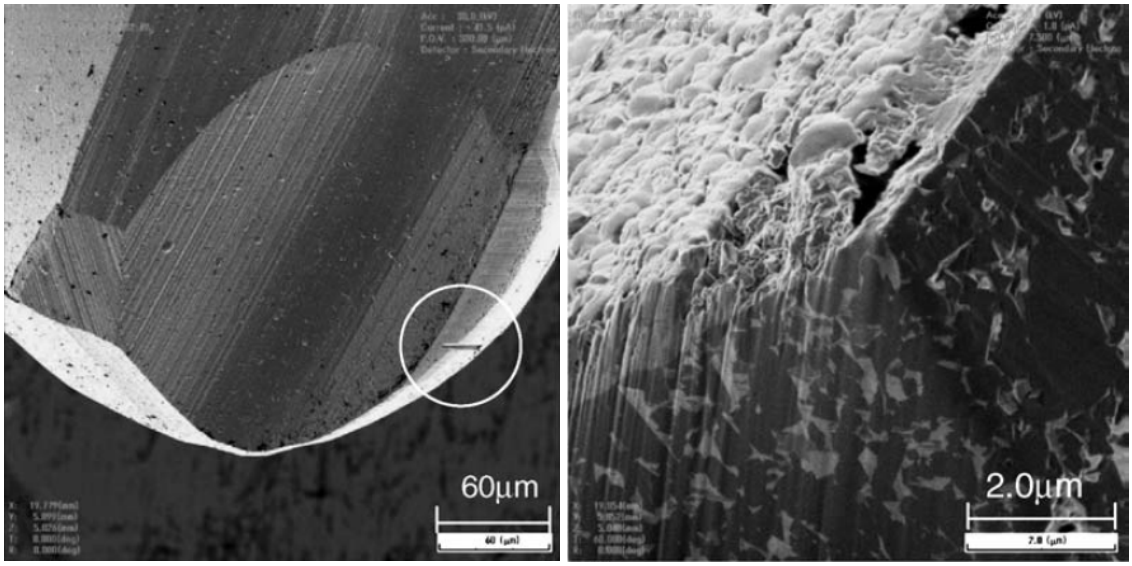

(a) (b)

Figure 3.2 - Scanning force ion microscopy images of cutting edge (a) rake face and (b) edge roundness (Matsumura et al., 2005)

The workpieces were crown glass-based microscope slides measuring 76 mm x 25 mm with a 1 mm thickness. The slides were fixed to a cavity of an aluminum mounting plate, and the cavity was designed to hold the cutting fluid, which was water in this study. The micromilling feed motion was provided using an Aerotech XYZ stage, over which the aluminum mounting plate was fixed. The stage feed axis (X-axis) had a resolution of 10 nm and accuracy within 1 μm, and the depth of cut was controlled by the Z-axis with a resolution and accuracy of 0.1 μm and 0.5 μm, respectively. The micromilling workstation was on a Newport isolation table.

Two-factor multiple-level experiments were designed to study the cutting regime transition in glass micromilling, and this experimental design is shown in Table 3.1. The two controlling factors were the tilt angle and the feed rate. The feed rates were selected based on a previous similar glass micromilling setup (Matsumura et al., 2005), and the largest tilt angle was selected as 60° due to the fixture design limitation. In addition, it was found that cutting performance started to deteriorate when the tilt angle was 60°, so the maximum 60° was considered a sufficient limit. Straight grooves were machined at a constant depth of cut (DOC) of 16 μm for all the tests based on the previous glass micromilling study (Matsumura et al., 2005). Machining was performed with the workpiece submerged in a water bath, and the water molecules were found to facilitate ductile micromilling of glass (Matsumura et al., 2005). A spindle speed of 20 kRPM was chosen since it has been shown to perform well in terms of tool wear for glass micromachining (Matsumura et al., 2005). Figures 3.3 and 3.4 illustrate a representative ball milling process and one of the machined grooves.

Table 3.1 - Two-factor multi-level design of experiments

Factors	Level
Tilt angle (degrees)	0, 15, 30, 45, 60
Feed rate (mm/min)	0.12, 0.24, 0.36, 0.48, 0.60, 0.72

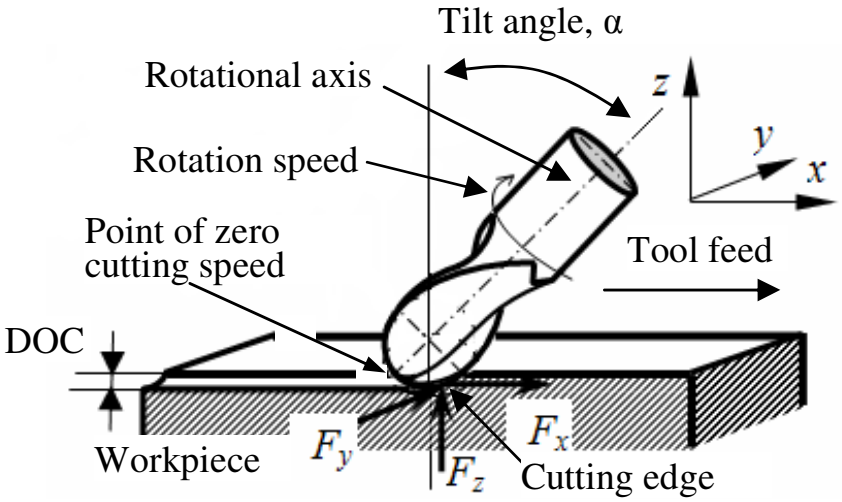

Figure 3.3 - Schematic of ball end micromilling

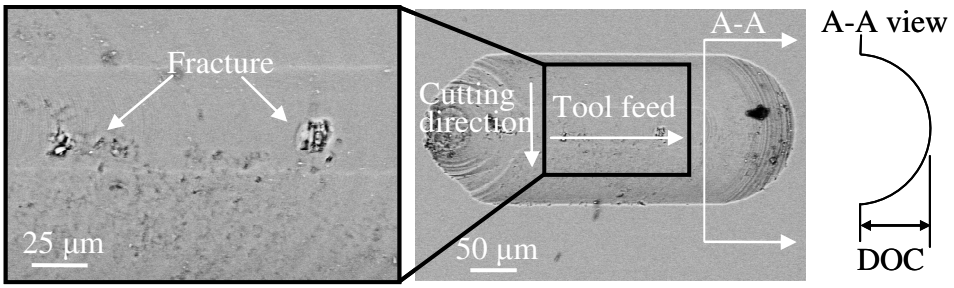

Figure 3.4 - Representative machined groove (feed rate = 0.12 mm/min, water bath, and tilt angle = 15°)

The tool wear was monitored throughout the machining experiments using an optical microscope and the flank wear was observed as the main wear pattern. The surface profile and finish of selected machined grooves were analyzed using a noncontact surface profilometer (Wyko NT-2000), and the average surface roughness values reported in this study were measured based on 80 μm lengths in the feed direction. The machined grooves were further examined using SEM (Hitachi S3400) after coating a nano-scale thick platinum layer.

Experimental Results and Discussion

Effect of Tilt Angle on Cutting Regime Transition

The cutting regimes in micromachining of brittle materials have proven to be important since ductile machining results in a smoother and more geometrically defined surface. Such a surface consists of fewer machining-induced microstructure defects when compared to a surface machined in the brittle regime. As discussed before, the cutting regime transition between the brittle and ductile regimes is greatly dependent upon the cutting configuration. In micromilling, the undeformed chip thickness changes as the tool engages and disengages from the workpiece as shown in Figure 3.5. The undeformed chip thickness starts at zero when the cutting edge engages the workpiece and increases to be a maximum value (t_{max}) before it decreases back to zero when the cutting edge disengages from the workpiece. The value of t_{max} is analogous to the feed per tooth and is mainly dependent upon the feed rate and the number of cutting edges/flutes.

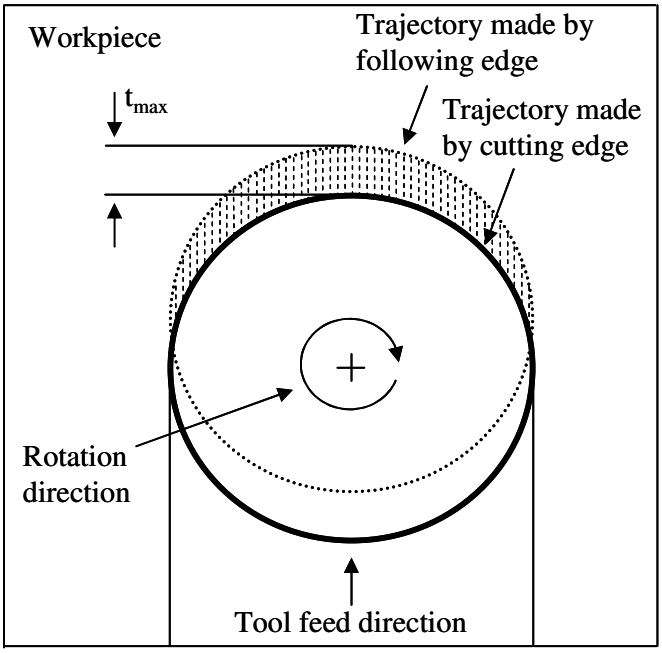

Figure 3.5 - Undeformed chip thickness in micromilling

In addition to the feed rate-dependent undeformed chip thickness, the tool tilt angle also has a pronounced effect on the cutting regime transition in glass machining. Generally speaking, when the tilt angle increases, the hydrostatic compressive stress in the cutting zone increases accordingly as a result of the increasing thrust forces (F_x and F_z in Figure 3.3) towards the workpiece, which helps to suppress the glass crack propagation in the cutting zone. However, if the tilt angle is too large, the effective cutting edge (equivalent to the width of cut) will be too long and the rubbing or ploughing effect might turn to be significant. To appreciate the effect of tilt angle on the cutting regime transition in glass micromilling, the glass grooves were machined with constant 16 μm depths based on the experimental designs as specified in Table 3.1.

It should also be pointed out that the cutting speed changes along the ball mill cutting edge when the axial depth of cut is smaller than the ball mill radius in micromilling. This is because the perpendicular distance (radial distance) between the cutting edge and the rotational axis changes along the effective cutting edge. The cutting speed is zero at the ball mill tip, and it increases along the cutting edge from the tip as a function of the rotation speed and the radial distance. When the tilt angle is zero, the ball end mill engages the workpiece using the lower bottom portion of the insert with a relatively low cutting speed. When the tilt angle increases from zero, the effective cutting speed also increases accordingly since the radial distance increases as the cutter tilts as shown in Figure 3.3. The tilt angle increase induces an increase in the cutting speed along the effective cutting edge (Figure 3.3), which leads to a competing phenomenon: an increased strain rate in the cutting zone to make the workpiece material harder to be cut due to the strain rate hardening effect and an increased temperature in the cutting zone to make the workpiece material easier to be cut due to the thermal softening effect.

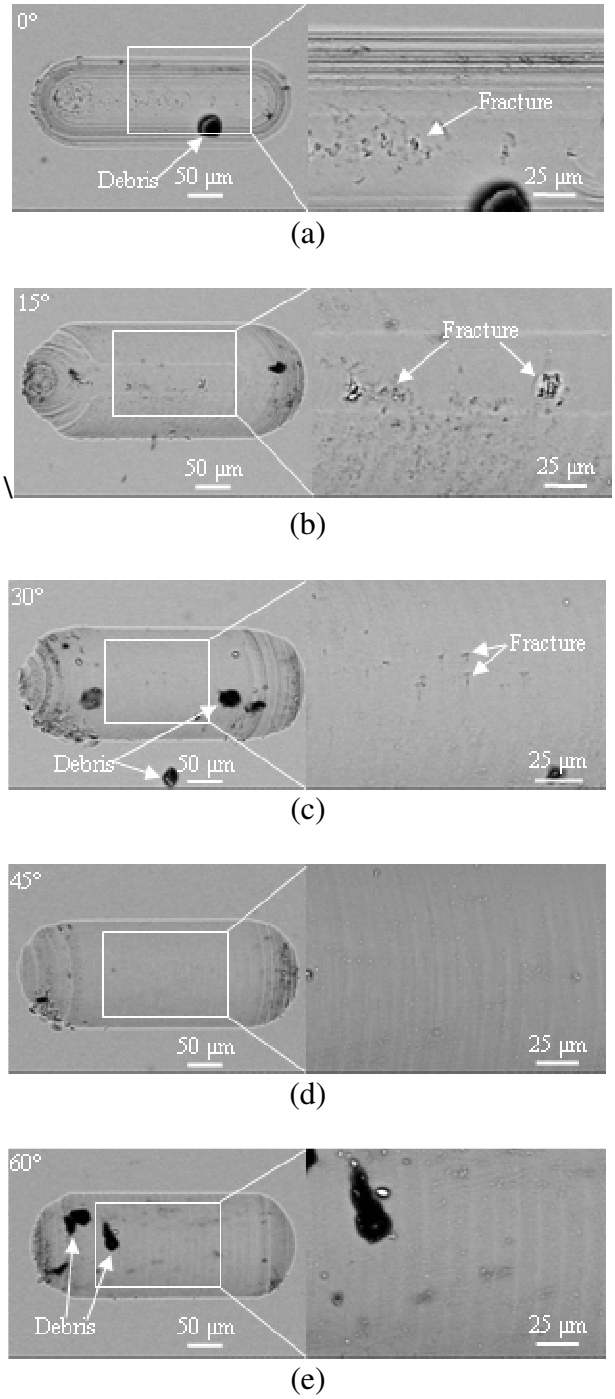

Figure 3.6 - 5 SEM micrographs of grooves machined at 0.12 mm/min under tilt angles of (a) 0°, (b) 15°, (c) 30 °, (d) 45°, and (e) 60° (the shown debris were due to stuck glass chips)

In characterizing the cutting regimes in glass micromilling, rubbing, ductile machining, and brittle machining regimes are hypothesized based on the relative value of undeformed chip thickness. As undeformed chip thickness increases from zero, the cutting regime experiences rubbing, ductile machining, and brittle machining, respectively, for a given cutting configuration. It is believed that rubbing will suppress fracture propagation but increase surface roughness, brittle machining will increase fracture propagation and surface roughness, and ductile machining will lead to a fracture-free, low surface roughness surface. Strictly speaking, rubbing is not responsible for any material removal, so only the cutting transition from brittle machining to ductile machining is usually of interest.

Figure 3.6 shows the grooves machined under the different tilt angle conditions at the feed rate of 0.12 mm/min. It can be seen that the fractured surfaces were common for the grooves machined with the 0°, 15°, and 30° tilt angles, but not with the grooves with 45° and 60°. A noticeable trend was observed as the amount of fractured surface decreased gradually with the increasing tilt angle until a smooth crack-free surface was obtained. As aforementioned, this observation was attributed to the effect of tilt angle. It is considered that a larger tilt angle helps to increase the hydrostatic stress in the cutting zone to facilitate ductile machining under the combined effect of increased thrust force and increased cutting speed.

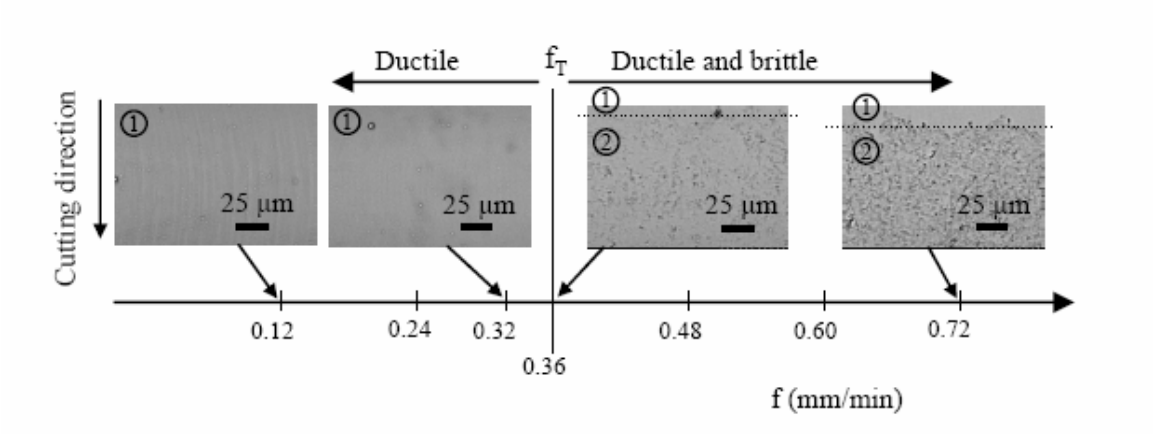

(a)

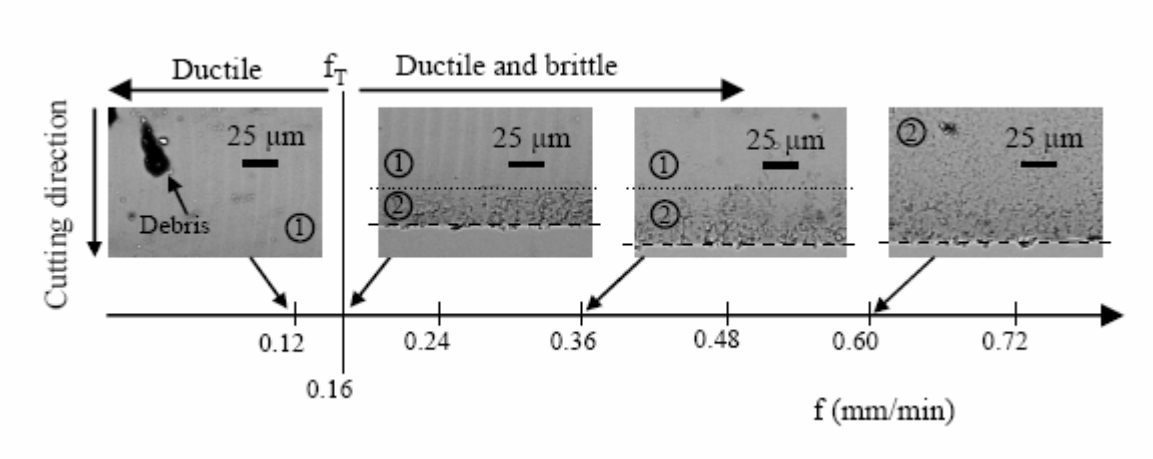

(b)

Figure 3.7 - SEM micrographs of machined groove surfaces as feed rate increases under (a) 45° and (b) 60° tilt angles (Circle 1 represents the ductile cutting regime surface, Circle 2 represents the brittle cutting regime surface, the solid line separates the two cutting regimes, and the dash line is the boundary of the groove. Once fracture was initiated, it propagated through the rest of the pass.)

As the 45° and 60° tilt angles were considered as the favorable tilt angle conditions, the effort was further made to investigate when the cutting regime transition occurs as a function of feed rate. In addition to the proposed experimental setup, two more feed rates, 0.32 mm/min for the 45° tilt angle and 0.16 mm/min for the 60° tilt angle, were performed in order to find the transition condition. Figure 3.7 shows this occurrence of the cutting regime transition for both the 45° and 60° tilt angles. Generally speaking, once the feed rate is larger than a transition feed rate (f_T), the cutting regime changes from purely ductile to ductile/brittle; and the transition feed rate is larger under 45° than that under 60° (0.32 mm/min vs. 0.16 mm/min) as discussed in the following.

For the groove machined at 45° at 0.32 mm/min, a crack-free surface was observed. When the feed rate increased to 0.36 mm/min (f_T for 45º), the fracture occurred during each tool pass shortly after the cutting edge engaged with the glass workpiece (within the entry zone). Once the fracture was initiated, this fracture continued to propagate throughout the cut pass until the cutting edge disengaged from the workpiece.

For the 60° case, it was found that the transition occurred at a relatively smaller feed rate. As shown in Figure 3.7(b), the crack-free surface was found at 0.12 mm/min and the fracture began to first occur near the exit zone when machining at 0.16 mm/min (f_T for 60º). However, a closer look at the SEM micrograph of the 0.16 mm/min groove revealed visual evidence of smaller microcracks that appeared to begin from the middle of the groove where the undeformed chip thickness was the largest. Between the entry zone and the middle of the groove the chip thickness increased as shown in Figure 3.5,

and the cutting regime appeared ductile in this region as observed. After the tool passed the middle of the groove, the undeformed chip thickness then decreased towards the exit zone. As expected, the fracture should not occur if there was no fracture in the middle of the groove since the critical undeformed chip thickness was not reached and would not be reached after passing the middle point (t_{max} at the groove bottom). However, the fracture was visible near the groove exit zone while there was no facture in the middle at the 0.16 mm/min feed rate. It is believed that the observed microcracks in the middle were propagated from the middle area to be fracture at the macro-scale after the middle point due to the excessive rubbing effect under the 60° tilt angle condition. This point will be further elaborated in discussing the surface roughness of machined grooves.

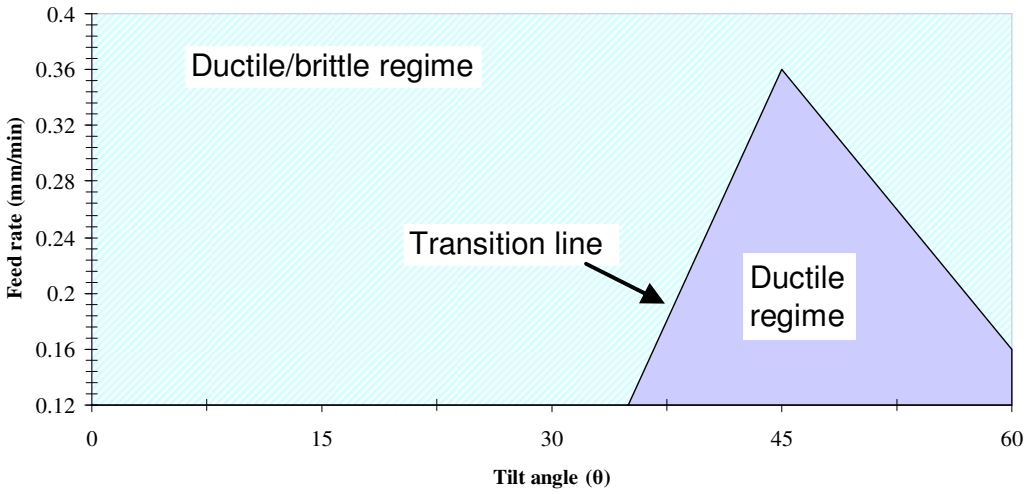

Figure 3.8 - Cutting regimes as a function of tilt angle and feed per tooth

Based on the visual inspection, glass machining is considered favorable with a tilt angle of 45° for the investigated machining setup (16 μm DOC, 2000 RPM, and water bath) since f_T under 45° is the largest. Figure 3.8 delineates the cutting regimes as a function of feed per tooth and tilt angle in this study. This plot can be used as an initial guide to select machining parameters for micromilling glass in the desirable cutting regime. It should be pointed out that the transition line is drawn as linear between the data points at each tilt angle for simplicity. In reality, the stress field surrounding the cutting edge in micromilling might not change linearly with respect to the tilt angle and the feed rate due to the complex geometry of the ball end mill. While the groove machined at a tilt angle of 30° and feed rate of 0.12 mm/min did result in the evidence of both regimes, the extent of brittle fracture was small. Although very low feed rates were not performed in this study, a ductile cut is expected as possible when the feed rate is lower than 0.12 mm/min if not excessively rubbing. Based upon the observations in this study, all the grooves showed some evidence of ductile machining under the conditions investigated.

Cutting Chips under Different Cutting Regimes

Cutting chips have been used to demonstrate the ductility of glass under controlled conditions where the chips are continuous and similar to those obtained in cutting of ductile metals (Takeuchi et al., 1996). Collecting all of the cutting chips in this study was difficult, since the cutting operations were conducted in a water bath and the resulting cutting chips were so small. Therefore, dry cutting with a relatively large feed rate (0.5 mm/min) was performed to observe the different chip morphologies. Prior to

micromilling, the workpiece surface was coated with a thin blue ink layer to help to identify the cutting chips. The continuous chips and dust-like particles were collected when using a 5 μm DOC (Figure 3.9(a)) while the crushed chips/particles were obtained when using a 10 μm DOC (Figure 3.9(b)).

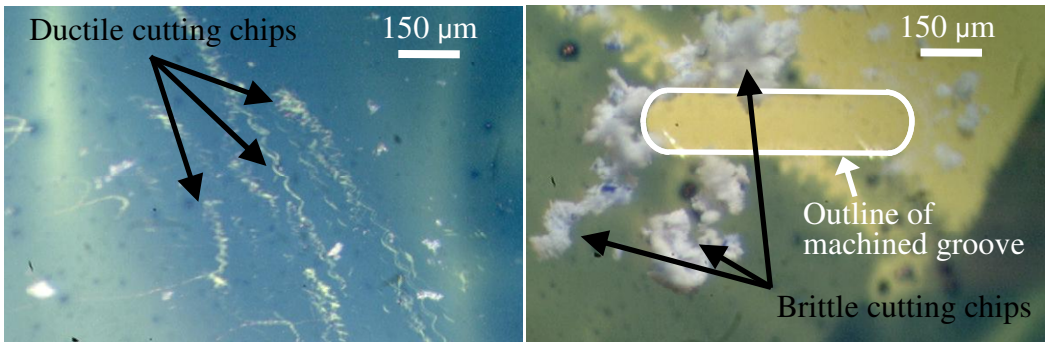

(a) (b)

Figure 3.9 - Typical (a) ductile and (b) brittle cutting chips under a 11.5º tilt angle

Surface Finish Analysis in Micromilling with Tilt Angle

Surface Finish along the Groove Cross-Section

The surface finish of the machined grooves was investigated using a surface profilometer to investigate the cutting regime transition based on the surface finish measurements. Figure 3.10(a) illustrates the surface profile of a representative groove machined using a 0.16 mm/min feed rate and 60° tilt angle. The surface images of the entry zone, groove bottom, and exit zone are also shown in Figure 3.10(a). The surface roughness values, as shown in Figure 3.10(b), were sampled at eight locations along the groove cross-section. Each measurement was based on a 80 μm sample length in the feed direction.

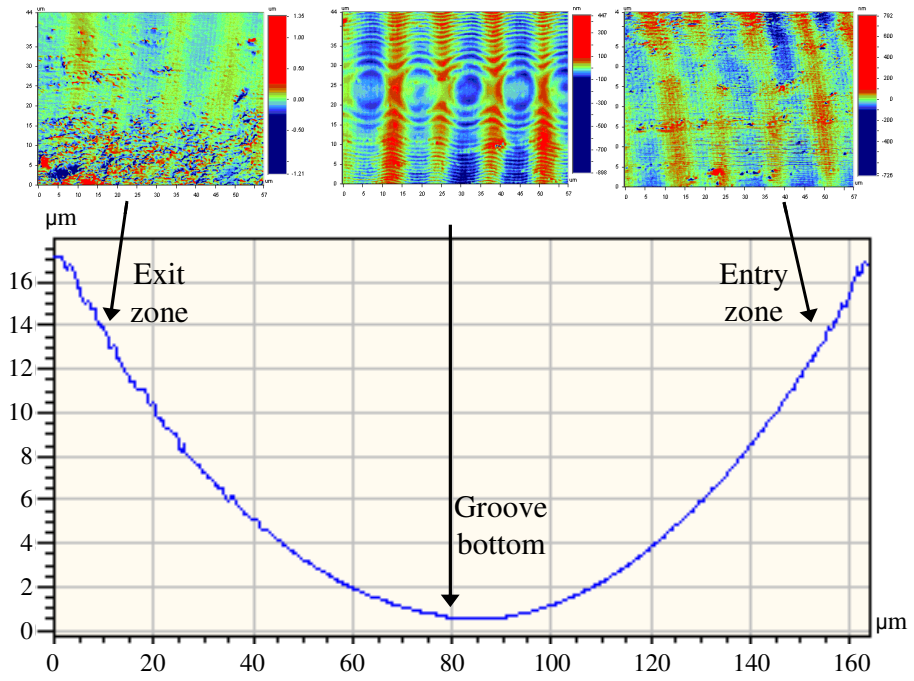

(a)

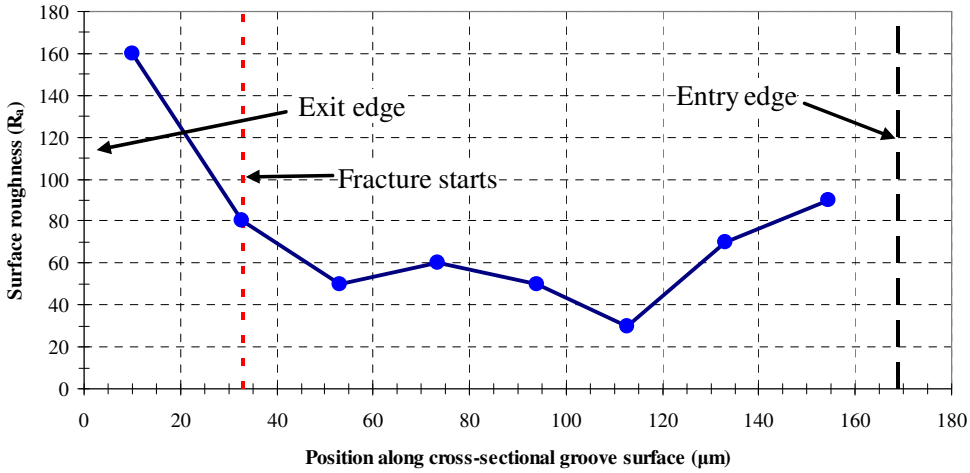

(b)

Figure 3.10 - (a) Surface profile with magnified images illustrating the tool exit zone, groove bottom, and entry zone and (b) plot of the average surface roughness (Ra).

As seen from Figure 3.10(b), the average surface roughness was 90 nm near the entry zone in the feed direction and decreased to a minimum value of 30 nm around the groove bottom as the tool continued to fully engage with the workpiece. Between the groove bottom and the exit zone brittle fracture was observed (Figure 3.7(b)), and this fracture is correlated with a sharp increase in the surface roughness from 80 nm to 160 nm as seen in Figure 3.10(b). The position of fracture initiation is marked with a dashed line in Figure 3.10(b) at a position of 33 μm measured from the tool exit edge. It should be noted the microcracks observed in the SEM images and discussed earlier did not reflect in a change in the surface profile before this fracture initiation position (33 μm) in Figure 3.10(b). The surface roughness decrease from the entry zone to the groove bottom is attributed to a decrease in the rubbing effect due to the exceeding of the minimum undeformed chip thickness for the workpiece, and the surface roughness increase from the groove bottom to the exit zone is attributed to the microcrack-induced fracture and the increasing rubbing effect.

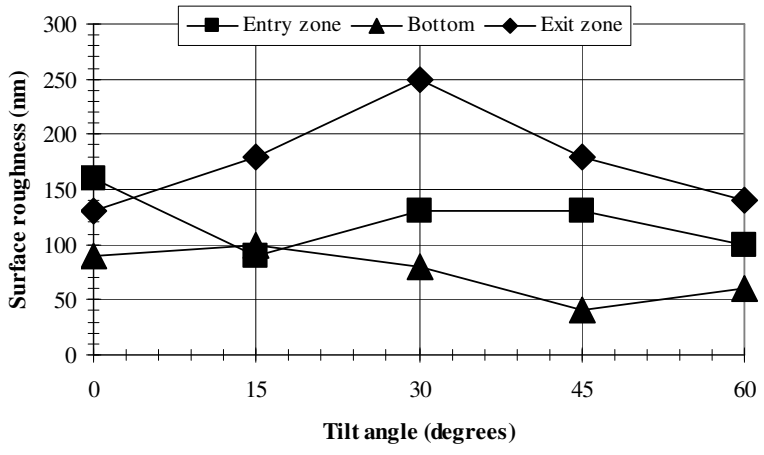

Figure 3.11 - Surface roughness versus tilt angle at entry zone, groove bottom, and exit zone (feed rate = 0.12 mm/min)

Effect of Tilt Angle

Figure 3.11 shows the average surface roughness measured at the entry zone, groove bottom, and exit zone when the glass was machined at 0.12 mm/min under various tilt angles. Although this cutting configuration is classified as in the ductile/brittle cutting regime as seen from Figure 3.8, the surface was observed to be dominated by the ductile cutting characteristics (fracture free). In general, for all the investigated feed rates, larger surface roughness values were obtained at the entry and exit zones under this cutting configuration while the smaller surface roughness values occurred at the groove bottom. During typical milling processes, when the feed rate increases the average surface roughness is also expected to increase as proportional to the square of the feed per tooth. As seen from Figure 3.5, a larger surface roughness is expected in the middle of groove due to the maximum feed rate-related undeformed chip thickness. However, the opposite observations were found under this micromilling cutting configuration. This is most likely due to the minimum chip thickness effect, which has been found to occur in micromachining when the undeformed chip thickness is comparable to that of the tool edge hone radius. If the undeformed chip thickness is smaller than a certain value, rubbing prevails instead of material removal, resulting in a higher surface roughness. For a 0.12 mm/min feed rate, it is possible to have a dominant rubbing effect at the entry and exit zones, which is more pronounced than that due to the possible milling-induced material removal. If the general surface roughness contribution due to the rubbing effect is stronger than that of possible material removal in micromilling, the similar surface roughness trend is expected, which was the case for

most experimental results in this study. It is concluded that the surface roughness decreases from the entry zone to the groove bottom then increases towards the exit zone under the ductile or ductile/brittle cutting regimes. It is also interesting to point out that the surface roughness value at the exit zone is usually higher than that of the entry zone.

Effect of Feed Rate under Different Tilt Angles

Figure 3.12 shows the average surface roughness along the groove bottom for the 45° and 60° tilt angles. It was observed that the favorable ductile regime machining can produce a surface with average surface roughness less than 60 nm using a 45° tilt angle. In comparison with average surface roughness values obtained with 60°, smaller roughness values were obtained with 45°, under which a higher transitional feed rate (f_T) was achieved.

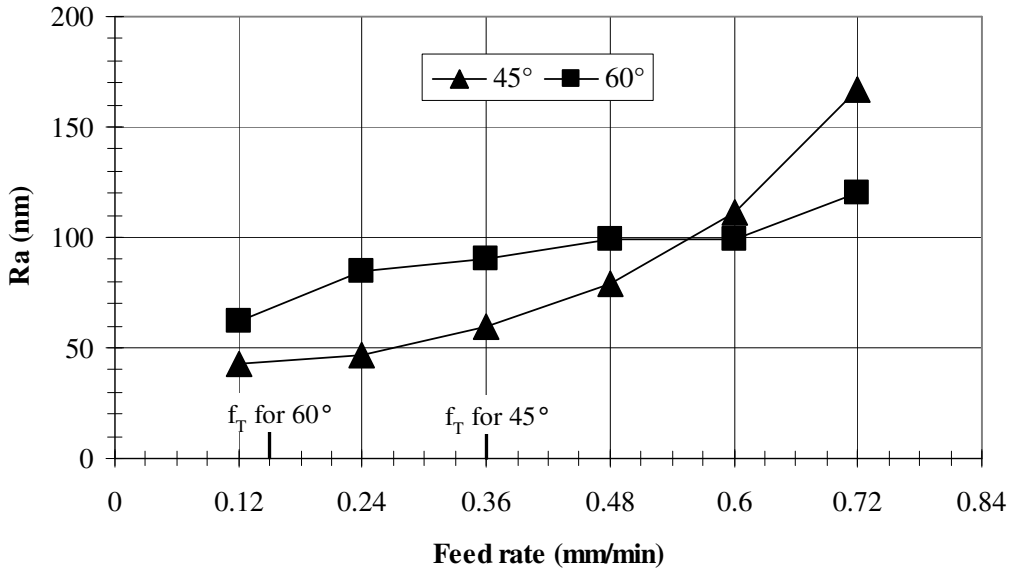

Figure 3.12 - Average surface roughness (R_a) along the groove bottom as a function of feed rate for 45° and 60° tilt angles.

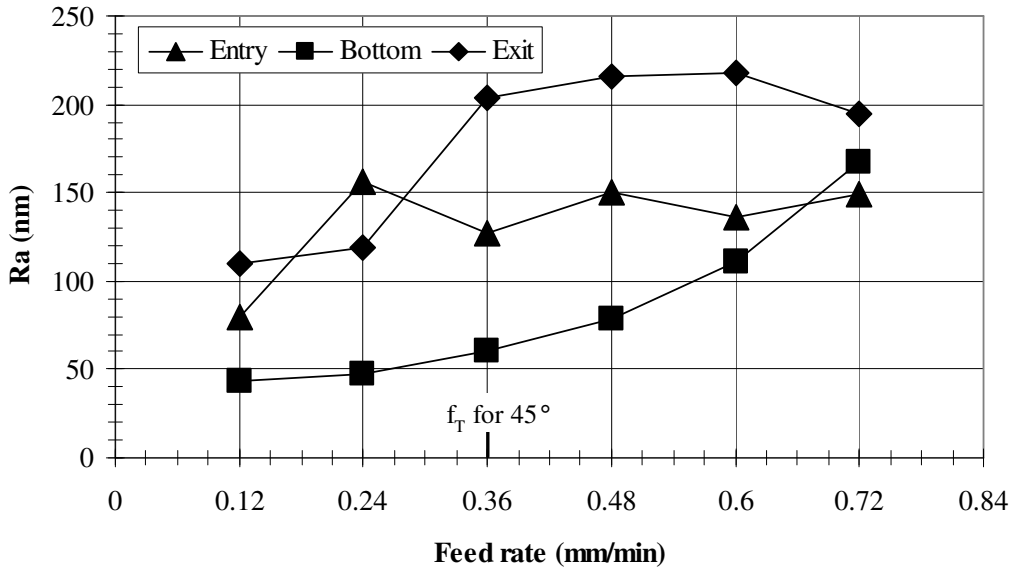

Figure 3.13 - Average surface roughness (Ra) at the different groove positions (45° tilt angle)

Figure 3.13 is a plot of the average surface roughness at the entry zone, groove bottom, and exit zone when machining with 45°. The quadratic trend of the average surface roughness along the groove bottom was observed as discussed before. It was found that ductile regime machining produced smallest average surface roughness values (typically less than 60 nm) at the groove bottom. Larger surface roughness values were found in the entry and exit zones due to the small values of undeformed chip thickness leading to excessive rubbing of the glass workpiece. In addition, after the transition feed rate (f_T = 0.36 mm/min), brittle cutting was observed in forms of fracture at the exit zone, and as a result, a significant surface roughness increase was observed, which was also much higher than that of the entry zone.

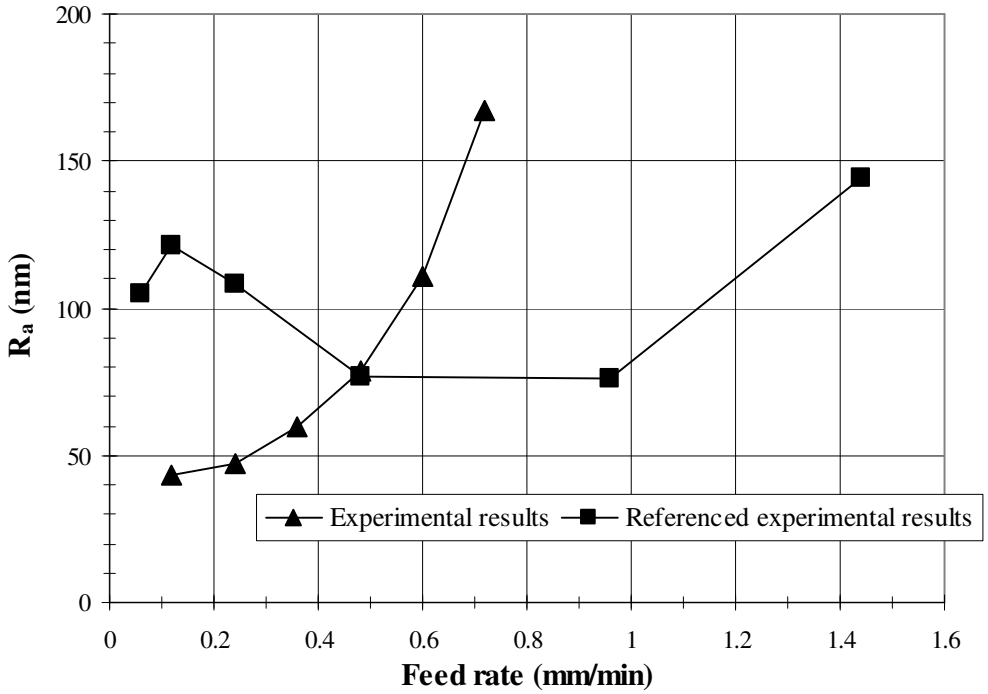

Figure 3.14 - Comparison of average surface roughness (R_a) along the groove bottom between this study and a previous study (Matsumura et al., 2005)

Figure 3.14 shows the comparison of the average surface roughness data (R_a) along the groove bottom in this study and those of a previous study by Matsumura and Ono (Matsumura et al., 2005) when machining with a 45° tilt angle under a similar micromilling configuration. While the measured surface roughness values for the both two studies are at the same order, Matsumura and Ono found that the average surface roughness did not monotonically increase as observed in this study, and their surface roughness values were much higher than those of this study when the feed rate was lower than 0.5 mm/min but lower when the feed rate was higher than 0.5 mm/min. The increasing trend of surface roughness values with feed rate found at the bottom of the groove in this study is indicative of a typical milling process. In this study, no cracks were visible at the lowest feed rate tested (0.12 mm/min) and resultantly there were no

high surface roughness values at the lower feed rates. However, Matsumura and Ono observed large scratches the surface machined with lower feed rates (Matsumura et al., 2005), which is thought to have an impact on their surface roughness measurements. Due to the extremely small values of undeformed chip thickness (on the order of 1 μm), high rigidity and accuracy are expected for better cutting configuration control, and the resulting cutting dynamics also might have an impact on actual undeformed chip thickness values and the cutting regime transition. Differences in the two milling setups are concluded to be the main cause in the discrepancies among the aforementioned surface roughness comparison.

Effect of Edge Serration

Limitations in current microtool fabrication can leave a serrated cutting edge where the cutting edge geometry is not consistent along the length of the flute, as is shown in Figure 2.12. As a result, the effect of edge serration can be profound on the chip formation and ensuing machined surface due to the inconsistency in cutting radius. Figure 3.15 illustrates the edge serration effect, and Figure 3.16 is an SEM image of the groove machined at 0.12 mm/min and 45° tilt angle. At the end of the cut shown in Figure 3.16(a) the tool is quickly disengaged from the workpiece. Left behind were ridges in the machined surface, as can be seen in Figure 3.16(b), due to the edge serration effect. However, only at the end of cut where the tool was quickly disengaged from the workpiece was the serrated surface visible, with exception of grooves machined with a 0° tilt angle. It was reasoned that material was removed via ductile cutting when the minimum chip thickness was first reached. Then during the next subsequent tooth passes

the minimum chip thickness was not reached. Instead, edge rubbing/ploughing occurred during these passes and smoothed the serrated surface. Once the minimum chip thickness was again reached material was once more removed via ductile cutting. This process continued until a smooth "polished" surface, with respect to the serrated surface, was produced after the tool had passed as seen in Figure 3.16(a). This could help explain why flank wear was the dominant wear pattern throughout a variety of conducted experiments under similar cutting conditions as observed by SEM. A selection of these images of the cutting tool is shown in Appendix C. Again, it should be noted that there was no visual evidence of a serrated surface behind the path of the cutting tool for any groove machined at the feed rates tested in this study for all tilt angles except those machined at 0° (groove machined at 0.12 mm/min shown in Figure. This was most likely due to inability of the cutting edge to viscously polish the serrated surface formed ahead of the tool due to low cutting speeds.

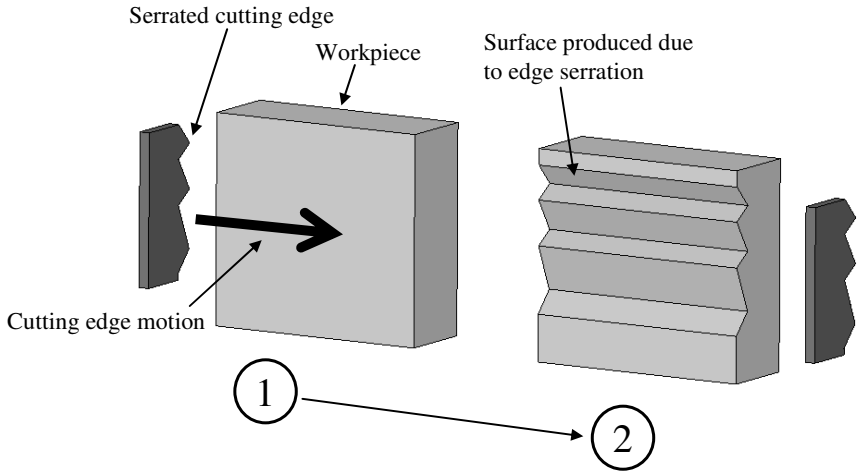

Figure 3.15 - Illustration of the edge serration effect during micro-cutting

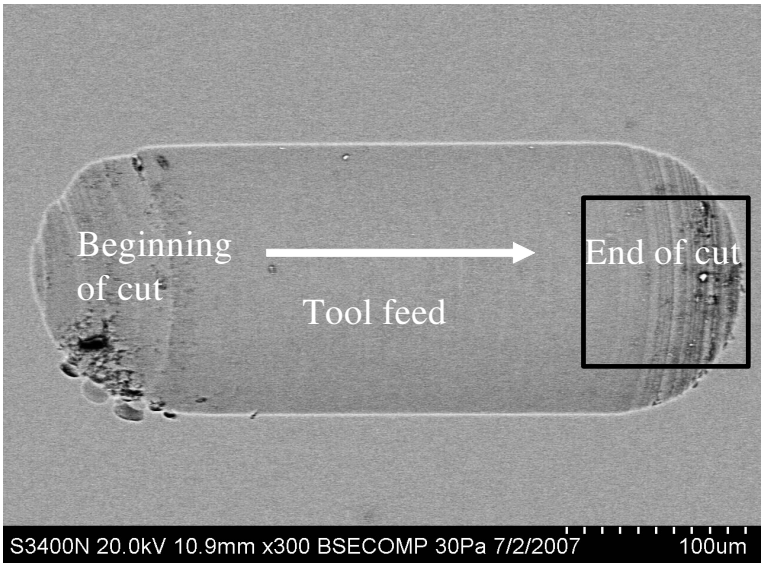

(a)

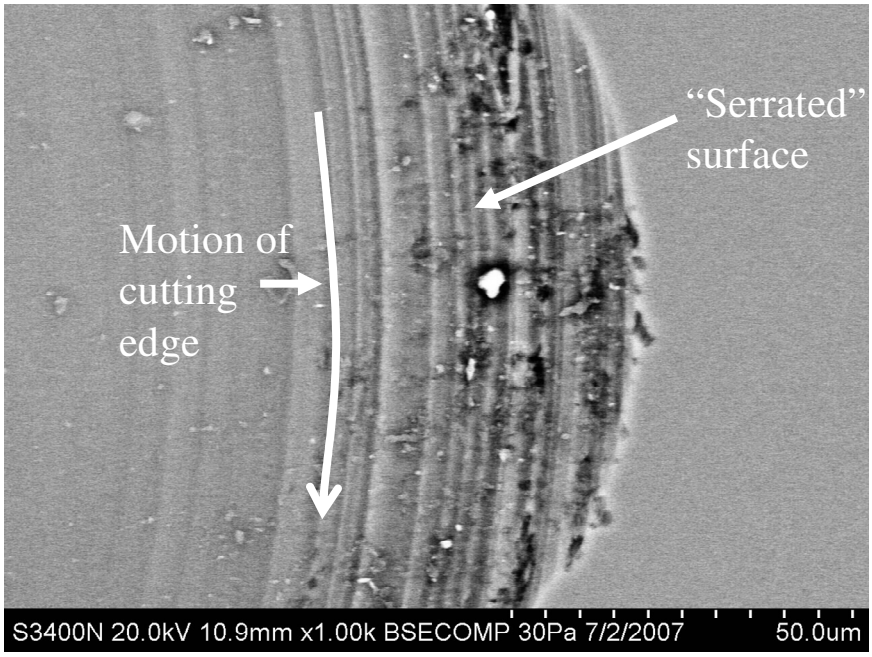

(b)

Figure 3.16 - SEM image of (a) groove machined at 0.12 mm/min and 45° tilt angle and (b) closer view at the end of cut

Based on the experimental observations in this study, the micromilling process draws some similarities with precision grinding. The serration along the cutting edge results in the effect of cutting at local asperities, which is similar to the grinding mechanism. In addition, each abrasive grit in grinding creates a large negative rake angle and the same can be realized with the ball end mill used in this study in which the cutting edge radius (~ 1 μm) is expected to be on the order of the chip load. In addition, chips produced in precision grinding are also on the micron to sub-micron range of the expected chip load in this study.

Conclusions

Straight crown glass grooves were machined using micromilling under different tilt angles to investigate the effect of tilt angle on the cutting regime transition of brittle material, which is glass in this study. The cutting regime transition was mainly characterized based on the machined surface which was analyzed using SEM and the non-contact profilometer. Some conclusions were drawn as follows which are expected to help to better understand the glass mechanical micromachining process:

- In characterizing the cutting regimes in glass micromilling, rubbing, ductile machining, and brittle machining regimes are hypothesized based on the relative value of undeformed chip thickness. Once the fracture was initiated as a sign of brittle machining, this fracture continued to propagate throughout the cut pass until the cutting edge disengaged from the glass workpiece;

- The crown glass can be better machined in the ductile mode by carefully selecting the tool tilt angle. A tilt angle of 45° had a highest ductile machining-related feed rate (0.32 mm/min) in this study and the surface finish was significantly better (less than 60 nm) at feed rates less than 0.32 mm/min;
- During each milling pass, surface roughness was found to decrease from the entry zone to the groove bottom and then increase to the exit zone regardless of the cutting regime due to the pronounced rubbing effect in micromilling;
- Brittle machining with 45° and 60° tilt angles was generally observed to first occur in the entry zone and the exit zone, respectively, as the feed rate gradually increased. As a result, a significant surface roughness increase was observed in the exit zone after the cutting regime transition-dependent feed rate was reached, which indicated the onset of brittle cutting regime;
- SEM images of the grooves machined in this study show evidence of the edge serration effect occurring in front of the tool during material removal. The serrated surface that is produced appears to be polished by edge rubbing during subsequent rotations of the tool, except for 0° tilt angle; and
- The micromilling process under the parameters and conditions in this study exhibited characteristics of the precision grinding process due to the tool geometry and expected chip size (tool edge serration effect, tool edge radius effect, micron to sub-micron chip size).

CHAPTER IV

UNDERSTANDING OF CUTTING REGIME CHANGE IN GLASS MICROMACHINING VIA STRESS AND TEMPERATURE MODELING

Introduction

Silica has drawn great interest in the research community since it serves as an ideal model of an amorphous material and is one of the primary constituents of the Earth's crust and mantle, and silica-based amorphous materials, such as optical glasses, have been formidable engineering materials in many fields. Within the upper and lower mantle of the Earth temperatures and pressures are extreme and thus create an interest into the high-pressure, high-temperature microstructure of silica and the associated physical and mechanical properties. However, studying the microstructure of silica under extreme conditions using conventional techniques, such as Raman spectroscopy and XRD, has been proven to be very difficult due to the limitations in the experimental setup. As a result, molecular simulation (Lacks, 1998; Huang et al., 2004;) and microindentation (Yoshida et al., 2005; Ji et al., 2006) methods have been the preferred approaches into gaining possible insight. Additional interest has risen into using mechanical micromachining. Mechanical micromachining offers the ability to study amorphous material under high stress and strain rate for both manufacturing and material testing applications.

In material testing applications such as ballistics testing, the material response is studied under situations that involve high impact and high strain rates. Manufacturing research has shown that certain controlled conditions can be used to mechanically

machine micro-scale features on silica-based glasses in the ductile regime, where the resulting surface is smooth and void of machining-induced cracks (Nakatsuji et al., 1990; Moriwaki et al., 1992). However, much research is still required to better understand the material response during the ductile machining of brittle materials. The occurrence of ductile regime machining has been correlated to the undeformed chip thickness (Nakatsuji et al., 1990; Moriwaki et al., 1992) and to a sufficient combination of hydrostatic pressure and temperature in the deformation zone (Komanduri, 1996). However, more research is required to better understand how the fracture toughness of glass changes with variation in pressure and temperature. Through investigating the cutting regime transition, this chapter presents a study of the fracture strength of glass as a function of the tilt angle and feed rate in the micromilling process. The mechanistic models implemented in this study for the prediction of the stress state and temperature in the cutting zone are first presented. The experimental design and methodology for predicting the stress state and temperature in the cutting zone are then presented. The predicted stresses are discussed and compared with previous experimental observations from Chapter III to draw conclusions regarding the effect of compressive stress on glass ductility. The findings from estimating the temperature in the cutting zone are offered and discussed.

Predicting Stress in Ball End Milling

Mechanical modeling of the machining process at the sub-micron level has proven to be difficult due to the size effects, process- and material-related, associated

with the scaling effects on the size of the deformation zone. Currently, a sufficient model for accurately determining the stress and temperature in the cutting zone during the micromilling process with a ball end mill does not exist. Thus, for this study an attempt is made to come up with a first-order approximation for the stress in the deformation zone using a conventional mechanistic modeling approach combined with experimental data gathered from micromilling experiments. The cutting tool modeled is a two-flute ball end mill, and the cutting edge is divided into small incremental segments. The cutting process at each segment is considered as an ideal two-dimensional orthogonal cutting process.

The assumptions for an ideal orthogonal cutting process assume that the tool is sharp and there is no contact along the clearance face of the tool. The shear surface is a plane extending upward from the tool and a continuous chip flows up the rake face of the cutting tool. The cutting edge is assumed to be a straight line extending perpendicular to the direction of motion and generates a plane surface as the work surface moves past it. The workpiece is assumed to be rigid. The velocity of the workpiece is considered to move uniformly relative to the tool. Lastly, the shear and normal stresses along the shear plane are assumed to be uniform (Shaw, 1984).

Ball End Milling Geometry

The geometric model of a typical industrial ball end mill with two cutting flutes is shown in Figure 4.1 considering constant-depth groove machining. The cutting edges lie along the tool envelope surface that consists of a cylindrical portion with radius R_0 and constant helix angle β_0 and a hemispherical end with the same radius R_0. The two flutes

meet at the tip O_1 of the hemispherical end that is grounded with a constant helix lead. Below the ball-shank meeting boundary A, the local helix angle β changes along the cutting edge and can be calculated at the cutting point P using Equation 4.1.

$$\beta = \tan^{-1}(\frac{R}{R_0}\tan\beta_0) \tag{4.1}$$

where R is the local cutting radius at cutting point P which is less than or equal to the nose radius R_0. Let φ represent the lag angle of the cutting point P from the flute's tip (where $\varphi = 0$) in counterclockwise rotation, then the cutting radius R can be calculated by Equation 4.2.

$$R = R_0\sqrt{1-(\varphi\cot\beta_0 - 1)^2} \tag{4.2}$$

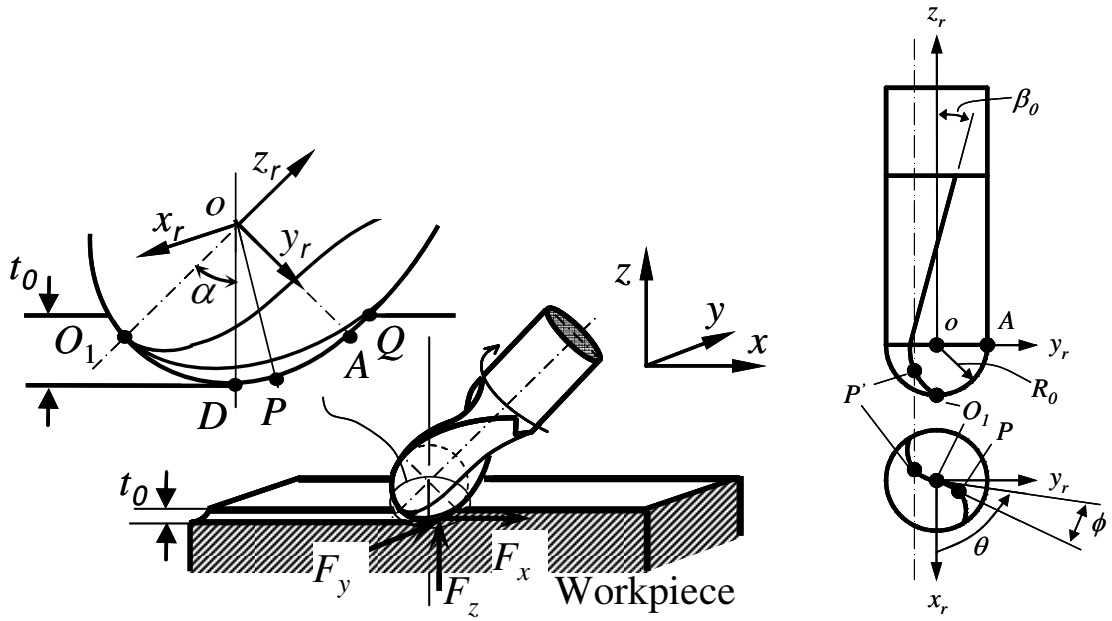

(a) (b)

Figure 4.1 - Illustration of two-flute ball end mill geometry in groove machining

For this study, the groove depth t_0 (16 μm) is much smaller than the nose radius R_0 (200 μm) and the cutting edge along the cylindrical portion (above the ball-shank meeting boundary A) never engages with the workpiece. Thus, only the cutting edge along the ball part of the tool is of interest. Each cutting edge along the ball part can be divided into infinitesimal cutter segments where the length of each segment can be described in terms of the lag angle φ, as shown in Equations 4.3 and 4.4.

$$dl = \sqrt{R_\varphi^2 + R^2 + R_0^2 \cot^2 \beta_0}\, d\varphi \tag{4.3}$$

$$\text{where } R_\varphi = \frac{-R_0(\varphi \cot \beta_0 - 1)\cot \beta_0}{\sqrt{1-(\varphi \cot \beta_0 - 1)^2}} \tag{4.4}$$

Therefore, since $t_0 \leqslant R_0$, the total contact length l_c of a flute along the ball part is computed by integrating Equation 4.3 to get Equation 4.5 with the limits of integration corresponding to the lag angle at the cutting edge engagement φ_1 and disengagement φ_2 from the workpiece.

$$l_c = \int_{\varphi_1}^{\varphi_2} \sqrt{R_\varphi^2 + R^2 + R_0^2 \cot^2 \beta_0}\, d\varphi \tag{4.5}$$

$$\text{where} \quad \varphi_1 = (1-\cos\alpha)\tan\beta_0 \text{ and}$$

$$\varphi_2 = (1-(1-t_0/R_0)\cos\alpha)\tan\beta_0$$

During the milling process the undeformed chip thickness is a typical factor which influences cutting force. However, in consideration of cutter and chip geometry, ball end milling is quite different from face or end milling with a cylindrical cutter due to the three-dimensional geometry of the ball part of the cutter. As the cutter rotates, each spherical shaped helical flute removes a different amount of chip along the engaged portion. Therefore, the undeformed chip thickness engaged in the ball end varies with

position along the helical flute during cutting. In this study the radial thickness of the undeformed chip measured from the center of the nose radius is used to estimate the cutting forces. The components of the radial thickness of undeformed chip can be seen in view of the x_r- and z_r-axes as shown in Figure 4.2. From view of the x_r-axis, the radial undeformed chip thickness varies with angle ψ as shown in Equation 4.6.

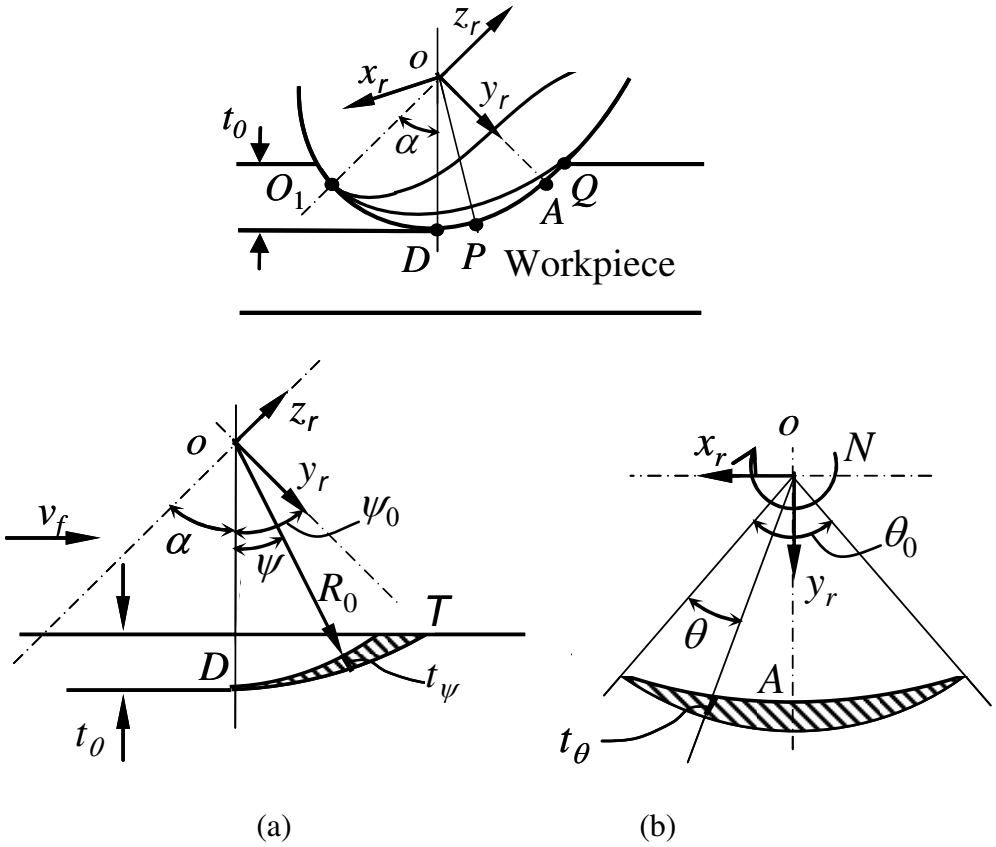

Figure 4.2 - View of undeformed chip thickness from (a) x_r-axis and (b) z_r-axis

$$t_{\psi} = \begin{cases} f_t \cos\alpha \sin\psi, & (0 \le \psi \le \psi_0) \\ f_t \cos\alpha, & (\psi > \psi_0) \end{cases} \tag{4.6}$$

where f_t is the theoretical feed per tooth in milling determined by Equation 4.7, α is the tilt angle of the tool, and ψ_0 is the angle ψ that corresponds to the ball-shank meeting boundary *A* and is found by Equation 4.8.

$$f_t = \frac{v_f}{nN} \tag{4.7}$$

$$\psi_0 = 90 - \alpha \tag{4.8}$$

where v_f is the feed rate (mm/min), n is number of flutes, N is the spindle speed (RPM), and α is the tilt angle of the tool. In micromilling, it is considered that the theoretical feed per tooth determined by Equation 4.7 may vary from the actual feed per tooth during the machining process due to the size effect. An effective feed per tooth will be introduced and discussed later in this chapter.

After point *A* the thickness remains unchanged until point *Q*. The maximum of angle ψ corresponds to the top of the groove (*Q*) and is denoted by ψ_T. When ψ_T is less than ψ_0 (only the ball part is engaged), it can be computed by Equation 4.9.

$$\psi_T = \cos^{-1}\left(1 - t_0 / R_0\right) \tag{4.9}$$

In addition to the maximum in view of the x_r-axis, the section of undeformed radial chip thickness also has a maximum in the x_r-y_r plane, as shown in Figure 4.2, and can be calculated by Equation 4.10.

$$t_\theta = f_t \cos\alpha \frac{\sin\theta \sin(\theta_0 - \theta)}{\sin^2(\theta_0 / 2)}, \quad (0 \le \theta \le \theta_0) \qquad (4.10)$$

where θ_0 is the range of tool-workpiece engagement as noted in Figure 4.2 and theta is the angle of tool rotation with respect to the tool engagement with the workpiece. Therefore, at any cutting element of a flute the engaged undeformed chip thickness can be expressed as Equation 4.11.

$$t(\psi, \theta) = f_t \cos\alpha \sin\psi \frac{\sin\theta \sin(2\psi - \theta)}{\sin^2(\psi)} \quad (0 \le \psi \le \psi_0, 0 \le \theta \le 2\psi) \qquad (4.11)$$

During milling the total contact area changes with the chip thickness, thus the contact stress acting on the cutter or the workpiece varies within every revolution. For a two-flute ball end mill, the cutting force meets the maximum twice a rotation during the milling process.

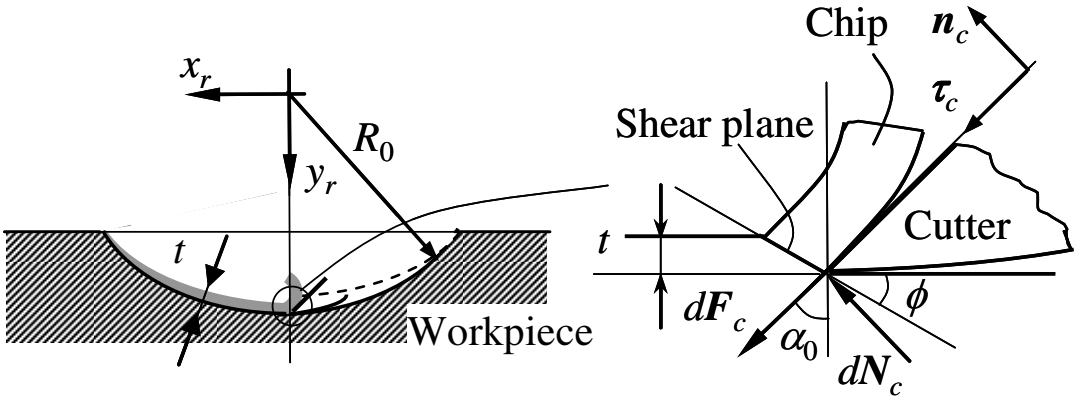

Figure 4.3 - Forces acting in the cutting zone

Modeling of Cutting Forces and Stresses

The cross section of the cutter is considered as a sharp blade with a rake angle α_0 as shown in Figure 4.3, and the contact length c between the rake face of the cutter and the chip thickness t at this section is assumed as can be found by using Equation 4.12. The chip thickness t can be found using Equation 4.11.

$$c = t \sin \phi \tag{4.12}$$

Over the years many analyses have been performed to determine the relationship of the shear angle to material properties and process variables. One of the earliest performed by M. E. Merchant proposed to assume that the shear angle changes to a value such that the cutting force is a minimum and is independent of the friction angle α_f (Kalpakjian et al., 2003). Consequently, the shear angle can then be estimated using Equation 4.13. The advantage to this relationship is that it correctly indicates a common trend that has been experimentally-verified in metal cutting. This trend point outs that as the rake angle α_0 decreases and/or as the friction angle α_f at the tool-chip interface increases the shear angle ϕ decreases and the resulting cutting chip is thicker (Kalpakjian et al., 2003).

$$\phi = 45^\circ + \frac{\alpha_0}{2} - \frac{\alpha_f}{2} \tag{4.13}$$

For orthogonal turning the cutting force acting on the workpiece can be estimated by Equation 4.14 (Shaw, 1984).

$$F_P = u_0 lt(1 - \frac{\alpha_b - \alpha_e}{100})(\frac{t_{ref}}{t})^{0.2} \tag{4.14}$$

where α_b is back rake angle, α_e is effective rake angle, t is undeformed chip thickness, l is cut depth, and u_0 is the specific cutting energy when α_e=0 and t=t_s. When the clearance face is assumed tangential to the machined surface and without contact force, for an infinitesimal cut width dl the cutting force acting on the workpiece, as shown in Figure 4.3, can be expressed by Equation 4.15.

$$d\boldsymbol{F} = d\boldsymbol{F}_c + d\boldsymbol{N}_c \tag{4.15}$$

However, for ball end milling, cutter orientation varies helically. Therefore, the cut width is not constant, and the direction of cutting force at one section differs from others. When the unit vectors of x-, y- and z-axes are named as $\boldsymbol{i}, \boldsymbol{j}$ and $\boldsymbol{k}$, those of x_r-, y_r- and z_r-axes can be calculated by Equation 4.16.

$$\begin{Bmatrix} \boldsymbol{i}_r \\ \boldsymbol{j}_r \\ \boldsymbol{k}_r \end{Bmatrix} = \begin{bmatrix} 0 & -1 & 0 \\ \cos\alpha & 0 & -\sin\alpha \\ \sin\alpha & 0 & \cos\alpha \end{bmatrix} \begin{Bmatrix} \boldsymbol{i} \\ \boldsymbol{j} \\ \boldsymbol{k} \end{Bmatrix} = [J_r] \begin{Bmatrix} \boldsymbol{i} \\ \boldsymbol{j} \\ \boldsymbol{k} \end{Bmatrix} \tag{4.16}$$

Then, the unit vectors along $d\boldsymbol{F}_c$ and $d\boldsymbol{N}_c$ can be computed by Equation 4.17.

$$\boldsymbol{\tau}_c = \boldsymbol{\tau}\cot\eta - \frac{\boldsymbol{\kappa}}{\sin\eta};\ \boldsymbol{n}_c = -\boldsymbol{\tau} \times \boldsymbol{\tau}_c \tag{4.17}$$

$$\text{where } \eta = \cos^{-1}(\boldsymbol{\tau} \cdot \boldsymbol{\kappa}),$$

$$\boldsymbol{\tau} = \frac{(-R\sin(\varphi + \varphi_{rm}) + R_\varphi \cos(\varphi + \varphi_{rm}))\boldsymbol{i}_r + (R\cos(\varphi + \varphi_{rm}) + R_\varphi \sin(\varphi + \varphi_{rm}))\boldsymbol{j}_r + R_0 \cot\beta_0 \boldsymbol{k}_r}{\sqrt{R^2 + R_\varphi^2 + R_0^2 \cot^2\beta_0}},$$

$$\text{and } \boldsymbol{\kappa} = \sin(\varphi + \varphi_{rm} - \alpha_0)\boldsymbol{i}_r - \cos(\varphi + \varphi_{rm} - \alpha_0)\boldsymbol{j}_r$$

where φ_{rm} is the equivalent rotation angle of a point on edge of the *m*th flute. Therefore, for a two-flute ball end mill, the equivalent rotation angle of a point on the second flute is $\varphi_{r2} = \varphi_{r1} + \pi$. To obtain the instantaneous cutting force the rotational angle is unchanged and the cutting force components in the x, y, and z directions, as denoted in Figure 4.1, are expressed in Equation 4.18.

$$d\boldsymbol{F}_{\boldsymbol{c}} = dF_c\boldsymbol{\tau}_c,\ d\boldsymbol{N}_{\boldsymbol{c}} = dN_c\boldsymbol{n}_c \quad \begin{cases} dF_x = dF_c\tau_{cx} + dN_c n_{cx} \\ dF_y = dF_c\tau_{cy} + dN_c n_{cy} \\ dF_z = dF_c\tau_{cz} + dN_c n_{cz} \end{cases} \qquad (4.18)$$

Therefore, for a two-flute ball end mill, the components in the directions of the *x*-, *y*- and *z*-axis of the total resultant cutting force acting on the workpiece can be calculated from Equation 4.19.

$$F_x = \sum_{i=1}^{2}\int_0^{l_c} dF_x\ ,\quad F_y = \sum_{i=1}^{2}\int_0^{l_c} dF_y\ ,\quad F_z = \sum_{i=1}^{2}\int_0^{l_c} dF_z \qquad (4.19)$$

One of the keys to understanding the mechanics of machining is the contact stresses between chip and tool surface, especially at the tool tip-workpiece interface. Cutting force and the stress distribution along the rake face have long been investigated both analytically and experimentally, but a satisfactory model is still expected because of the difficulty in accurately reflecting the insight into the behavior of the material at the tool-chip contact area (Zorev, 1963; Childs et al., 1989; Buryta et al., 1994; Lee et al., 1995; Li, 1997; Buryta et al., 1998; McClain et al., 2002). Focusing on the compressive stress in the local area of the cutter tip, the stress distribution is assumed based on a combination of the results from previous researchers (Zorev, 1963; Childs et al., 1989;

Buryta et al., 1994). Then Equation 4.20 can be used to compute the resultant cutting force for an infinitesimal cut width *dl* acting on the tool.

$$\begin{cases} dF_c = \dfrac{1}{2} a \tau_m dl \\ dN_c = \dfrac{25}{48} a \sigma_m dl \end{cases} \tag{4.20}$$

Paying attention to Figure 4.4, the differential friction and normal force components can be expressed as Equation 4.21.

$$\begin{cases} dF_c = dF_P \dfrac{\sin \alpha_f}{\cos(\alpha_f - \alpha_0)} \\ dN_c = dF_P \dfrac{\cos \alpha_f}{\cos(\alpha_f - \alpha_0)} \end{cases} \tag{4.21}$$

where $\alpha_f = \tan^{-1}(dF_c / dN_c)$ is the frictional angle between tool face and workpiece. Equation 4.22 then results by taking account for Equation 4.14 in consideration of $\alpha_b = \alpha_0$ and $\alpha_e = 0$ and substituting into Equation 4.21.

$$\begin{cases} dF_c = u_0 t dl (1 - \dfrac{\alpha_0}{100})(\dfrac{t_{ref}}{t})^{0.2} \dfrac{\sin \alpha_f}{\cos(\alpha_f - \alpha_0)} \\ dN_c = u_0 t dl (1 - \dfrac{\alpha_0}{100})(\dfrac{t_{ref}}{t})^{0.2} \dfrac{\cos \alpha_f}{\cos(\alpha_f - \alpha_0)} \end{cases} \tag{4.22}$$

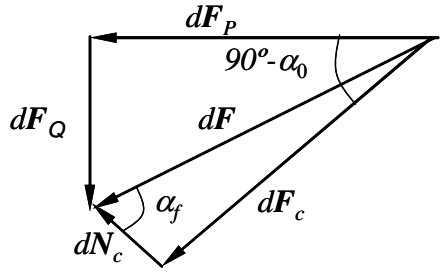

Figure 4.4 - Components of cutting forces in different directions

Therefore, the maximum normal stress σ_m can be computed by substitution of Equation 4.22 into Equation 4.20 for given machining conditions. With additional consideration of Equation 4.13, Equation 4.23 results.

$$\begin{cases} \dfrac{\tau_m}{2} = u_0\left(1-\dfrac{\alpha_0}{100}\right)\left(\dfrac{t_{ref}}{t}\right)^{0.2}\dfrac{\sin\alpha_f}{\cos(\alpha_f-\alpha_0)}\left(\csc\phi\right) \\ \dfrac{25}{48}\sigma_m = u_0\left(1-\dfrac{\alpha_0}{100}\right)\left(\dfrac{t_{ref}}{t}\right)^{0.2}\dfrac{\cos\alpha_f}{\cos(\alpha_f-\alpha_0)}\left(\csc\phi\right) \end{cases} \tag{4.23}$$

As the material removal is considered duo to shear yield in the shear plane, it is significant to study the stress state in the shear plane for understanding of the brittle-to-ductile transition during machining of soda lime glass. In addition, the compressive stress is also important as fracture has been found to primarily initiate in the primary deformation zone during machining of brittle materials. The stress state of an infinitesimal element (σ_{s1}, σ_{s2}, and τ_s) in the shear plane, shown in Figure 4.5, of the workpiece and the in-plane principal stresses (σ_1, σ_2) can be determined by Equations 4.24 and 4.25, respectively, through plane stress transformation.

$$\begin{cases} \sigma_{s1} = -\sigma_m(1+\cos(2(\alpha_0-\phi)))/2 - \tau_m\sin(2(\alpha_0-\phi)) \\ \sigma_{s2} = -\sigma_m(1-\cos(2(\alpha_0-\phi)))/2 + \tau_m\sin(2(\alpha_0-\phi)) \\ \tau_s = \sigma_m\sin(2(\alpha_0-\phi))/2 - \tau_m\cos(2(\alpha_0-\phi)) \end{cases} \tag{4.24}$$

$$\begin{cases} \sigma_1 = -(\sigma_m - \sqrt{\sigma_m^2+4\tau_m^2})/2 \\ \sigma_2 = -(\sigma_m + \sqrt{\sigma_m^2+4\tau_m^2})/2 \end{cases} \qquad \zeta = \frac{1}{2}\tan^{-1}\frac{2\tau_m}{\sigma_m} \tag{4.25}$$

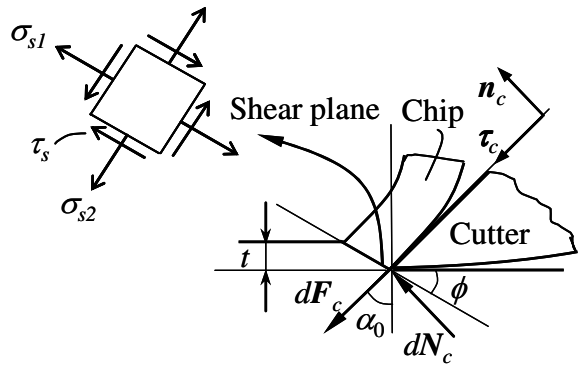

Figure 4.5 - State of stress in the shear plane

Estimating Temperature in Ball End Milling

Most of the input power during the cutting process is dissipated and converted into heat, which will have an effect on the temperature in the cutting zone. Previous research has shown that glass becomes more ductile at temperatures close to the glass transition temperature and can be more easily viscously deformed, as opposed to brittle fracture, when the temperature in the deformation zone in indentation is increased (Le Bourhis et al., 2000 ; Le Bourhis et al., 2003). Thus, predicting the temperature can be valuable, as well as predicting compressive stress, in figuring out machining conditions/parameters that lead to ductile machining of optical glass and other brittle materials.

It is considered that temperature in the cutting zone potentially scales proportionally with the cutting speed of the engaged cutting edge. The total input power in conventional cutting is the product of the cutting force F_C and cutting velocity V_C as expressed in Equation 4.26 (Kalpakjian et al., 2003).

$$Power = F_C V_C \tag{4.26}$$

In micromilling with a ball end mill the cutting speed is controlled by the spindle speed and the cutting radius. As the tilt angle of the machine tool is increased the portion of the tool edge that engages with the workpiece changes. Associated with this change is an increase in the cutting radius. The increase in cutting radius will increase the cutting speed and, thus, more power is dissipated into the cutting zone according to Equation 4.26. If more power is dissipated into the cutting zone the temperature of the workpiece in the cutting zone will increase. While this approach cannot accurately depict the actual temperature in the cutting zone it can be a valuable tool in determining the relative effect of different tilt angles on the average temperature rise in the cutting zone.

In machining with ball end mills the cutting radius changes along the cutting flute as illustrated in Figure 4.6. If d is the projection onto the z_r-axis of the distance measured from the tip of the hemispherical end to the cutting point P then the local cutting radius R at point P can be determined using Equation 4.27. Accordingly, Equation 4.28 can then be used to calculate the cutting velocity at cutting point P.

$$R(d) = \begin{cases} \sqrt{{R_0}^2 - (R_0 - d)^2} & (d < R_0) \\ R_0 & (d \geq R_0) \end{cases} \tag{4.27}$$

where R is the local cutting radius, R_0 is the radius of the ball nose, and d is measured along the z_r-axis from the tip of the hemispherical end to the cutting point P.

$$V_C(d) = \omega R(d) \tag{4.28}$$

where V_C is the cutting speed at the cutting point P and ω is the rotation speed of the spindle in rad/sec. Increasing the tilt angle of the tool will engage the cutting edge with

the workpiece at higher cutting radii of the ball mill and thus increase the cutting speed. Based on consideration that higher cutting speeds will generate higher temperatures in the cutting zone, the larger tilt angles are expected to result in an increased workpiece softening effect in machining constant-depth grooves in brittle material. Consequently, larger tilt angles are predicted to be more favorable for ductile machining because of this softening effect.

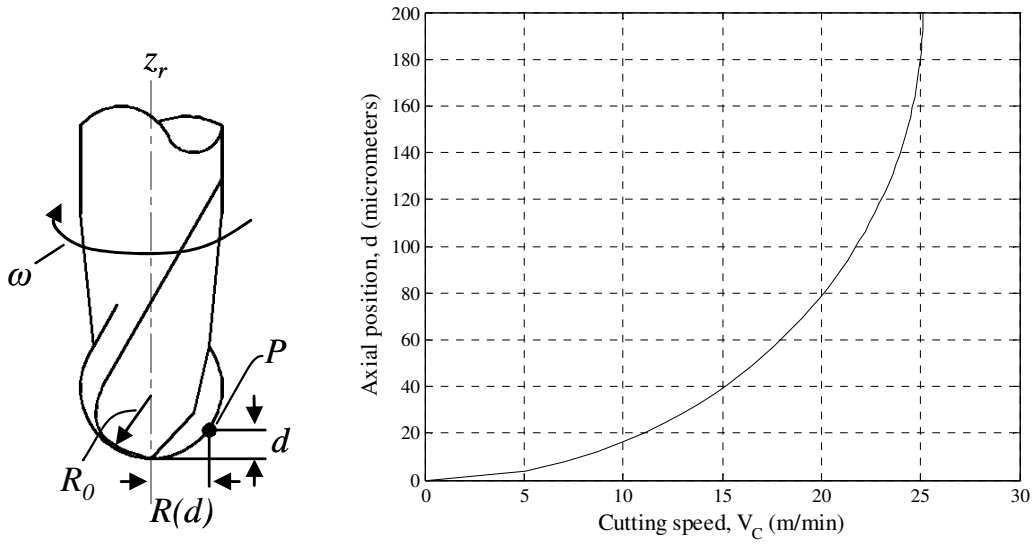

(a) (b)

Figure 4.6 - Cutting velocity in milling: (a) Schematic of ball end mill and (b) plot of the cutting speed V_C with change in position d for a ball end mill with 200 μm nose radius and rotating at 20 Krpm

Another approach was employed to estimate the general temperature rise in the cutting chip. For orthogonal cutting the general temperature rise ΔT (K) in the chip generated can be estimated using Equation 4.29.

$$\Delta T = \frac{\beta F_C V_C}{MRR \rho c} \tag{4.29}$$

where β is typically 0.9, F_C is the cutting force (N), V_C is the cutting velocity (m/min), MRR is the material removal rate (m^3/min), ρ is the density of the workpiece material (kg/m^3), and c is the specific heat (J/(kg-K)).

Experimental Investigation and Discussion

Experimental Design

A one-factor multiple level machining experiment was designed to collect force data for a range of chip loads by varying the feed rate during glass micromilling, and this experiment design is shown in Table 4.1. Each level was tested three times and the averaged force data is reported in Figure 4.8. The averaged force data and associated average chip area are used to estimate the average specific cutting energy. The average specific cutting energy was then plotted versus average chip thickness (under consideration of $f_t = f_{eff}$) and a power law trend was fit to the data. Unless otherwise specified, all machining parameters and cutting conditions employed in gathering the force data were selected based on the results from the cutting regime transition study in Chapter III in order to compare findings and investigate why ductile machining happens. The controlling parameter for this study was the feed rate and the selected levels were found to exhibit all cutting regimes in glass micromilling, as identified in Chapter III for a 45° tilt angle. In the previous study the 45° tilt angle was found to result in the highest ductile machining-related feed rate, 0.32 mm/min, and grooves with high surface finish.

For this study, straight grooves were also machined at a constant 16 μm depth of cut (t_0) in a water bath using a 20 kRPM spindle speed for all the tests. The resulting force measurements are reported in Figure 4.8.and average specific cutting energies are reported in Figure 4.9.

Table 4.1 - Design of cutting experiment

Factor	Levels
Feed rate (mm/min)	0.28, 0.32, 0.40, 0.64, 0.72, 0.80, 0.88, 0.96

To estimate the specific cutting energy the cutting forces generated during the micromilling of glass grooves were measured on a Kistler 9257B force dynamometer. Force signals were then converted into output voltages using three #5010 Kistler dual mode charge amplifiers with built-in low-pass filters with a fixed 180 kHz cut-off frequency. To avoid aliasing, a Krohn-Hite #3384 filter was also used to establish low-pass cut-off frequencies below 180 kHz. Final force signals were displayed in Dynaware V2.4.1.5 data acquisition software and imported to Matlab V7.1.0.246 technical computing software for further signal conditioning and analysis.

To accurately measure the small-scale forces (< 1 N) test runs were conducted to consider the instrument offset error and signal drift. Small static loads less than 1 N were applied to the dynamometer to simulate loads analogous to those produced during the micromilling process. Signal drift was found to be negligible when restricting the time duration of measurements to a 10 second period. The initial offset error in each collected force signal was corrected using Matlab by averaging the first second of data points (prior to tool engagement with workpiece) and subtracting this average from each data point in the final force signal. This process was executed for each force signal measured.

Effective Feed Rate and Specific Cutting Energy in Glass Micromilling

In conventional milling the theoretical chip thickness is largely determined by the feed per tooth (Equation 4.7). However, the undeformed chip thickness in micromilling might be different in micromilling due to size effects, the rigidity of the machine tool, and tool edge radius. The minimum chip thickness may not be met during each pass of the tool; as a result, rubbing occurs instead of material removal. Typically, in micromachining it has been found that a chip will not form until the undeformed chip thickness is a fraction of the tool edge radius. This fraction has been found to be 0.2 - 0.4 in the micromachining of aluminum and steels (Weule et al., 2001; Vogler et al., 2004; Liu et al., 2006). In this study, the theoretical feed per tooth (~ 10 nm/tooth) is much smaller than the tool edge radius (~ 1 μm). In addition, SEM images and profilometer data of machined grooves in Chapter III provided evidence of rubbing. For this study, the effective feed per tooth in micromilling f_{eff} is introduced and defined as the actual feed of the tool that meets the minimum chip thickness requirement for material removal

To further investigate the actual feed of the tool during micromilling the feed mark spacing was examined using the SEM images of machined grooves from the previous experimental study in Chapter III. The feed mark spacing can give valuable information into chip formation as the spacing can indicate the chip thickness that is actually being removed during a cutter pass in which cutting is performed and not edge rubbing/elastic deformation. Hence, it can give an estimation of the effective feed per tooth. The feed mark spacing along the groove bottom for the 0.24 mm/min and 45° tilt

angle condition was estimated using SEM to be approximately 2 μm which was much larger than the theoretical feed per tooth of 4 nm.

In conventional milling the average surface roughness of the machined surface can be estimated based on the kinematics of the milling process using Equation 4.30.

$$R_a = \frac{s_z^2}{32r} \tag{4.30}$$

where R_a is the average floor surface roughness, in end milling s_z is the feed per tooth in milling, which is considered analogous to the feed mark spacing in this study, and r is the radius of the tool cutting edge. The average surface roughness R_a along the groove bottom was previously measured to be 47 nm for the 0.24 mm/min and 45° tilt angle condition (Figure 3.11). Inputting this R_a value into Equation 4.30 along with a tool edge radius of 1 μm, s_z was solved for and found to be 1.2 μm. This compared reasonably with the 2 μm measurement of the feed mark spacing using SEM than with the theoretical feed per tooth (6 nm/tooth). In addition, the feed mark spacing visible on other machined grooves using various feed rates and tilt angles also compared favorably with results from Equation 4.30. Hence, it was considered that Equation 4.30 was a good estimation for the effective feed per tooth f_{eff} under the conditions tested in this study.

For this study, s_z was considered to vary linearly with the feed rate v_f (mm/min) as shown in Equation 4.31.

$$s_z = a v_f + b \tag{4.31}$$

In the previous experimental study in Chapter III the surface roughness data was measured mostly for grooves machined with 45° and 60° tilt angles in order to investigate

the surface finish for surfaces produced through ductile and/or brittle cutting. The average surface roughness data measured along the bottom of the grooves machined with these two tilt angles were used with Equation 4.30 to calculate s_z. Then a linear trend line in the form of Equation 4.31 was found by fitting the calculated s_z values with the corresponding feed rate v_f. While a linear trend line was found to fit the data well for the conditions in this study, it is not necessarily recommended for feed rates outside the realm of this study. For example, a nonzero b value would indicate a nonzero feed per tooth when the feed rate v_f is zero, which would not be realistic. For this study, a was assumed constant for all feed rates for the same cutting tool since the edge radius is the same, and the coefficient b was considered to vary. With this being considered, the linear coefficient a was found using the least squares method where an optimum value for a was found to be 1.07. The coefficient b was then found for each tilt angle using the measured surface roughness data for the 0.12 mm/min condition, as shown in Figure 3.11. The resulting a and b coefficients for the linear trends for s_z with respect to the feed rate v_f are shown in Table 4.2, and the plots for the linear trends are given in Figure 4.7. In considering s_z as the effective feed per tooth $f_{eff,}$ the linear trends were then used to estimate an average specific cutting energy curve with respect to the average chip thickness values calculated using the effective feed per tooth.

Table 4.2 - Coefficients for the s_z and v_f linear relationship (a = 1.07)

Tilt Angle, α (°)	b
0	1.57
15	1.66
30	1.47
45	1.15
60	1.27

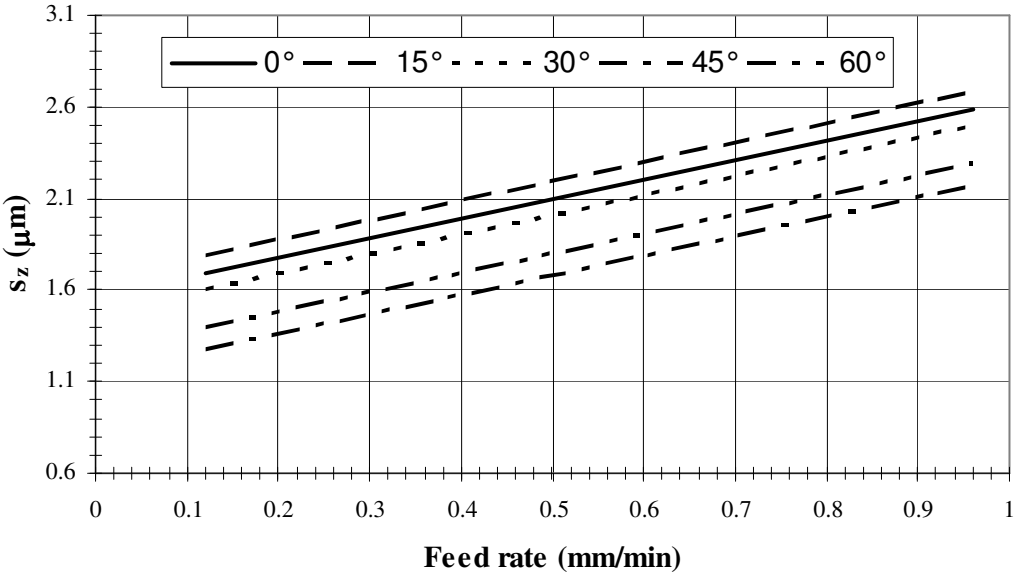

Figure 4.7 - Plotted linear trends for s_z versus feed rate for the tilt angles considered in this study

In order to predict the maximum normal and shear stresses (Equation 4.23) the specific cutting energy needed to be determined. Specific cutting energy is the energy required to remove one unit amount of material. In the standard milling configuration using cylindrical end mills the specific cutting energy can be calculated by dividing the machining forces by the chip area per unit time. However, in milling the cutting forces and chip area vary during a tooth pass, so, instead, average specific energies can be

approximated using average milling forces and average chip area. For this study in micromilling with a ball end mill, the average chip area A_C was calculated through consideration of the average chip thickness when $f_t = f_{eff}$ and the depth of cut t_0 as shown in Equation 4.32.

$$A_C = \frac{f_{eff}\, t_0}{2} \tag{4.32}$$

where f_{eff} is the effective feed per tooth determined by the linear trend given in the form of Equation 4.31 with the coefficients in Table 4.2. Equation 4.33 is then used to calculate the average specific cutting energy.

$$u_0 = \frac{F_C}{A_C} \tag{4.33}$$

where u_0 is the average specific cutting energy and F_c is the average cutting force.

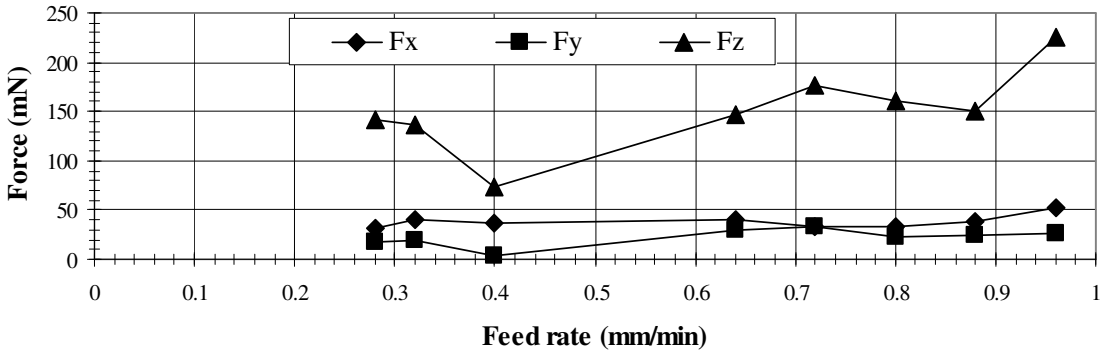

Figure 4.8 - Measured cutting forces using orientation shown in Figure 4.1

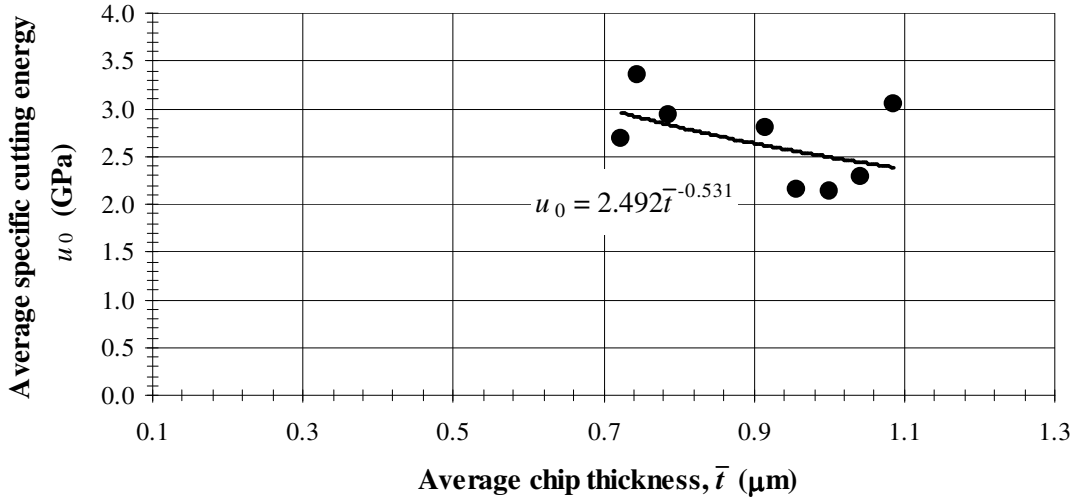

Figure 4.9 - Average specific cutting energy versus the average chip thickness for the feed rates given in Table 4.1. The fitted linear trend line, Equation 4.34, is also shown.

The cutting forces generated during the ball end milling of linear, constant-depth grooves in glass were measured, and the average values for each level of feed rate are reported in Figure 4.8. The average specific cutting energy, shown in Figure 4.9 was calculated at each level of feed rate using Equation 4.33 by inputting the measured average cutting force, F_x, and the average cross sectional area (Equation 4.32). In micro-cutting an increase in the specific cutting energy with decrease in chip load is observed due to the size effect. As seen in Figure 4.9, a similar trend was found in this study. The values of the average specific cutting compare favorably with the reported 3.1 GPa specific grinding energy when grinding soda lime glass with a diamond wheel at 5 μm depth of cut (Huerta et al., 1976a). The micromilling process in Chapter III was likened to that of grinding in that cutting appears to occur along local asperities on the cutting edge. The tool edge radius to chip load ratio (~ 1) was expected to yield a high effective

negative rake angle. A power law trend was used to fit the specific cutting energy data and later on implemented into the cutting force model to predict the state of stress in the shear plane. The power law trend captures the effect of decreasing specific cutting energy with increase in the chip thickness that is typical in micro-cutting. The trend is shown in Figure 4.9 and given in Equation 4.34 as follows:

$$u_0 = 2.492\bar{t}^{-0.531} \tag{4.34}$$

where u_0 is the average specific cutting energy in GPa and $\bar{t}$ is the average chip thickness in μm.

Stress Prediction

In this study the normal and shear stresses in the shear plane were predicted for given conditions during glass micromilling. The conditions and parameters were chosen in order to compare the results with the previous experimental results in Chapter III. Accordingly, the groove geometry for the predictions was based on the micromilling of linear grooves at a constant DOC (t_0) of 16 μm with a ball end mill. The workpiece for the simulations was crown glass, whose machining behavior during micromilling is based on the specific cutting energy curve Equation 4.34. The spindle speed was kept constant at 20 kRPM throughout all simulations. The geometry of the cutting tool used for the simulation is the same as the geometry used in the previous study in Chapter III.

The rake (α_0), friction (α_f), and shear (ϕ) angles and the chip thickness (t), shown in Figure 4.3, are needed to describe the orthogonal cutting process. The rake angle of

the machine tool changes locally and the values given by the manufacturer are reported in Appendix B. However, no information was given for tilt angles less than 30° tilt angles. Thus, as an average for this study, the rake angle is considered to be 0° for all tilt angles. The friction angle is chosen to be 51° as this value is found to be typical in the machining of metals (Kalpakjian et al., 2003). The shear angle is calculated to be 20° using the shear-angle relationship presented in Equation 4.13.

The machining of glass is expected to change from ductile deformation to brittle fracture when the undeformed chip thickness exceeds a critical chip thickness. In milling the undeformed chip thickness varies with the engagement between the cutting tool and workpiece. For machining linear constant-depth grooves the largest undeformed chip thickness values will occur when the cutting edge is located at the middle of the groove (centerline of the tool path), as illustrated in Figure 4.2(b), so when the cutting edge is at this position the probability of brittle fracture is expected to be at its highest. The distribution of the chip thickness at this location is shown in Figure 4.2(a) and given by Equation 4.6. For simplicity an average chip thickness (f_{eff} /2) in consideration of the effective feed rate was used in this study for creating an average specific cutting energy curve based on machining experiments and for the subsequent prediction of stresses.

The stress was predicted in order to estimate the stress state in the shear plane during glass micromilling and the controlling factors and levels are shown in Table 4.3. The controlling factors for this study were the feed rate and tilt angle. The levels for both the feed rate and tilt angle were selected in order to compare the results with the previous experimental study in Chapter III. In addition, the tested feed rate range was expanded to

incorporate the feed rates used to generate force data for the average specific cutting energy curve shown in Figure 4.9.

Table 4.3 - Controlling factors in simulations

Factors	Level
Tilt angle (degrees)	0, 15, 30, 45, 60
Feed rate (mm/min)	0.12, 0.36, 0.60, 0.8, 0.96

As shown in Figure 4.10, the predicted shear stresses are significantly large for cutting of glass. Thus, the compressive stress is very important for suppressing crack propagation from the shear plane. It is expected that as the compressive stress is reduced the chance for brittle fracture increases. The predicted compressive stresses given in Figure 4.11 are found to compare favorably with the experimental results in Chapter III. When machining at 0.12 mm/min it was found that a groove could be machined in the ductile mode with a 45° and 60° tilt angle. Machining with a 30° tilt angle resulted in small pits scattered along the groove bottom but cutting was still found to be dominated by the ductile regime. Accordingly, the predicted compressive stresses are highest for these three tilt angles at the 0.12 mm/min. Increasing the feed rate results in a reduced compressive stress. In Chapter III, increasing the feed rate to 0.24 mm/min resulted in fracture for all tilt angles except 45°. For all feed rates considered, 45° is predicted to result in the highest compressive stress in comparison to the other tilt angles. This was found in good agreement with experiments as the 45° tilt angle produced the highest ductile-regime related feed rate of 0.32 mm/min. Based on the results of this prediction and experimental results for the machining conditions/parameters used in this study it can

be concluded that the compressive stress normal to the shear plane needs to be at least in the 29-31 GPa range in order for cutting in the ductile regime to be favorable.

Effect of Tilt Angle and Feed Rate on Cutting Regime Transition via Stress Modeling

Compressive stress in the cutting zone during machining has been shown to increase the ductility of work material. Four ways in which the compressive stress affects the behavior of materials are as follows (Kalpakjian et al., 2003):

- It substantially increases the strain at fracture;
- It has little or no effect on the shape of the true stress-true strain curve but only extends it;
- It has no effect on the strain or the maximum load at which necking begins; and
- The mechanical properties of metals are generally not altered.

The predicted compressive stresses shown in Figure 4.11 indicates that a increase in the tilt angle from 0° to 45° will increase the compressive stress normal to the cutting zone shear plane. This correlates with the experimentally observed trends in Chapter III in which increasing the tilt angle from 0° at 0.12 mm/min resulted in decreasing amount of fracture until no evidence of fracture was found when machining with a 45° tilt angle. In addition, the predicted compressive stresses decrease with in increase in feed rate regardless of tilt angle and this was also observed in experiments. Increasing the feed rate above the transition-related feed rate further increased the occurrence of fracture. Consequently, based on the results of this study it can be concluded that the fracture toughness of the material during cutting can be increased according to adjustment of the tilt angle and/or feed rate due to the effect of the compressive stress.

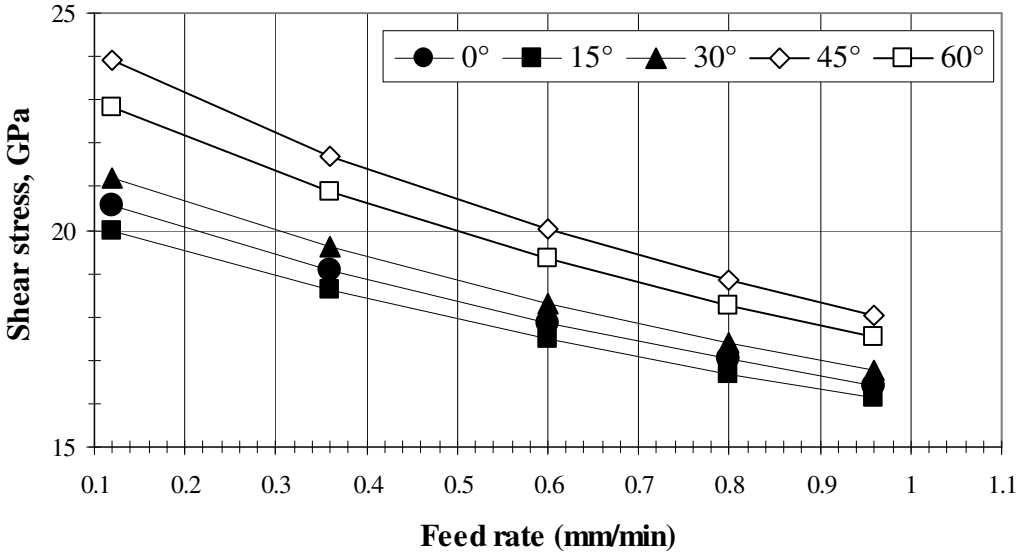

Figure 4.10 - Predicted shear stress versus tilt angle

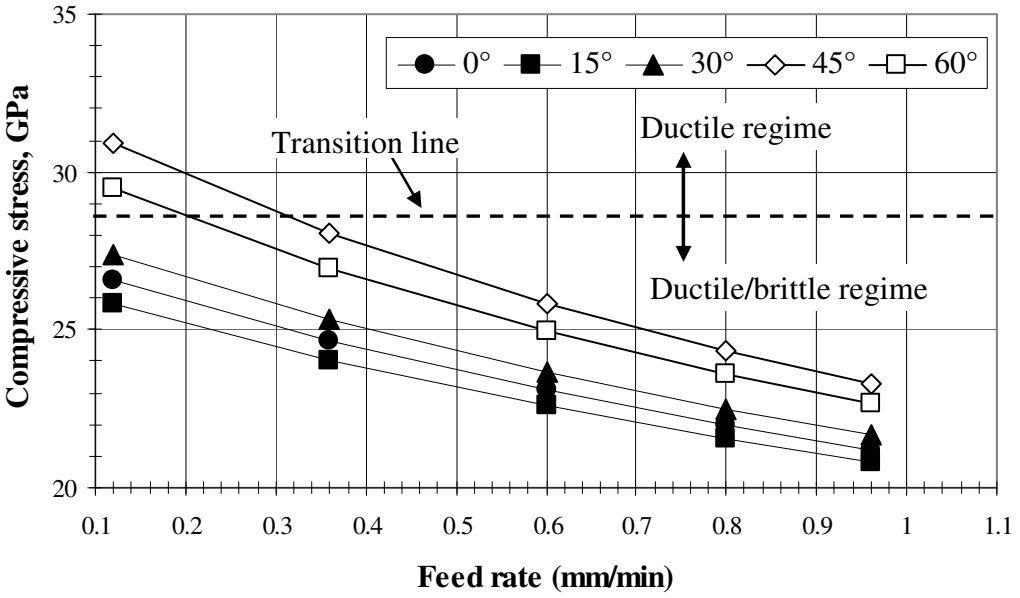

Figure 4.11 - Predicted compressive stress versus feed rate (the dashed line is the transition line that correlates with the observed cutting regimes in Chapter III)

Temperature Prediction and Discussion

Fracture toughness data as a function of temperature was not found for the crown glass workpiece in this study. However, soda lime glass is believed to exhibit similar mechanical and thermal behavior, since both optical glasses have a similar amount of SiO_2 (~ 70%) and a similar glass softening temperature (Le Bourhis et al., 2003; Yoshida et al., 2005; Ji et al., 2006). The density and specific heat for soda lime glass is 2.5 kg/m^3 (Bansal et al., 1986) and 884 J/(kg-K) (Tipler, 1999), respectively. Using these material properties with the measured cutting force data (Figure 4.8) and associated machining parameters the general temperature rise in glass micromachining can be estimated. However, it should be noted that the material removal rate in Equation 4.29 is based on a conventional machining assumption, which is that a cutting chip is being generated during every pass of the cutting edge. In Chapter III under similar machining conditions/parameters as simulated in this study it was found that a chip may not be formed every tooth pass. Hence, an effective feed rate was introduced in this study and used to predict the temperature in the cutting zone.

The 45° tilt angle and 0.32 mm/min feed rate condition was selected from the parameters tested in this study. All other parameters such as the spindle speed, geometry of the ball end mill, and depth of cut were kept the same. The temperature rise ΔT was then calculated using Equation 4.29 to be 86 K. This result compares reasonably with the 30-40 K temperature rise simulated under similar conditions in micro-cutting of Al-7075-T6, as well as a 320-330 K temperature rise in Ti-6Al-4V (Lu et al., 2007). The higher temperature rise for Ti-6Al-4V was reasoned to be because of the lower thermal

conductivity, 6-7 W/(m-K) for Ti-6Al-4V, in comparison to 167 W/(m-K) for aluminum alloys. The low thermal conductivity was reasoned to make the heat difficult to transfer outside the deformation zone during the chip formation (Lu et al., 2007). Accordingly, the thermal conductivity for glass, 1.25 W/(m-K) is significantly lower than both titanium and aluminum alloys (Holloway, 1973). Therefore, it would be expected that the temperature rise in glass micro-cutting would be greater than that of predicted 320-330 °C in Ti-6Al-4V. Indentation of soda lime float glass has shown that the glass workpiece will soften and the fracture toughness will increase around half of the glass softening temperature (~ 600 °C) (Le Bourhis et al., 2000). As a result, the calculated temperature rise for the simulated condition in this study needed to be approximately 300 °C to significantly increase the ductility of the glass workpiece at the tip of the tool cutting edge. Since ΔT = 86 °C correlates to an absolute temperature around 384 K (110 °C), which was much smaller than 300 °C, it was then concluded that the temperature effect, as predicted using a conventional approach, in the micromilling of glass under the presented conditions and parameters was not significant enough to increase the ductility of the workpiece at the tool tip and was no longer considered in this study.

Indentation studies of soda lime glass have shown that when the temperature in the deformation zone is elevated the glass turns to be more ductile. An increase in the fracture toughness (Figure 2.4) and a decrease in both hardness (Figure 2.5) and elastic modulus (Figure 2.6) have been observed. However, the temperature predicted in this study based on a conventional approach was found to be too small to increase ductility. It should be noted that the cutting process on the micro-scale is very complicated

involving elastic/plastic deformation, high strain rates and temperatures for which material properties vary during the process. Accordingly, it is not expected that the temperature predicted using a conventional approach is accurate as previously indicated by the results of Lu et al., and the temperature in the cutting zone will be revisited in future work as the machining-related micro-scale phenomena on the workpiece material behavior are better understood.

Conclusions

The stress and temperature in the cutting zone shear plane have been investigated for the micromilling of glass with a ball end mill. A mechanistic model of the ball end milling process and experimental results/observations were used to predict the shear and compressive stresses in the shear plane. Temperature generated in the primary deformation zone of the micromilling process was investigated using a conventional approach. Some conclusions were drawn that are expected to prove insight in predicting the ductile-brittle transition in glass machining:

- An effective feed rate has been introduced in order to predict the actual chip thickness due to the size effect during the micromachining process;
- A specific cutting energy curve has been generated using measured force data and predicted cross-sectional area with consideration of the effective feed rate;
- The trends for the predicted compressive stress are found to agree well with experimental observations of the cutting regimes in Chapter III. The fracture toughness of glass in the cutting zone during micromilling has been shown to be

pressure dependent. It is concluded that the compressive stress normal to the shear plane must be at least 29-31 GPa to best facilitate ductile machining using the machining conditions/parameters in this study; and

- The temperature in the cutting zone in micromilling under the presented conditions is predicted using a conventional approach to be too small to increase the ductility of glass in the cutting zone during machining.

CHAPTER V

CONCLUSIONS AND RECOMMENDATIONS

Conclusions

In this work, the ductile-brittle cutting regime transition as a function of feed rate and tool tilt angle during the micromilling of glass has been studied both experimentally and through simulation. Emerging micro-scale applications have increased the demand for the use of brittle materials due to their excellent thermal, chemical, and wear resistance characteristics, as well as a high stiffness to density ratio. However, brittle materials have to be machined using nontraditional methods that can involve hazardous operations. Fortunately, it is found that the glass can be machined in a ductile regime under certain controlled cutting conditions. Machining in the ductile regime can produce continuous cutting chips and a smooth surface with no evidence of fracture. It is known that the cutting regime transition from brittle to ductile cutting regimes is attributed to the effect of pressure and temperature in the cutting zone. The transition has also been correlated to the undeformed chip thickness. However, the mechanism behind ductile regime machining still cannot be fully explained and further machining research is required to find optimum cutting configurations to produce high quality micro-scale features. In this work, cutting conditions were selected for the micromilling process and performed on crown glass. The effect of tilt angle on the cutting regime transition was evaluated through experimental observation, mainly through SEM, and through the resulting surface finish measured by a noncontact profilometer. The stress state in the cutting zone shear plane was also predicted through a combined approach involving

mechanistic ball end mill modeling and implementation of experimental data/observations, and the ensuing predicted stresses were correlated with experimentally observed results. The temperature in the cutting zone was also predicted based on a conventional approach. Conclusions for this work are as follows:

- Cutting regimes of glass micromilling can be rubbing, ductile machining, and brittle machining depending on uncut chip thickness.

During each milling pass, surface roughness was found to decrease from the entry zone to the groove bottom and then increase to the exit zone regardless of the cutting regime due to the pronounced rubbing effect in micromilling. Increasing the undeformed chip thickness prior to reaching the critical chip thickness decreased the rubbing effect and promoted ductile cutting, which produced the highest quality surface finish without introducing brittle fracture into the machined surface. Once the critical chip thickness was reached, brittle cutting initiated and fracture continued to propagate throughout the cut pass until the cutting edge disengaged from the glass workpiece.

- Tilt angle and feed rate can be optimized to achieve ductile cutting regime in glass micromilling.

The occurrence of the cutting regime transition was found to occur at a certain feed rate, as is typical in glass micromachining. A tilt angle of 45° had a highest ductile machining-related feed rate (0.32 mm/min) for the conditions in this micromilling study. Ductile machining was also found to occur when machining at the lowest feed rate tested, 0.12 mm/min, with a 60° tilt angle. Machining at this feed rate with all other tilt tested angles (0°, 15°, 30°) resulted in brittle cutting. While machining with a 30° tilt angle at

0.12 mm/min produced minimal fracture on the machined surface where most of the groove was cut in the ductile regime, brittle machining was found to be dominant with 0° and 15° tilt angles regardless of the feed rate tested.

- Surface finish in glass micromilling correlates well with cutting regimes.

The best surface roughness values were found to occur when the groove was machined in the ductile mode. A tilt angle of 45° had a highest ductile machining-related feed rate (0.32 mm/min) in this study and the surface finish was significantly better (less than 60 nm) at feed rates less than 0.32 mm/min. Brittle machining with 45° and 60° tilt angles was generally observed to first occur in the entry zone and the exit zone, respectively, as the feed rate gradually increased. As a result, a significant surface roughness increase was observed in the exit zone after the cutting regime transition-dependent feed rate was reached, which indicated the onset of brittle cutting regime. During each milling pass, surface roughness was found to decrease from the entry zone to the groove bottom and then increase to the exit zone regardless of the cutting regime due to the pronounced rubbing effect in micromilling..

- Higher compressive stress in the shear plane facilitates ductile cutting while cutting zone temperature is assumed negligible.

The fracture toughness has been shown to be pressure dependent in glass micromilling. Conditions in experiments that resulted in ductile cutting, namely larger tilt angles and smaller feed rates, were predicted to result in the highest compressive stresses normal to the cutting zone shear plane. For the machining conditions in this study, it was concluded that these compressive stresses needed to be at least 29-31 GPa to

best facilitate ductile machining. The temperature was predicted negligible to further increase the ductility of glass in the cutting zone during machining.

Recommendations on Future Work

- Study of effective undeformed chip thickness and chip formation process in glass micromilling.

In this work, an effective feed rate in glass micromilling was predicted based on measured surface roughness, feed rate, and tool geometry. In estimating the specific cutting energy average chip thicknesses were used based on the predicted effective feed rate. A more extensive study could be conducted to determine the actual feed rate. Such an experiment might include a high speed camera which would be used to monitor machining experiments in effort to try and capture visual evidence of continuous or discontinuous chip generation, as well as insight into how many tool passes are required before the cutting chip is formed and removed. Generation of continuous chips during micromilling would provide further proof and insight into the ductile cutting regime. In this study the machining was performed in a water bath and it was found to be difficult to extract the cutting chips. In addition, the resulting surface finish and SEM images of machined grooves indicated the impact of the minimum chip thickness on chip formation that is typical in mechanical micromachining. Insight into the actual undeformed chip thickness and chip formation would more clearly define the different cutting regimes in terms of the machining parameters and conditions.

- Characterization of machined glass surface and subsurface.

In this study, ductile cutting conditions have been identified with micromilling process parameters and conditions through experiments and analysis of surface finish. The next step would be to characterize the surface and subsurface in terms of its mechanical properties. Evaluation of the mechanical properties of machined surfaces on the micro-scale is very important in producing a product of consistent and high quality. Machining brittle materials in the ductile regime is expected to produce a stronger surface due to minimal induced defects/fracture on the machined surface. Accordingly, machined surfaces produced through various cutting regimes during micromilling could be quality tested in terms of its mechanical properties using micro-scale evaluation techniques such as nanoindentation. Data from nanoindentation can be used to determine hardness, elastic modulus, strain-hardening exponent, fracture toughness (for brittle materials), and viscoelastic properties (Fischer-Cripps, 2004). Also, the nano-scale indentation depths provide a better evaluation of surface properties on the micro-scale in comparison to more conventional techniques. The performance of micro-scale parts depend more on surface properties than the bulk due to the small size scale of its features.

Cracks in brittle materials can initiate in indentation at the elastic-plastic boundary formed beneath the tip of the indenter. These cracks may or may not propagate to the surface. As a result, the indented surface may appear to be ductile but actually have fracture beneath the surface. Similarly, in micromachining Nakamura et al. evaluated the occurrence and extent of subsurface crack formation by obliquely sectioning and chemical etching the workpiece after machining and observing the crack formation via a scanning force microscope and a scanning laser microscope. In some

cases, subsurface cracks were found to form before the critical depth of cut of cracks formed on the surface (Nakamura et al., 2003). A similar study could be conducted to analyze the subsurface of machined features using the micromilling process. In addition, the effect of subsurface damage on the resulting surface mechanical properties could be analyzed using the aforementioned nanoindentation technique.

- Stress and temperature modeling in micromilling of amorphous materials.

Modeling of the machining process on the macro-scale has been proven in industry to be beneficial in a variety ways including the selection of optimal process parameters in fabricating a machined product with high quality quickly at low cost and prediction of tool condition and resulting machined surfaces. However, micro-scale phenomena due to the scaling effects require the use of new models to describe the machining process. Currently, minimal research has been performed in development of models for the micromilling for brittle materials. Such a model would be very beneficial in analyzing the cutting regime transition and predicting optimal machining parameters for the fabrication of micro-scale devices composed of amorphous/brittle materials. This study was conducted based on a stress model based on many conventional machining assumptions due to lack of insight into the underlying mechanics of the process at the micro-scale. However, the results of this work will help further develop the understanding of the machining mechanics on the micro-scale and brittle material behavior under the high stress and strain rates typical in micromachining. The prediction of cutting zone temperature in this work was also based on a conventional approach.

Once more insight is realized into the machining-related phenomena on the micro-scale it is recommended that the temperature in the cutting zone again be readdressed.

- Relationship among fracture toughness, cutting regime, and process information.

In this work, stress and temperature modeling was used to predict machining stress and cutting zone temperature in glass micromilling. The compressive stress in the shear plane was correlated with an apparent increase in fracture toughness through the experimental observation of the different cutting regimes. While it was apparent that the fracture toughness of glass could be changed through the control of the compressive stress in the shear plane by process parameters and conditions, the actual relationship among the fracture toughness, cutting regime, and process information is still not clearly understood and a more extensive study is needed to gain more insight.

APPENDICES

Appendix A

Technical Drawings for Micromilling Workstation

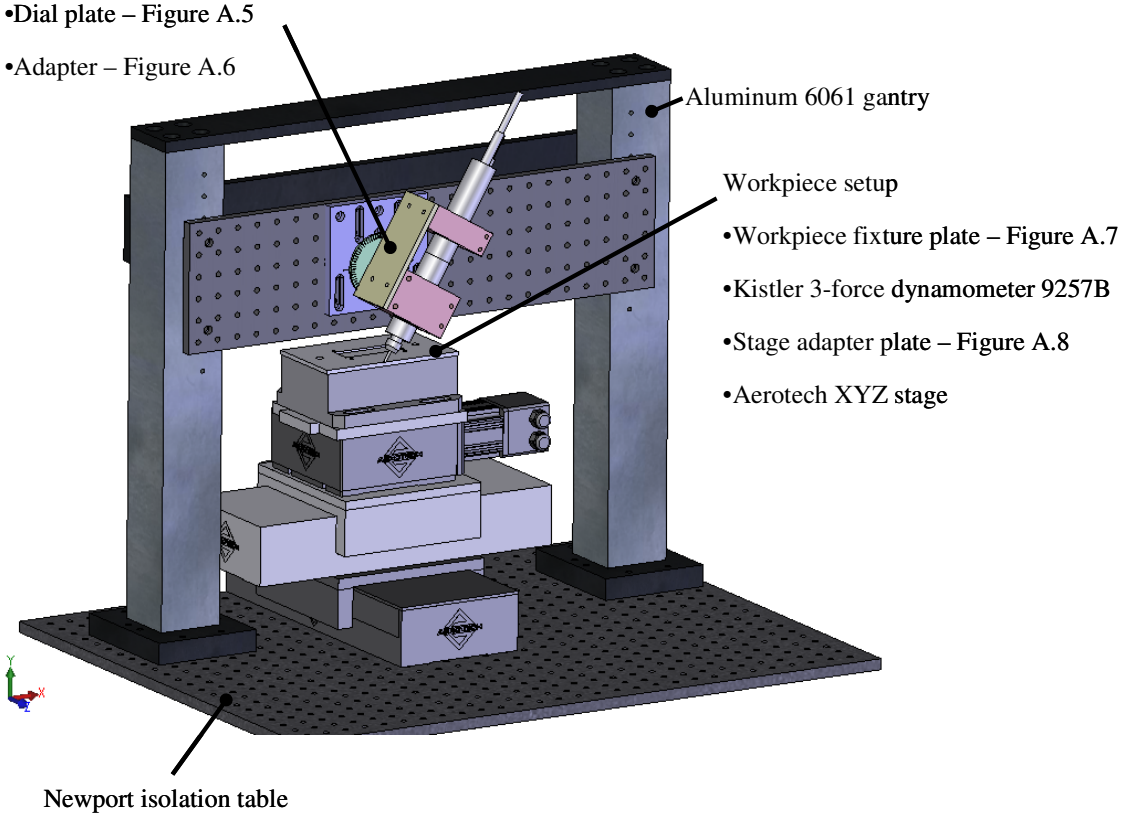

Figure A.1 - Micromilling workstation

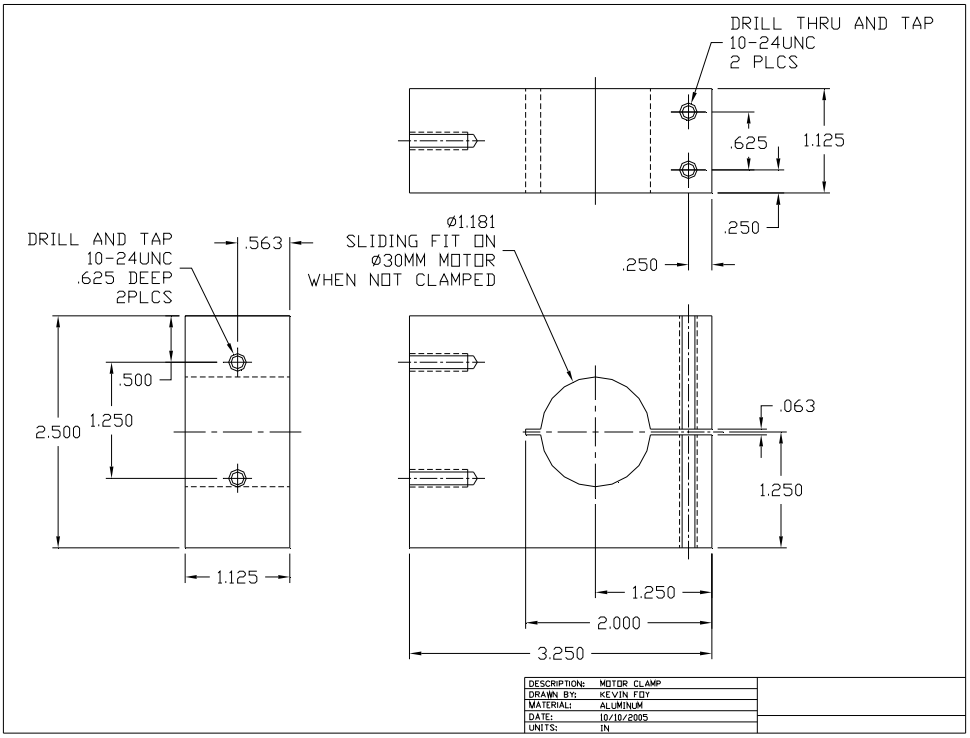

Figure A.2 - Motor clamp

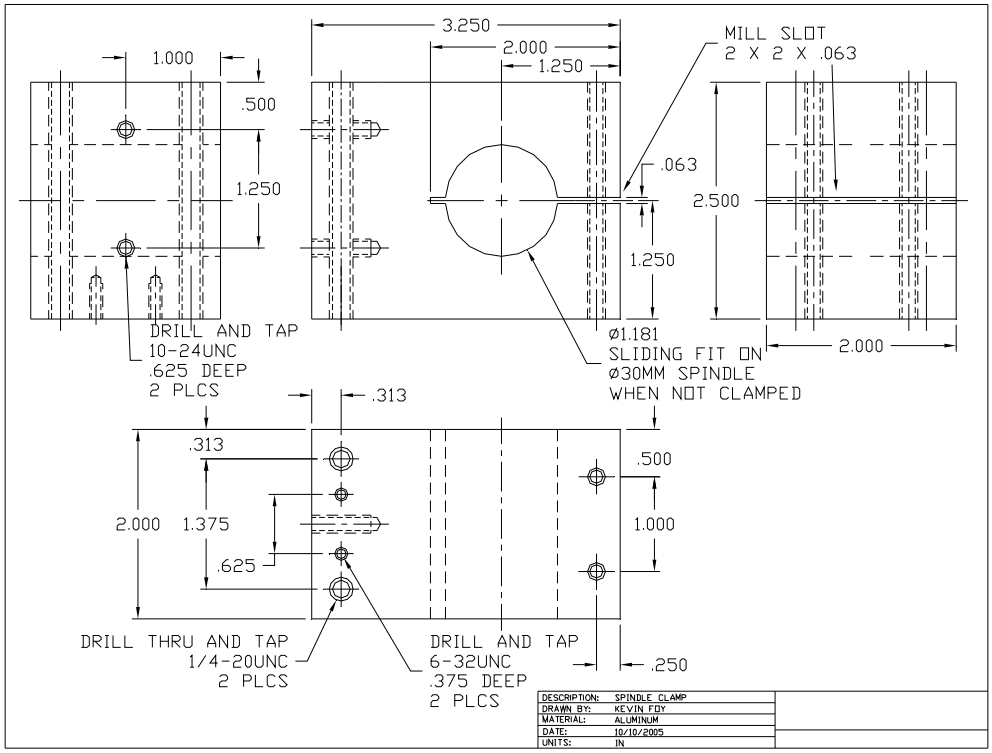

Figure A.3 - Spindle clamp

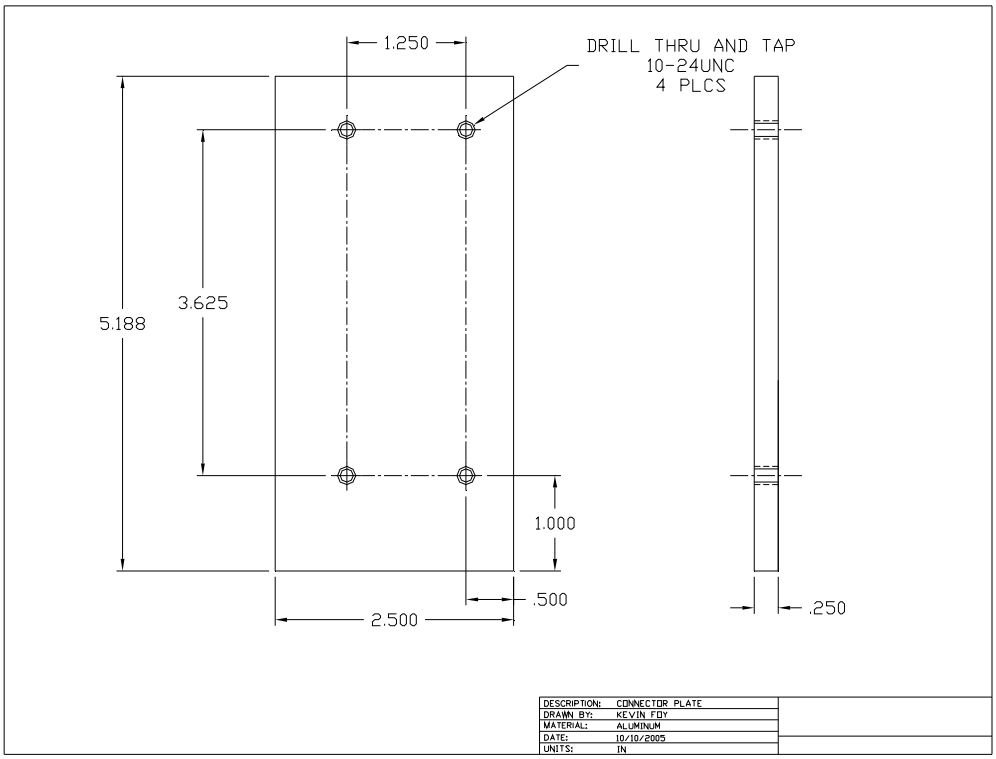

Figure A.4 - Connector plate

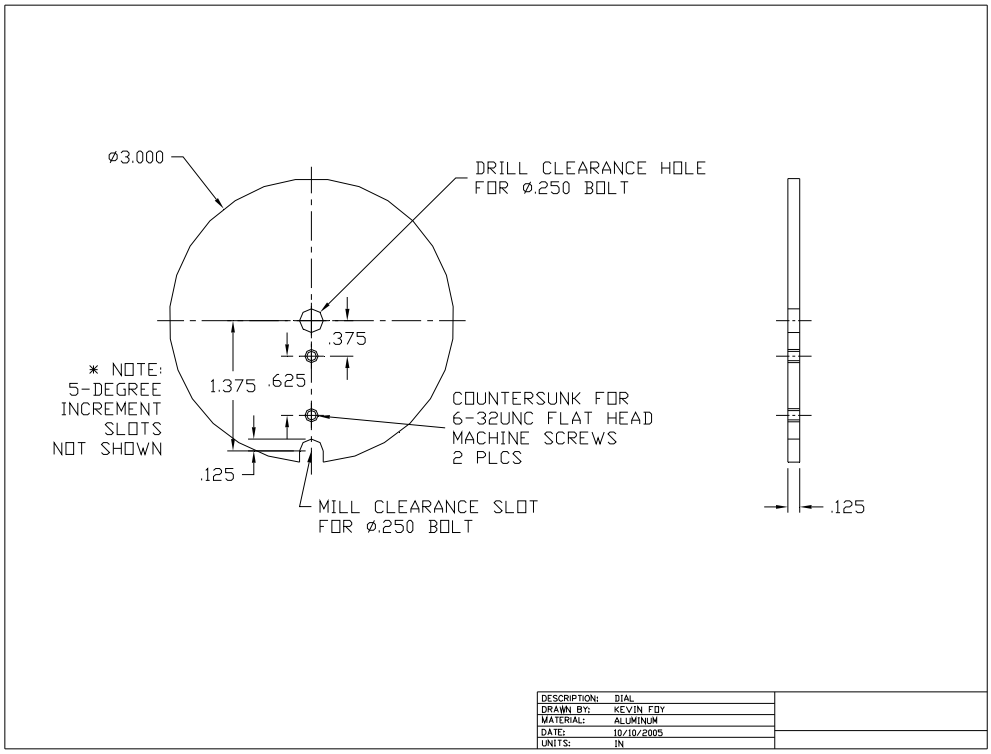

Figure A.5 - Dial plate

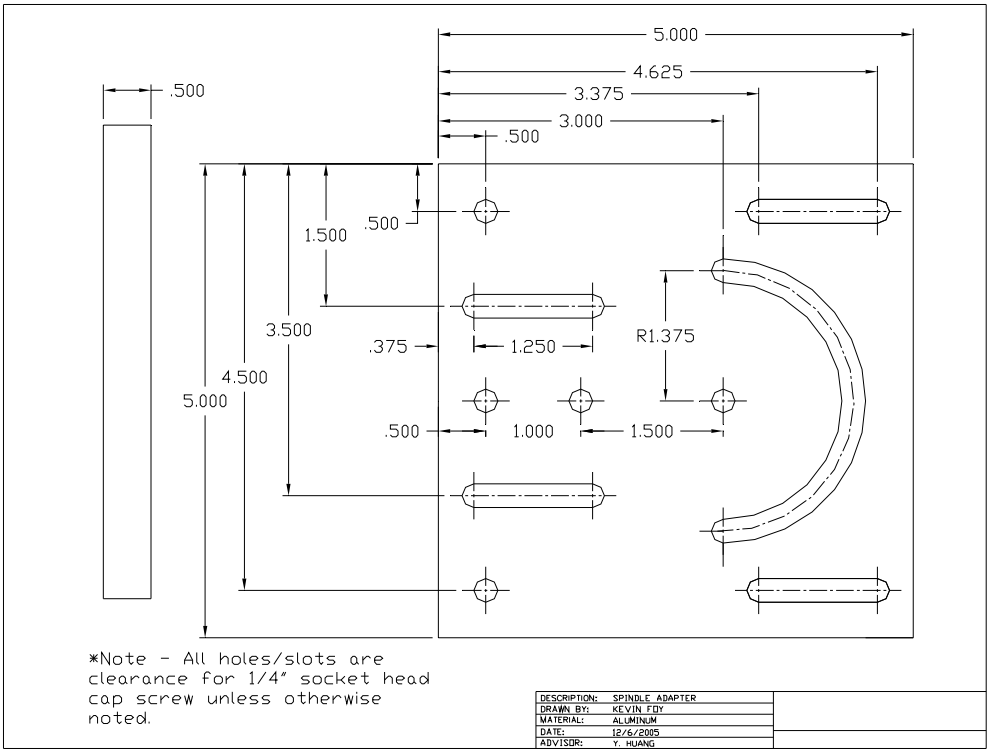

Figure A.6 - Spindle adapter

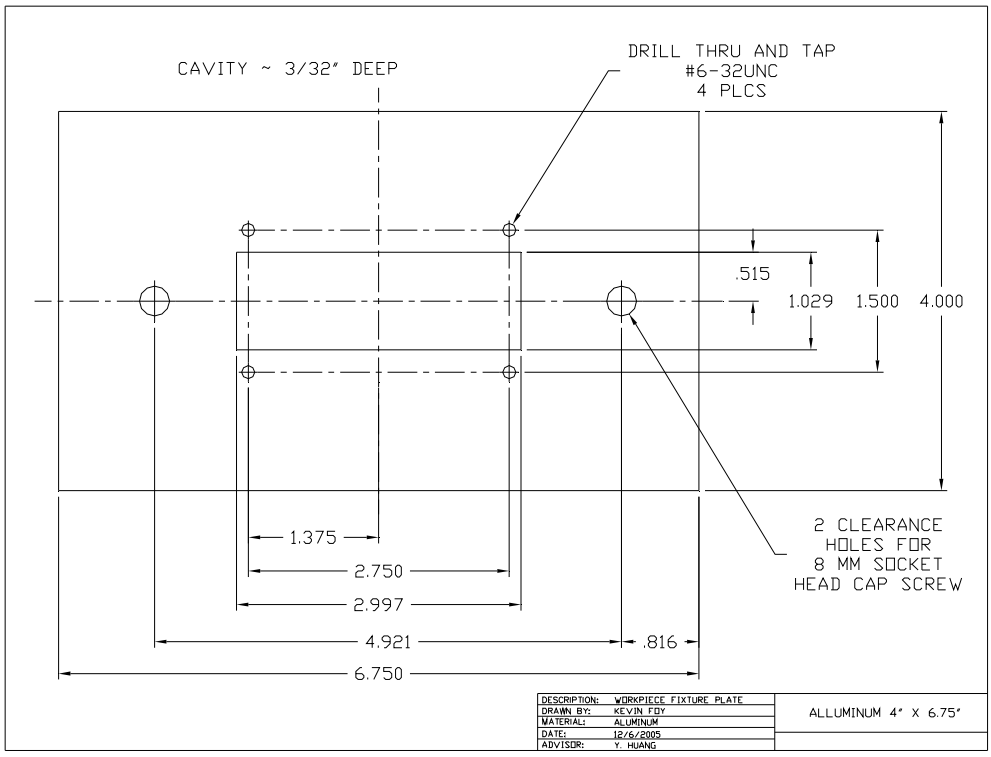

Figure A.7 - Workpiece fixture plate

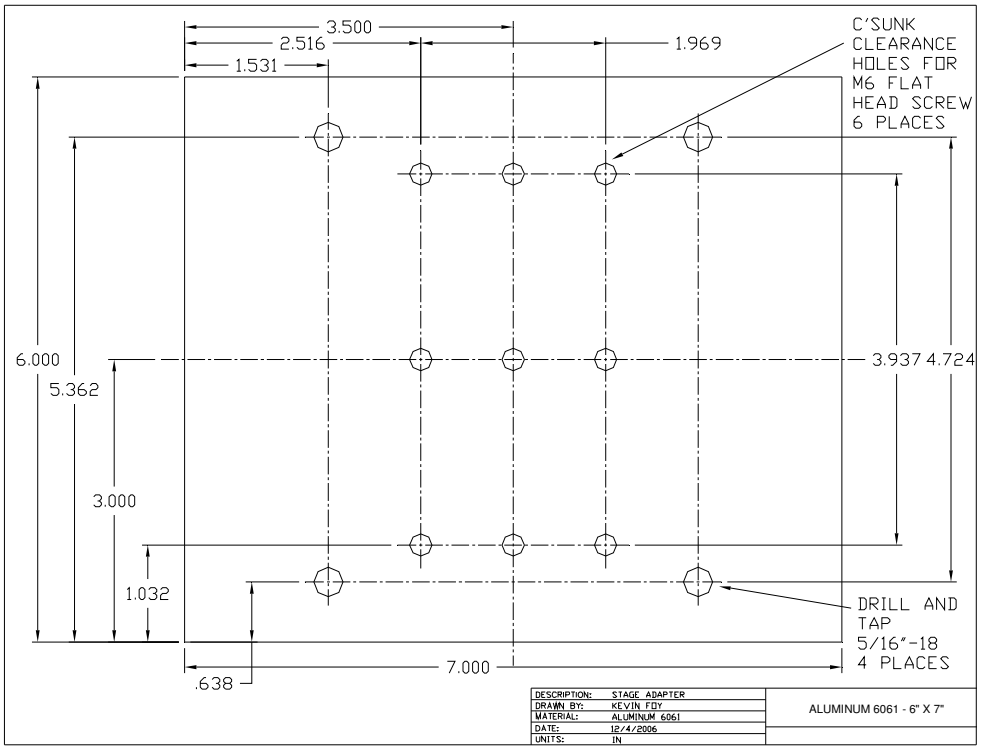

Figure A.8 - Stage adapter

Appendix B

Tool Manufacturer Information for Mitsubishi Ball End Mill #VC-2ESB Series

ミラクル® エンドミルシリーズ

VC-2ESB Size up

2枚刃 ミラクル®ショートボールエンドミル(ES)

最適な突き出し長さを実現！

特長
●小型マシニングセンタでのダイレクトミーリング加工に最適なエンドミルシリーズです。
●剛性の高い1D刃長とシャンク長を最短に設定することにより、HSK、焼きばめホルダでの使用に高性能を発揮します。
●耐熱性に優れた「高硬度加工用ミラクルコーティング」の適用によって長寿命を実現します。
●ドライ切削においても優れた性能を示します。

VC-2ESB Size up
2枚刃 ミラクル®ショートボールエンドミル(ES)
R ±0.01
D1<6 0 − -0.028
6≦D1 0 − -0.036

UWC VC 30°

●小型マシニングセンタでのダイレクトミーリング加工に最適なエンドミルシリーズです。

図1 図2

単位:mm

呼び記号	ボール半径 R	外径 D1	刃長 ap	首下長 L3	首径 D5	全長 L1	シャンク径 D4	刃数 N	在庫	タイプ
Size up VC2ESBR0015N006	0.15	0.3	0.3	0.6	0.27	30	4	2	●	図1
Size up VC2ESBR0020N008	0.2	0.4	0.4	0.8	0.36	30	4	2	●	図1
Size up VC2ESBR0030N012	0.3	0.6	0.6	1.2	0.56	30	4	2	●	図1
Size up VC2ESBR0040N016	0.4	0.8	0.8	1.6	0.76	30	4	2	●	図1
VC2ESBR0050	0.5	1	1	–	–	30	4	2	●	図1
Size up VC2ESBR0050N025	0.5	1	1	2.5	0.96	30	4	2	●	図1
VC2ESBR0075	0.75	1.5	1.5	–	–	30	4	2	●	図1
Size up VC2ESBR0075N040	0.75	1.5	1.5	4	1.46	30	4	2	●	図1
VC2ESBR0100	1	2	2	–	–	40	6	2	●	図1
Size up VC2ESBR0100N060	1	2	2	6	1.96	40	6	2	●	図1
VC2ESBR0150	1.5	3	3	–	–	40	6	2	●	図1
Size up VC2ESBR0150N080	1.5	3	3	8	2.96	40	6	2	●	図1
VC2ESBR0200	2	4	4	–	–	40	6	2	●	図1
Size up VC2ESBR0200N080	2	4	4	8	3.96	40	6	2	●	図1
VC2ESBR0250	2.5	5	5	–	–	40	6	2	●	図1
Size up VC2ESBR0250N120	2.5	5	5	12	4.96	40	6	2	●	図1
VC2ESBR0300	3	6	6	–	–	40	6	2	●	図2
Size up VC2ESBR0300N130	3	6	6	13	5.85	40	6	2	●	図2
VC2ESBR0350	3.5	7	7	–	–	50	8	2	●	図1
VC2ESBR0400	4	8	8	–	–	50	8	2	●	図2
VC2ESBR0500	5	10	10	–	–	60	10	2	●	図2
VC2ESBR0600	6	12	12	–	–	65	12	2	●	図2

1

●：標準在庫品

Figure B.1 - Manufacturer catalog page for VC-2ESB Series. Product #VC2ESBR0020N008 was the ball end mill used in experiments

MITSUBISHI

2008/1/21

件名：VC-2ESB のボール切れ刃形状調査

平素より弊社切削工具をご使用いただきありがとうございます。
ご依頼のありました、ボールエンドミル（VC-2ESB R0.2）の切れ刃形状について調査を行いましたので、以下にご報告させていただきます。

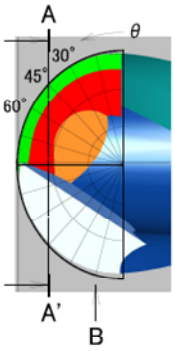

図 1：ボール切れ刃外観

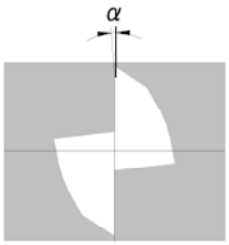

図 2：半径方向すくい角 α
（A-A'断面）

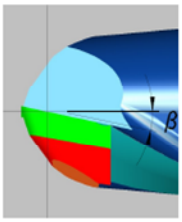

外周刃ねじれ角：30°
図 3：軸方向すくい角 β
（矢視 B）

表 1：ボール切れ刃のすくい角

切れ刃位置 θ	30°	45°	60°
半径方向すくい角 α	3°	0°	-4°
軸方向すくい角 β	11°	12°	14°

以上

MITSUBISHI MATERIALS CORPORATION
AKASHI PLANT
179-1, Nishioike, Kanagasaki, Uozumicho, Akashi, Hyogo, 674-0071 JAPAN

Figure B.2 - Manufacturer information for local rake angle (α) and local helix angle (β) for VC-2ESB Series

Appendix C

SEM Images of Cutting Tool - Post-Experiments

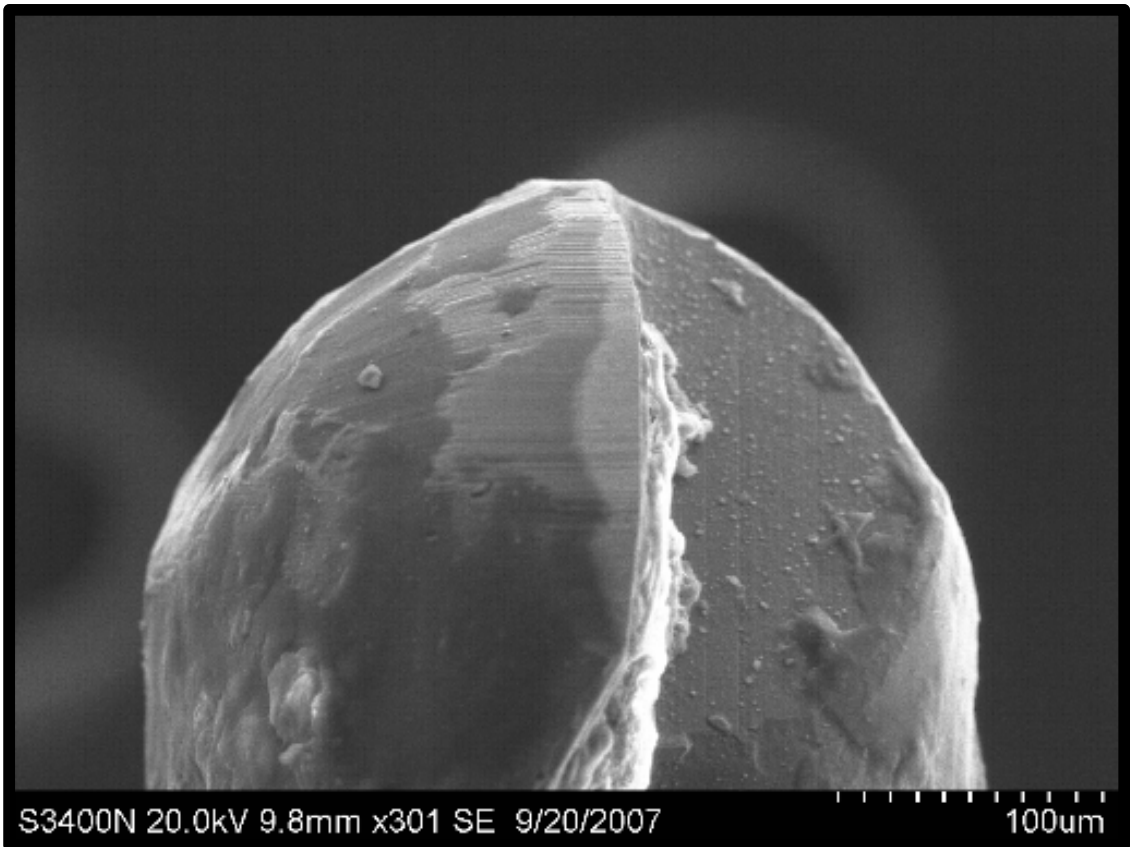

Figure C.1 - SEM image of ball end mill used in this study and other cutting experiments (nose radius - 200 μm, 2 flutes, cemented carbide)

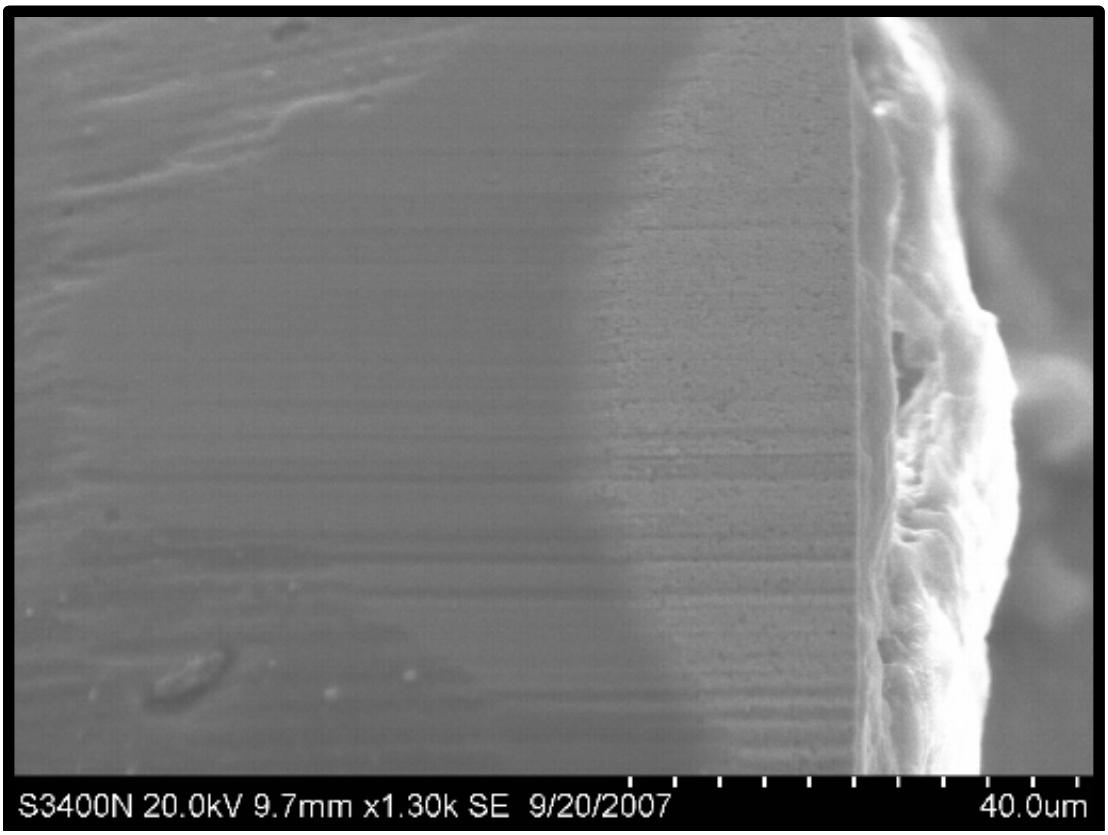

Figure C.2 - Closer view of the flank face shown in Figure C.1

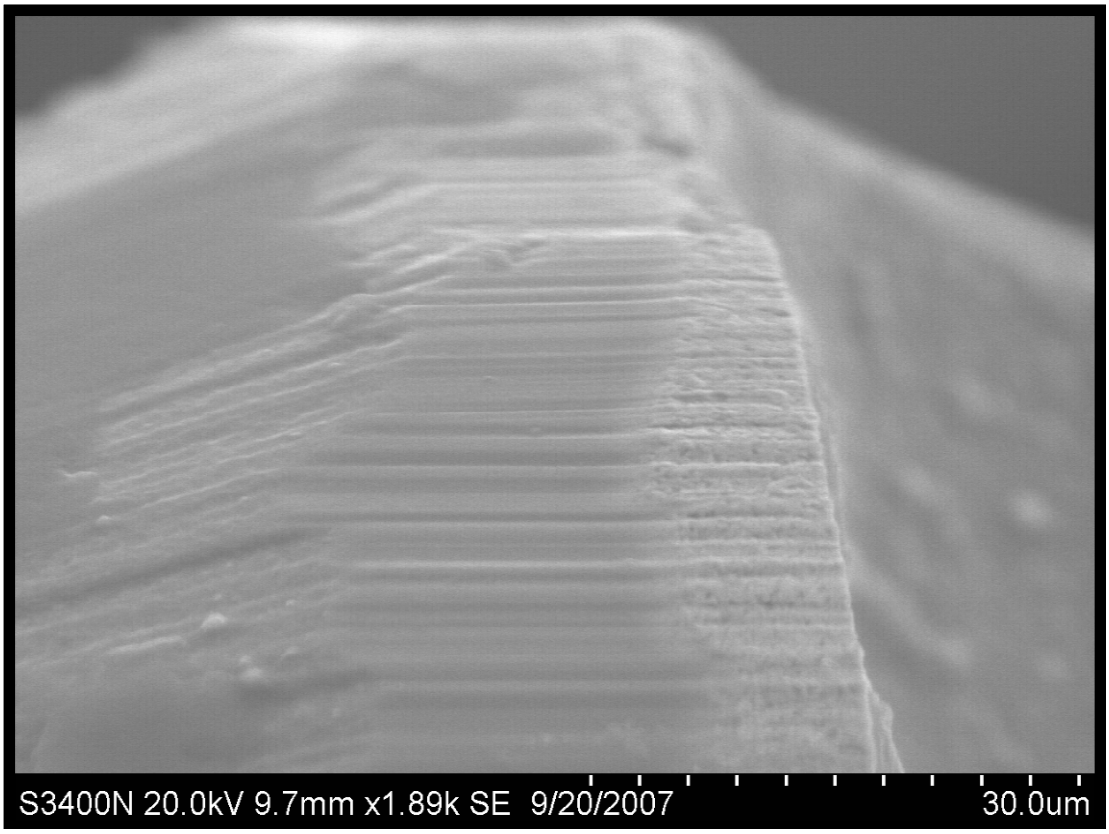

Figure C.3 - Another view of the flank face shown in Figure C.1

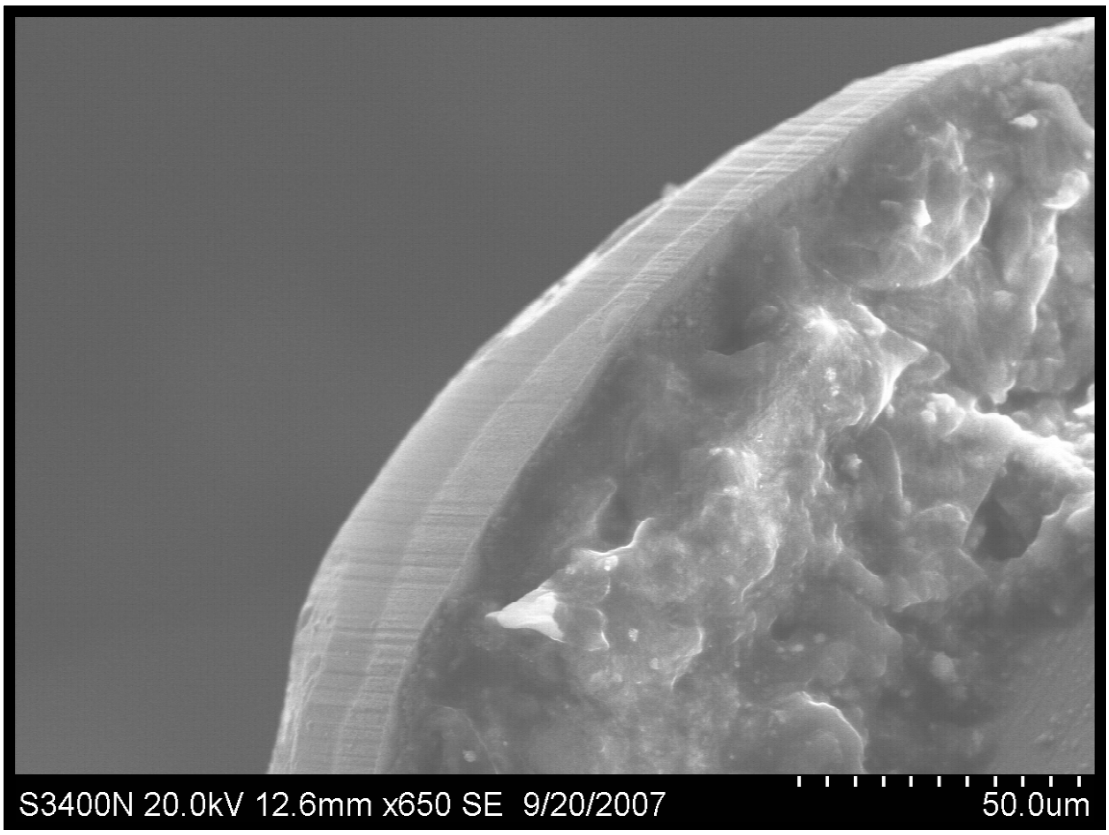

Figure C.4 - Another view of the cutting edge shown in Figure C.1 illustrating adherence of glass cutting chips along the rake face

REFERENCES

Antoniadis, A., Bilalis, N, Savakis, C., Maravelakis, E., Petropoulos, G., 2003, "Influence of Machining Inclination Angle on Surface Quality in Ball End Milling," *Proceeding of International Conference on Advances in Materials and Processing Technologies*, AMPT2003, Dublin, Ireland, July 8-11, pp. 1-4.

Bansal, N., Doremus, R., 1986, *Handbook of Glass Properties*, Academic Press, Inc., Orlando, FL.

Bifano, T., Dow, T., Scattergood, R., 1991, "Ductile-Regime Grinding: A New Technology for Machining Brittle Materials," *Journal of Engineering for Industry*, Vol. 113, pp. 184-189.

Brehm, R., van Dun, K., Teunissen, J., Haisma, J., 1979, "Transparent Single-Point Turning of Optical Glass: A Phenomenological Presentation," *Precision Engineering*, Vol. 1, pp. 207-213.

Bridgman, P., Simon, I., 1953, "Effects of Very High Pressures on Glass," *Journal of Applied Physics*, Vol. 24, pp. 405-413.

Buryta, D., Sowerby, R., Yellowley, I., 1994, "Stress Distributions on the Rake Face During Orthogonal Machining," *International Journal of Machine Tools and Manufacture*, Vol. 35, pp. 721-739.

Buryta, D., Sowerby, R., 1998, "Experimental Determination of Rake Face Stress Distributions," *Key Engineering Materials*, Vol. 138-140, pp. 57-126.

Childs, T., Mahdi, M., 1989, "On the Stress Distribution Between the Chip and Tool During Metal Turning," *Annals of CIRP*, Vol. 38, pp. 55-58.

Chiu, W.-C., Endres, W., Thouless, M., 2000, "An Experimental Study of Orthogonal Machining of Glass," *Machining Science and Technology*, Vol. 4, pp. 253-275.

Chiu, W.-C., Endres, W., Thouless, M., 2001, "An Analysis of Surface Cracking During Orthogonal Machining of Glass," *Machining Science and Technology*, Vol. 5, pp. 195-215.

Cohen, H., Rustum, R., 1961, "Effects of Ultrahigh Pressures on Glass," *Journal of the American Ceramic Society*, Vol. 44, pp. 523-524.

Dornfeld, D., Min, S., Takeuchi, Y., 2006, "Recent Advances in Mechanical Micromachining," *Annals of the CIRP*, Vol. 55, pp. 745-768.

Fang, F., Zhang, G., 2003, "An Experimental Study of Edge Radius Effect on Cutting Single Crystal Silicon," *International Journal of Advanced Manufacturing Technology*, Vol. 22, pp. 703-707.

Fang, F., Zhang, G., 2004, "An Experimental Study of Optical Glass Machining," *International Journal of Advanced Manufacturing Technology*, Vol. 23, pp. 155-160.

Filiz, S., Conley, C., Wasserman, M., Ozdoganlar, B., 2007, "An Experimental Investigation of Micro-Machinability of Copper 101 Using Tungsten Carbide Micro-Endmills," *International Journal of Machine Tools and Manufacture*, Vol. 47, pp. 1088-1100.

Fischer-Cripps, A., 2004, *Nanoindentation*, Springer, New York.

Galeener, F., 1987, "Structural Models for Amorphous SiO_2," edited by Weeks, R., Kinser, D., *Effects of Modes of Formation on the Structure of Glasses*, Trans Tech Publications, Brookfield, VT, pp. 305-314.

Gan, J., Wang, X., Zhou, M., Ngoi, B., Zhong, Z., 2003, "Ultraprecision Diamond Turning of Glass with Ultrasonic Vibration," *International Journal of Advanced Manufacturing Technology*, Vol. 21, pp. 952-955.

Grimsditch, M., 1984, "Polymorphism in Amorphous SiO_2," *Physical Review Letters*, Vol. 52, pp. 2379-2381.

Holloway, D., 1973, *The Physical Properties of Glass*, Wykeham Publications, London.

Huang, L., and Kieffer, J., 2004, "Amorphous-Amorphous Transitions in Silica Glass. I. Reversible Transitions and Thermomechanical Anomalies," *Physical Review B*, Vol. 69, pp. 224203-1-224203-11.

Huerta, M., Malkin, S., 1976a, "Grinding of Glass: The Mechanics of the Process," *Journal of Engineering for Industry*, Vol. 98, pp. 459-467.

Huerta, M., Malkin, S., 1976b, "Grinding of Glass: Surface Strength and Fracture Strength," *Journal of Engineering for Industry*, Vol. 98, pp. 468-473.

Hwang, D., Choi, T., Grigoropoulos, C., 2004, "Liquid-Assisted Femtosecond Laser Drilling of Straight and Three-Dimensional Microchannels in Glass," *Applied Physics A*, Vol. 79, pp. 605-612.

Inamura, Y., Katayama, Y., Utsumi, W., Funakoshi, K., 2004, "Transformations in the Intermediate-Range Structure of SiO_2 Glass Under High Pressure and Temperature," *Physical Review Letters*, Vol. 93, pp. 015501-1-015501-4.

Ji, H., Keryvin, V., Rouxel, T., Hammouda, T., 2006, "Densification of Window Glass Under Very High Pressure and Its Relevance to Vickers indentation," *Scripta Materialia*, Vol. 55, pp. 1159-1162.

Kailer, A., Nickel, K., and Gogotsi, Y., 1999, "Raman Microspectroscopy of Nanocrystalline and Amorphous Phases in Hardness Indentations," *Journal of Raman Spectroscopy*, Vol. 30, pp. 939-946.

Kalpakjian, S., Schmid, S., 2003, *Manufacturing Processes for Engineering Materials*, Prentice Hall, New Jersey.

Kese, K., Li, Z., Bergman, B., 2005, "Method to Account for True Contact Area in Soda-Lime Glass During Nanoindentation with the Berkovich Tip," *Materials Science and Engineering A*, Vol. 404, pp. 1-8.

Kese, K., Tehler, M., Bergman, B., 2006, "Contact Residual Stress Relaxation in Soda-Lime Glass. Part I. Measurement Using Nanoindentation," *Journal of the European Ceramic Society*, Vol. 26, pp. 1003-1011.

Ko, T., Kim, H., Lee, S., 2001, "Selection of the Machining Inclination Angle in High-Speed Ball End Milling," *International Journal of Advanced Manufacturing Technology*, Vol. 17, pp. 163-170.

Komanduri, R., 1996, "On Material Removal Mechanisms in Finishing of Advanced Ceramics and Glasses," *Annals of CIRP*, Vol. 45, pp. 509-513.

Kurkjian, C., Kammlott, G., Chaudhri, M., 1995, "Indentation Behavior of Soda-Lime Silica Glass, Fused Silica, and Single-Crystal Quartz at Liquid Nitrogen Temperature," *Journal of the American Ceramic Society*, Vol. 78, pp. 737-744.

Lacks, D., 1998, "Localized Mechanical Instabilities and Structural Transformations in Silica Glass Under High Pressure," *Physical Review Letters*, Vol. 80, pp. 5385-5388.

Le Bourhis, E., Metayer, D., 2000, "Indentation of Glass as a Function of Temperature," *Journal of Non-Crystalline Solids*, Vol. 272, pp. 34-38.

Le Bourhis, E., Rouxel, T., 2003, "Indentation Response of Glass with Temperature," *Journal of Non-Crystalline Solids*, Vol. 316, pp. 153-159.

Lee, L., Liu, X., Lam, K., 1995, "Determination of Stress Distribution on the Tool Rake Face Using a Composite Tool," *International Journal of Machine Tools and Manufacture*, Vol. 35, pp. 373-382.

Li, X., 1997, "Development of a Predictive for Stress Distributions at the Tool-Chip Interface in Machining," *Journal of Materials Processing Technology*, Vol. 63, pp. 169-174.

Liu, K., Li, X., Liang, S., Liu, X., 2004a, "Nanometer Scale Ductile Mode Cutting of Soda-Lime Glass," *Transactions of NAMRI/SME*, Vol. 32, pp. 39-45.

Liu, K., Li, X., Rahman, M., Liu, X., 2004b, "A Study of the Cutting Modes in the Grooving of Tungsten Carbide," *International Journal of Advanced Manufacturing Technology*, Vol. 24, pp. 321-326.

Liu, X., DeVor, R., Kapoor, S., 2004c, "The Mechanics of Machining at the Microscale: Assessment of the Current State of the Science," *Transactions of the ASME*, Vol. 126, pp. 666-678.

Liu, X., DeVor, R., Kapoor, S., 2006, "An Analytical Model for the Prediction of Minimum Chip Thickness in Micromachining," *Transactions of the ASME*, Vol. 128, pp. 474-481.

Liu, X., DeVor, R., Kapoor, S., 2007a, "Model-Based Analysis of the Surface Generation in Microendmilling - Part 1: Model Development," *Journal of Manufacturing Science and Engineering*, Vol. 129, pp. 453-460.

Liu, X., DeVor, R., Kapoor, S., 2007b, "Model-Based Analysis of the Surface Generation in Microendmilling - Part 1: Model Development," *Journal of Manufacturing Science and Engineering*, Vol. 129, pp. 461-469.

Lu, D., Li, J., Rong, Y., Grevstad, A., Usui, S., 2007, "Temperature and Stress Distribution Analysis in Micro-Cutting of TI-6AL-4V and AL7050-T6 with Advantedge," *Proceedings of the ASPE 22nd Annual Meeting*, Dallas, TX, Oct. 14-19, pp. 1-4.

Mackenzie, J., 1963, "High-Pressure Effects on Oxide Glasses: I, Densification in Rigid State," *Journal of the American Ceramic Society*, Vol. 46, pp. 461-470.

Marians, C., and Hobbs, L., 1987, "A Language for the Study of Network Silica Glasses," edited by Weeks, R., Kinser, D., *Effects of Modes of Formation on the Structure of Glasses*, Trans Tech Publications, Brookfield, VT, pp. 31-36.

Matsumura, T., Hiramatsu, T., Shirakashi, T., Muramatsu, T., 2004, "A Study on Cutting Force in the Milling Process of Glass," *Transactions of NAMRI/SME*, Vol. 32, pp. 463-470.

Matsumura, T., Ono, T., 2005, "Glass Machining with Ball End Mill," *Transactions of NAMRI/SME*, Vol. 33, pp. 319-326.

McClain, B., Batzer, S., Maldonado, G., 2002, "A Numeric Investigation of the Rake Face Stress Distribution in Orthogonal Machining," *Journal of Materials Processing Technology*, Vol. 123, pp. 114-119.

Michel, M., Mikowski, A., Lepienski, C., Foerster, C., Serbena, F., 2004, "High Temperature Microhardness of Soda-Lime Glass," *Journal of Non-Crystalline Solids*, Vol. 348, pp. 131-138.

Morgan, C., Vallance, R., Marsh, E., 2004, "Micro Machining Glass with Polycrystalline Diamond Tools Shaped by Micro Electro Discharge Machining," *Journal of Micromechanics and Microengineering*, Vol. 14, pp. 1687-1692.

Moriwaki, T., Shamato, E., Inoue, K., 1992, "Ultraprecision Ductile Cutting of Glass by Applying Ultrasonic Vibration," *Annals of CIRP*, Vol. 41, pp. 141-144.

Nakatsuji, T., Kodera, S., Hara, S., Matsunaga, H., Ikawa, N., Shimada, S., 1990, "Diamond Turning of Brittle Materials for Optical Components," *Annals of CIRP*, Vol. 39, pp. 89-92.

Nakamura, M., Sumomogi, T., Endo, T., 2003, "Evaluation of Surface and Subsurface Cracks on Nano-Scale Machined Brittle Materials by Scanning Force Microscope and Scanning Laser Microscope," *Surface and Coatings Technology*, Vol. 169-170, pp. 743-747.

Oxley, P., 1989, *The Mechanics of Machining: An Analytical Approach to Assessing Machinability*, Wiley, New York.

Patten, J., Cherukuri, H., Yan, J., 2004, "Ductile-Regime Machining of Semiconductors and Ceramics," *High-Pressure Surface Science and Engineering*, edited by Gogotsi, Y., Domnich, V., Institute of Physics Publishing, Philadelphia, PA, pp. 543-632.

Patten, J., Gao, W., Yasuto, K., 2005, "Ductile Regime Nanomachining of Single-Crystal Silicon Carbide," *Transactions of the ASME*, Vol. 127, pp. 522-532.

Peter, K., 1970, "Densification and Flow Phenomena of Glass in Indentation Experiments," *Journal of Non-Crystalline Solids*, Vol. 5, pp. 103-115.

Polian, A., Grimsditch, M., 1990, "Room-Temperature Densification of *a*-SiO_2 Versus Pressure," *Physical Review B*, Vol. 41, pp. 6086-6087.

Rouxel, T., Sangleboeuf, J., 2000, "The Brittle to Ductile Transition in a Soda-Lime-Silica Glass," *Journal of Non-Crystalline Solids*, Vol. 271, pp. 224-235.

Shang, H., Rouxel, T., Buckley, M., Bernard, C., 2006, "Viscoelastic Behavior of a Soda-Lime-Silica Glass in the 293-833 K Range by Micro-Indentation," *Journal of Materials Research*, Vol. 21, pp. 632-638.

Shaw, M., 1984, *Metal Cutting Principles*, Oxford University Press, New York.

Shimada, S., Ikawa, N., Inamura, T., Takezawa, N., Ohmori, H., Sata, T., 1995, "Brittle-Ductile Transition Phenomena in Microindentation and Micromachining," *Annals of CIRP*, Vol. 44, pp. 523-526.

Sreejith, P., Ngoi, B., 2001, "New Materials and Their Machining," *International Journal of Advanced Manufacturing Technology*, Vol. 18, pp. 537-544.

Sreejith, P., 2005, "Machining Force Studies on Ductile Machining of Silicon Nitride," *Journal of Materials Processing Technology*, Vol. 169, pp. 414-417.

Susman, S., Volin, K., Price, D., Grimsditch, M., Rino, J., Kalia, R., Vashishta, P., 1991, "Intermediate-Range Order in Permanently Densified Vitreous SiO_2: A Neutron-Diffraction and Molecular-Dynamics Study," *Physical Review B*, Vol. 43, pp. 1194-1197.

Takeuchi, Y., Sawada, K., Sata, T., 1996, "Ultraprecision 3D Micromachining of Glass," *Annals of CIRP*, Vol. 45, pp. 401-404.

Tipler, P., 1999, *Physics for Scientists and Engineers*, W.H. Freeman, New York, NY.

Voldman, J., Gray, M., Schmidt, J., 1999, "Microfabrication in Biology and Medicine," *Annual Review of Biomedical Engineering*, Vol. 1, pp. 401-425.

Volger, M., Liu, X., Kapoor, S., DeVor, R., and Ehmann, K., 2002, "Development of Meso-Scale Machine Tool (mMT) Systems," Transactions of NAMRI/SME, Vol. XXX, pp. 653-661.

Vogler, M., DeVor, R., and Kapoor, S., 2004, "On the Modeling and Analysis of Machining Performance in Micro-Endmilling, Part I: Surface Generation," *Journal of Manufacturing Science and Engineering*, Vol. 126, pp. 685–694.

Weule, H., Huntrup, V., Tritschler, H., 2001, "Micro-Cutting of Steel to Meet New Requirements in Miniaturization," *CIRP Annals - Manufacturing Technology*, Vol. 50, pp. 61–64.

Williams, R., Huang, Y., Melkote, S., Kinsey, B., Sun, W., Yao, D., 2005, "Recent Advances in Micro/Meso-Scale Manufacturing Processes," *Proceeding of 2005 ASME International Mechanical Engineering Congress and Exposition*, Orlando, Florida, IMECE2005-79889, pp. 1-22, Nov. 5-11.

Yoshida, S., Sangleboeuf, J., Rouxel, T., 2005, "Quantitative Evaluation of Indentation-Induced Densification in Glass," *Journal of Materials Research*, Vol. 20, pp. 3404-3412.

Yoshino, M., Ogawa, Y., Aravindan, S., 2005, "Machining of Hard-Brittle Materials by a Single Point Tool Under External Hydrostatic Pressure," *Journal of Manufacturing Science and Engineering*, Vol. 127, pp. 837-845.

Yoshino, M., Matsumura, T., Umehara, N., Akagami, Y., Aravindan, S., Ohno, T., 2006, "Engineering Surface and Development of a New DNA Micro Array Chip," *Wear*, Vol. 260, pp. 274-286.

Zhou, M., Ngoi, B., Yusoff, M., Wang, X., 2006, "Tool Wear and Surface Finish in Diamond Cutting of Optical Glass," *Journal of Materials Processing Technology*, Vol. 174, pp. 29-33.

Zorev, N., 1963, "Interrelationship Between Shear Processes Occurring Along Tool Face and on Shear Plane in Metal Cutting," *Proceeding of International Conference on Production Engineering Research*, Pittsburgh, PA, Nov. 5-11, pp. 42-49.